VERIFICATION OF CIRCUMFERENTIAL AND AXIAL STRAINS IN AXISYMMETRIC WOUND ROLL MODELS

By

KAZI MD. ISMAEL MURTAZA

Bachelor of Science in Mechanical Engineering

Bangladesh University of Engineering and Technology

Dhaka, Bangladesh

2006

Submitted to the Faculty of the
Graduate College of the
Oklahoma State University
in partial fulfillment of
the requirements for
the Degree of
MASTER OF SCIENCE
May, 2009

VERIFICATION OF CIRCUMFERENTIAL AND

AXIAL STRAINS IN AXISYMMETRIC

WOUND ROLL MODELS

Thesis Approved:

Dr. J. K. Good

Thesis Adviser

Dr. H. B. Lu

Dr. R. Singh

Dr. A. Gordon Emslie

Dean of the Graduate College

ACKNOWLEDGMENTS

I would like to thank the Almighty for giving me the strength to do what I have done in the course of this project. I am grateful to him in every way.

My sincere appreciation to Dr. J. K. Good for everything he has done for me. He has inspired and motivated me to a great extent. His intuition has proved to be very helpful for me. I thank him for his wisdom and insight. In addition I thank him for being very considerate and supportive of me all the way.

I would like to thank Mr. Ron Markum for guiding me throughout my work and constantly helping me with anything I need.

I thank my family members and my friends who have stood by me through everything. Their encouragement and support have made the rough times smoother.

TABLE OF CONTENTS

LIST OF TABLES

Tables Page

LIST OF FIGURES

Figure Page

LIST OF SYMBOLS AND ABBREVIATIONS

WHRC	Web Handling Research Center
HSWL	High Speed Web Line
PET	Polyester Film
MD	Machine Direction
CMD	Cross Machine Direction
E_r	Radial Young's modulus
E_θ	Tangential Young's modulus
G_{rz}	Shear Modulus
ε_r	Radial Strain
ε_θ	Tangential Strain
ε_z	Axial Strain
σ_r	Radial Stress
σ_θ	Tangential Stress
σ_z	Axial Stress
$\nu_{r\theta}$	Poisson's ratio of stress in θ-direction to strain in r-direction
$\nu_{\theta r}$	Poisson's ratio of stress in r-direction to strain in θ-direction
ν_{zr}	Poisson's ratio of stress in r-direction to strain in z-direction
$\nu_{\theta z}$	Poisson's ratio of stress in z-direction to strain in θ-direction
$\varepsilon_\theta(r)$	Tangential strain at certain radius, r

$\varepsilon_z(r)$	Axial strain at certain radius, r
$\varepsilon_\theta(gage)$	Tangential strain at gage's radius
$\varepsilon_z(gage)$	Axial strain at gage's radius
r	Radius
d	Diameter
R_{outer}	Outer radius of core
Y	Distance of neutral axis
R	Radius of curvature
P	Normal pressure
K_1	Material constant
K_2	Material constant
δ_{ij}	Level of interference
u_i, u_j	Nodal points
T_w	Web tension
t	Web thickness
w	Web width
α	Reinforcement factor
pli	pounds per linear inch
fpm	feet per minute

CHAPTER I

INTRODUCTION TO THE NATURE OF STRESS AND STRAIN IN WOUND ROLLS

The term web is used to describe thin materials. A web may be defined as a material whose length is much greater than its width and whose width is much greater than its thickness. Webs are manufactured and processed in a continuous, flexible strip form. Web materials are very common these days in manufacturing industries and are made from a wide range of materials. Common categories of web materials include plastic, paper, textiles, metals, and composites. Many of the products we use daily are essentially web materials. Web materials are often thin and fragile and must be wound into rolls to prevent them from being damaged. The rolls are then unwound and rewound in subsequent web processes.

However, there are several problems that accompany the conveniences wound web materials have to offer. The winding process, depending on the tension at which the web is wound, can cause damage to the web material. While it is this tension that is holding the wound roll together, it is this very tension that is responsible for the stress

levels inside the wound rolls. The quality of the wound roll can depend on the stresses which exist in it. If this is not controlled properly, several defects may occur including buckling and tearing.

This study focuses on verifying an axisymmetric wound roll model which was developed by Cagri Mollamahmutoglu, here at Oklahoma State University. This model predicts the internal stresses and strains in the wound roll. In the axisymmetric sense, these stresses include radial, axial, shear and circumferential components. The stresses that develop are affected by

1. Winding tension level or profile with radius.
2. The start and finish diameter of the wound roll.
3. The material properties of the wound roll. Some of which are state dependent.
4. The material properties and dimensions of the core.
5. The thickness variation across the web width and through its length.
6. The length variation of the web across the width and through its length.

The stresses are relatable to wound roll defects. The radial stresses can be related to "blocking" defects. Given adequate pressure or radial stress, uncoated and coated web surfaces will stick together. The surfaces may be so well adhered, the web cannot be unwound without tearing. Another defect which is common in wound rolls is known as circumferential corrugation as shown in Figure 1. These corrugations are similar to the buckling that can occur in cylindrical shells that are subjected to axial loads. Corrugations in wound rolls are detrimental to roll quality. When the web on the roll shown in figure 1 is unwound the buckled waves will remain in the web. The wound roll with the corrugations wound into it may reside in storage for a period of days, weeks, or even

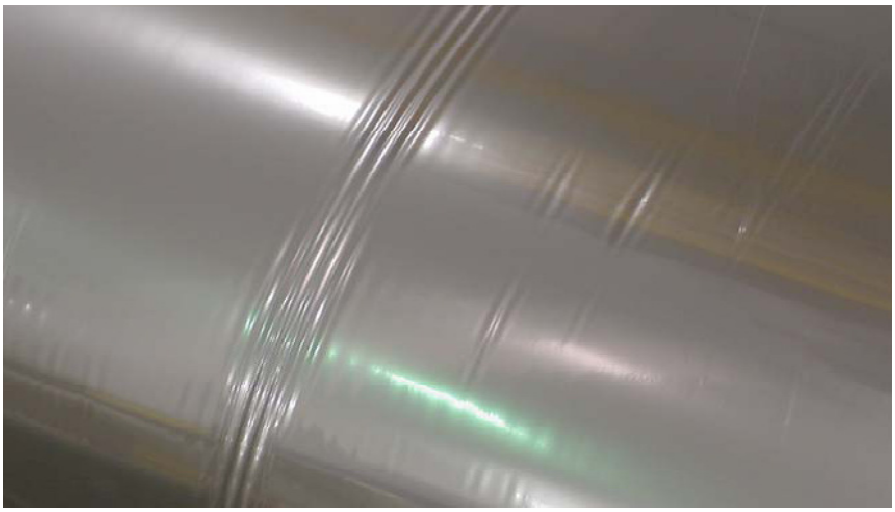

Figure 1: Circumferential Corrugations

months. Many webs are viscoelastic in some time frame and so the corrugations that may have been the result of elastic winding stresses will remain in the web for some period of time after unwinding. Many web operations requiring coating, printing or laminating and if the web will not lie flat defects will result.

To predict buckling phenomena requires knowledge of the stresses which act in or on the layer that is buckling. These stresses are calculated by axisymmetric winding models such as that of Mollamahmutoglu. All models incorporate assumptions which affect the behavior of the output stresses. These models are largely not validated.

My research will focus on validating the stresses output by 2D axisymmetric winding models. If the stresses or strains computed by the model agree with the laboratory measurements, the model and its underlying assumptions will be validated. With a verified model future research will be possible. For example if the axial stresses produced by the model are known to be valid, failure theories can be developed that predict when circumferential corrugations will occur.

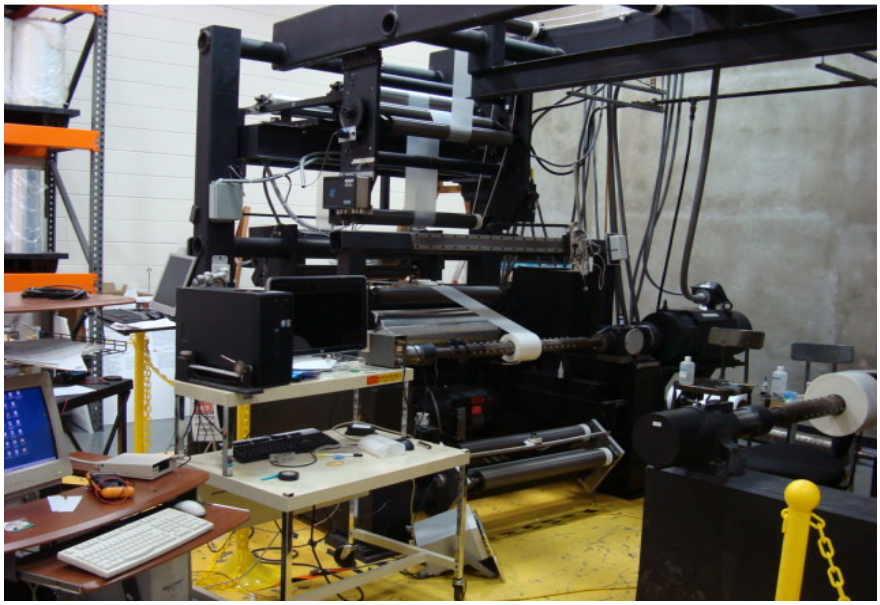

Figure 2: Experimental Area of the HSWL

CHAPTER II

LITERATURE REVIEW

In order to determine the stresses inside wound rolls, numerous procedures have been developed. This is because the quality of a wound roll depends on the stresses which exist in it. These procedures are known as winding models. They aid in the detail study of wound rolls. A wound roll is three dimensional; hence, the winding process introduces stresses and strains which vary in all three directions. So ideally, a wound roll should be considered as an accreted finite width spiral of layers. This, however, would make it very complicated to analyze. To simplify this, a wound roll is considered to be a series of concentric accreted hoops of web in a cylinder form [9]. Other assumptions that simplify the condition are also made in winding models. This literature review will focus on two dimensional winding models where stresses are evaluated as a function of r (radial) and z (axial) location.

Two-Dimensional Models

Since this study is based on a two-dimensional model, two-dimensional models will be elaborately discussed, with special attention to the model being verified, in this chapter. However, a few of the key two-dimensional models will be reviewed here briefly.

Kedl's Model

Kedl [12] described a model that calculated the stresses throughout a wound roll as a function of both radius and width. The roll was divided into an arbitrary number of widthwise segments. Each segment was treated as a separate roll with its own winding tension dependent on its outer radius. The effect of CMD non-uniformity was thus computed. In order to compute the tension, segment diameters were determined by using a special model which was based on stacking thick walled cylinders with orthotropic properties. Calculations of the wound-in pressure and tension were computed from any existing model that allowed the compressive roll modulus to be a function of pressure. Two types of tests were run to evaluate the model. The first type used measured cross-web caliper of a 29 inch wide polyester web as a base for cross-web stress computations. The second type assumed a uniform cross-web caliper on 12 inch wide polyester web that was wound on an aluminum core with a 1.0 inch wide by 0.008 inch thick radial step in the center. The experimental results obtained in this study showed that the model adequately predicted the center wound roll as a function of cross-web caliper variation over the web width.

Cole and Hakiel's Model

Cole and Hackiel developed the first 2D winding model [3]. All other models to that date were one dimensional models that predicted pressure and circumferential stress as a function of the radial location on a roll. Cole and Hackiel recognized that web materials often have thickness variation across their width. They recognized that as such webs wind that non-cylindrical rolls result. They also recognized that those lateral locations that had the greatest thickness would also have the greatest outside radius. Since the wound roll can have but one angular velocity this meant there was a linear velocity variation across the width of the outer layer dependent on the variation in the radius of that layer across the roll width. The web tension could thus no longer be assumed uniform. This was important because the web or winding tension is the most important input given to a winding model in terms of the effect on the internal stresses in the wound roll.

Although apparently Cole and Hakiel's model [3] was two dimensional, further investigation showed that it can be best described as a pseudo two dimensional model. The reason for this is, they consider the roll's finite width with the segmentation to thin slices and treat each slice as a discrete one dimensional model. This is an approximation because it neglects displacement continuity across the slices and it is not able to treat the wound roll as a whole. This model is mentioned here since it was one of the first two-dimensional models to be introduced. Cole and Hakiel conducted a study in which the roll was divided in the widthwise direction into a discrete number of segments. The theoretical stresses and displacements within the segments were calculated by solving a second order differential equation in radial pressure with non-constant coefficients that

Hakiel had employed in an earlier one dimensional model [1]. In the experimental part of the study, two strain gages were mounted onto each segment of the core of the roll to measure the circumferential strain in the core. Pressure readings were obtained with the segmented, instrumented core. Since the relation between the external pressure on a ring and the circumferential strain on the outside of a ring is known, the contact pressure between the inside of the roll and the outside of the core could be inferred. Pressure readings were taken by stopping the winder several times during the winding process while the tension was maintained. The pressure could be compared to the radial stress predicted by the model at the radial location of the core. Hakiel also measured the variation in roll diameter across the roll width each time the winder was stopped.
Cole and Hackiel's model models generated radial and circumferential stress as a function of radius (σ_r and σ_θ) and the radial location of layers, sector by sector. Each sector was assumed to exist in a plane stress condition. Since all axial stresses (σ_z) were assumed to be zero, axial stress output was not possible

Determination of Relationship between the Material Constants and Stress and Strain

Normal Pressure, Normal Strain and Radial Modulus of Elasticity

Earlier one-dimensional models assumed linear isotropic material properties for modeling the constitutive relations. Web materials may exhibit a linear relationship between stresses and strains in the plane of the web. Pfeiffer proved that the out-of-plane behavior was non-linear [2]. If a stack of web coupons are subject to an out of plane pressure, the relation between stress (pressure) and normal or radial strain will be found

to be non-linear. Pfeiffer found that an exponential relationship could be used to curve fit pressure versus strain.

$$P = -\sigma_r = K_1\left(e^{K_2 \cdot \varepsilon_r} - 1\right) \quad \text{(2.1)}$$

The derivative of the pressure with respect to the strain will be the radial modulus of elasticity.

$$E_r = \frac{d\sigma_r}{d\varepsilon_r} = K_2\left(P + K_1\right) \quad \text{(2.2)}$$

where K_1 and K_2 are determined experimentally, by curve fitting pressure versus strain data collected from stack compression tests.

Poisson's Ratio:

The in-plane Poisson's ratios of webs ($\nu\theta z$ and $\nu z\theta$) have magnitudes that are comparable or greater than the common value of 0.3. The Poisson's ratios which couple the out-of-plane pressure to a circumferential or axial strain ($\nu_{r\theta}$ or ν_{rz}) have been found to be (1) very small and as such (2) very hard to measure. Willet and Poesch [8] and Good and Markum [5] have measured these Poisson's ratios on the order of 0.01. In addition to $\nu_{r\theta}$ and ν_{rz} being small use of 1D & 2D winding models show that the stresses output are quite insensitive to $\nu_{r\theta}$ and ν_{rz} . The in-plane values of Poisson's Ratio are quite important in their impact on the axial stresses (σ_z) developed.

Lee and Wickert's model

Lee and Wickert [10] developed a model which predicted the stress field within a wound roll. The wound roll examined in their study comprised core and web regions of

finite width. In this model, the radial, circumferential, axial, and shear stresses could vary in the radial and axial directions. This model accounts for the anisotropic and nonlinear behavior of web material. In one-dimensional models, core stiffness was considered to be uniform across the roll's width. This was re-examined in this two-dimensional analysis. Winding tension was not allowed to vary across the roll width. Regardless of the shape of the outside of the winding roll, winding tension was assumed constant across the roll width.

Hoffecker and Good's model

Hoffecker and Good [11] developed a two-dimensional model that employed an axisymmetric finite element method. A series of quadrilateral elements were used to model a layer, or group of layers, in the wound roll. The web thickness was allowed to vary linearly across the width of each quadrilateral. The primary output of finite element codes in solid mechanics were nodal deformations. Strains and stresses were secondary outputs since they depend on the knowledge of the deformation of the finite elements. The outer lap was formed as a cylinder of guessed constant radius but non-uniform thickness across the width. Multi point constraints were then used to make the inside of the outer lap conform to the outside of the lap beneath. The circumferential stress was then integrated over the web width and thickness to determine the level of winding tension associated with the "guessed" radius. If the computed winding tension was larger than the actual winding tension the "guessed" radius of the outer lap had been chosen too small. The "guessed" radius would be iterated until the computed winding tension matched the actual winding tension within some tolerance. However, implementation of

multipoint constraints requires defining additional degrees of freedom, increasing solution arrays' dimensions and this situation burdens the computational work.

Output of two-dimensional models

The outputs of two-dimensional models differ slightly from the one-dimensional models. Two-dimensional models are able to output radial pressure, circumferential stress, axial stress, and shear stress in the r-z plane as a function of the axisymmetric location. Roll deformation and outer shape can also be calculated across the roll width. Two-dimensional models allow defects to be studied that could not be studied with one-dimensional models. Blocking or sticking defects were mentioned in the introduction. The highest pressure locations in the wound roll are often the result of web non-uniformity over the web width. Thus, these high pressure(r-z) locations could not be captured with a 1D model that outputs pressure only as a function of radius (r). The axial stresses that cause corrugations also require a 2D axisymmetric model that predicts these stresses as a function of r-z location.

The objective of this study is to verify a novel algorithm, developed by Cagri Mollamahmutoglu under the supervision of Dr. Good at Oklahoma State University, used to compute the axial strains in wound rolls. An introduction to the basics of his model is given here.

Mollamahmutoglu's Model:

Mollamahmutoglu's model uses an axisymmetric finite element method in which a series of quadrilateral elements are used to model a layer, or group of layers in a roll.

The model uses an accretive process. So, as each layer is accreted onto the outside of the roll, the new outside radius becomes part of the solution vector.

An important thing to note about his model is that he allows no slippage between the outer layer and the layer beneath. The inside nodes on the outer layer and outsides node on the layer beneath are common. Thus no relative slip is allowed in his formulation. Now let us consider the following figure.

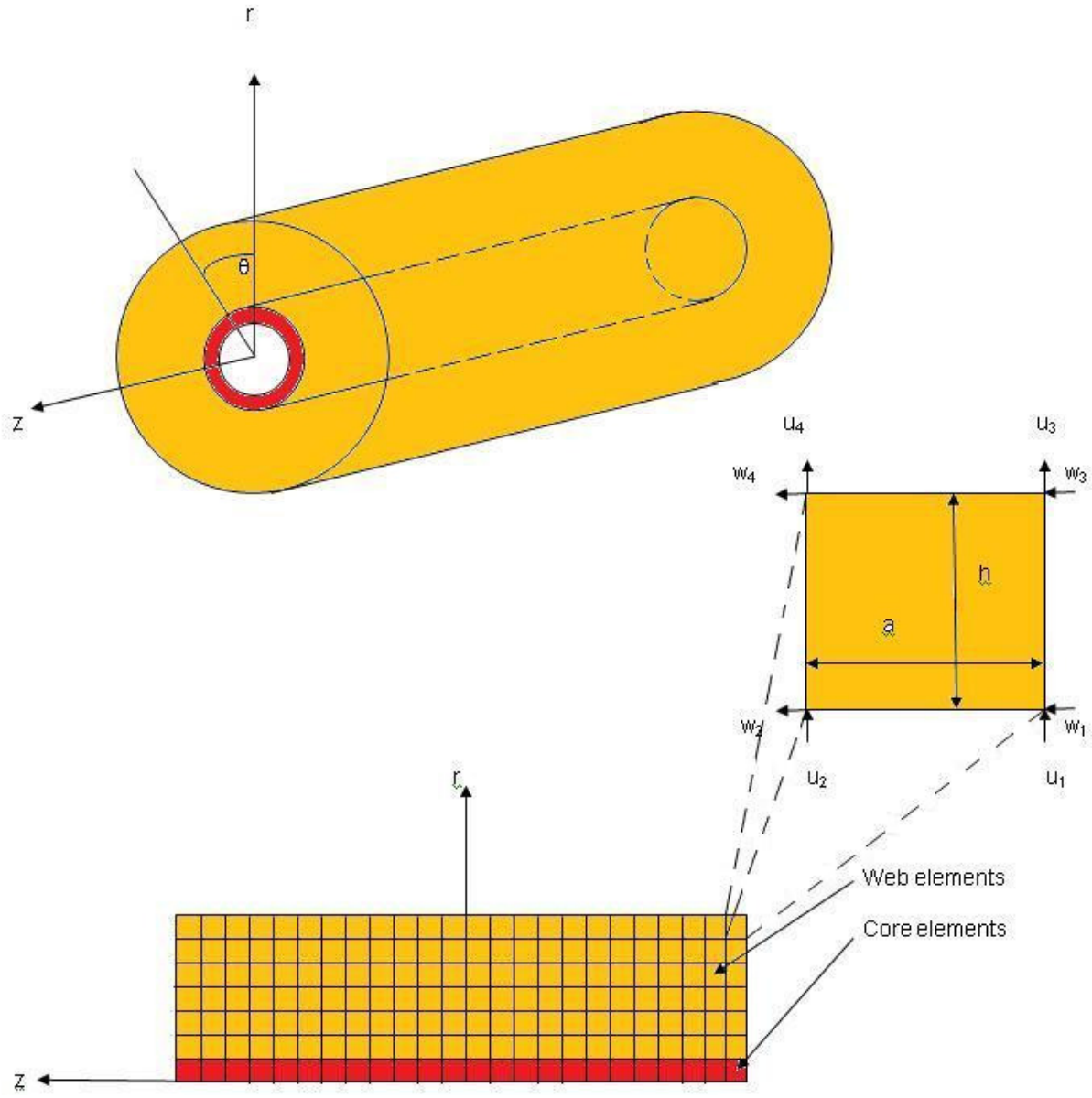

Figure 3: Finite element mesh

One element is magnified in the diagram. We see that it has 4 nodes and 8 degrees of freedom. The deformations of these nodes, and hence the element is given by the following equations:

$$\begin{pmatrix} u \\ w \end{pmatrix} = \begin{pmatrix} N_1 & 0 & N_2 & 0 & N_3 & 0 & N_4 & 0 \\ 0 & N_1 & 0 & N_2 & 0 & N_3 & 0 & N_4 \end{pmatrix} \begin{pmatrix} u_1 \\ w_1 \\ u_2 \\ w_2 \\ u_3 \\ w_3 \\ u_4 \\ w_4 \end{pmatrix} \text{ or, } [u] = [N]\,[q] \quad \ldots\ldots\ldots\ldots\ldots\ldots\ldots\ldots\ldots\ldots \quad (2.3)$$

Here, the shape functions are given by

$$N_1(\eta,\xi) = (1-\eta)(1-\xi)/4$$

$$N_2(\eta,\xi) = (1-\eta)(1+\xi)/4$$

$$N_3(\eta,\xi) = (1+\eta)(1-\xi)/4$$

$$N_4(\eta,\xi) = (1+\eta)(1+\xi)/4$$

The elemental stiffness matrix is an 8x8 matrix like this:

$$\begin{bmatrix} K^1_{11} & K^1_{12} & K^1_{13} & K^1_{14} & K^1_{15} & K^1_{16} & K^1_{17} & K^1_{18} \\ & K^1_{22} & K^1_{23} & K^1_{24} & K^1_{25} & K^1_{26} & K^1_{27} & K^1_{28} \\ & & K^1_{33} & K^1_{34} & K^1_{35} & K^1_{36} & K^1_{37} & K^1_{38} \\ & & & K^1_{44} & K^1_{45} & K^1_{46} & K^1_{47} & K^1_{48} \\ & & & & K^1_{55} & K^1_{56} & K^1_{57} & K^1_{58} \\ & & & & & K^1_{65} & K^1_{66} & K^1_{67} \\ & SYM & & & & & K^1_{77} & K^1_{78} \\ & & & & & & & K^1_{88} \end{bmatrix}$$

This element stiffness matrix is derived by performing numerical integration on

$$k^e = 2\pi \int_{-1}^{1} \int_{-1}^{1} r\mathbf{B}^{\mathbf{T}}\mathbf{D}\mathbf{B}\det\mathbf{J}\, d\xi d\eta \quad \ldots\ldots\ldots\ldots\ldots\ldots\ldots\ldots\ldots\ldots\ldots\ldots\ldots\ldots\ldots\ldots\ldots\ldots\ldots\ldots\ldots\ldots\ldots\ldots \quad (2.4)$$

where the element strain-displacement matrix **B** is defined like this:

$$B = \begin{bmatrix} B_1 \\ B_2 \end{bmatrix}$$

Where B_1 is a 3x8 matrix and B_2 is a 1x8 row matrix that relate the element strains (ε_r, ε_z ,γ_{rz} , ε_θ) to the nodal deformations [q].

For defining the load vector, a pre-strain formulation is used. The pre-strain formulation incorporates the tangential stress caused by the web line stress into the model. Basically, it computes the tangential stress of the sectors that the web width is divided into and using these stresses calculates the corresponding nodal loads of each element of the last layer. An integral part of the pre-strain formulation is the determination of the relaxation radius. The relaxation radius is the radius of the outer layer of web in a stress free state. The wound roll maybe larger than the relaxation radius, then the new layer cannot relax completely. The actual relaxation amount is determined by the surface stiffness of the wound roll, the web and relaxation radius [9]. The relaxation radius is computed in the following way.

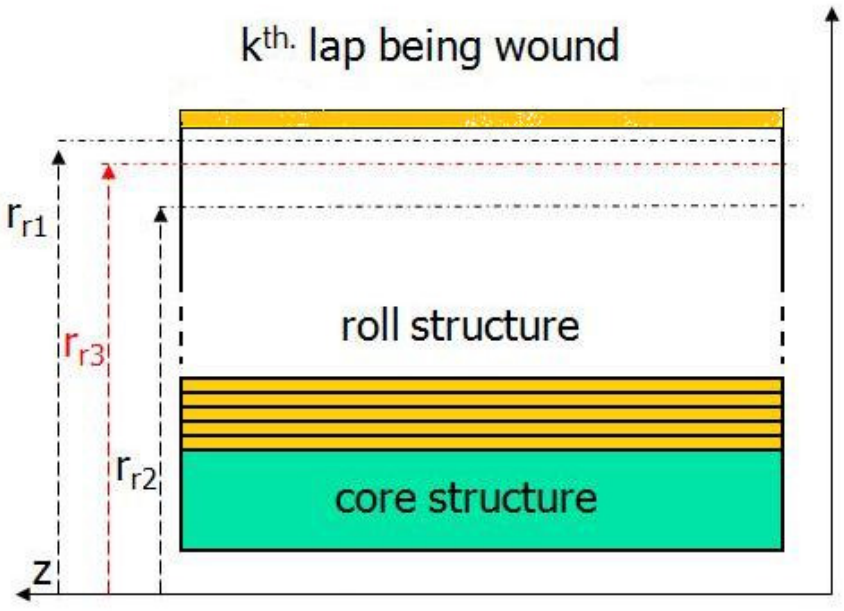

Figure 4: Pre-strain Formulation.

From the figure we see that the k^{th} layer is being wound onto the roll. A relaxation radius (r_{r1}) is calculated using the following formula:

$$T_{\theta i} = E_{\theta i}((r_{i+1} + r_i)/(2r_r) - 1)$$

Here, r_r is the relaxation radius and for the first iteration, $r_r = r_{r1}$. Furthermore, since we are not considering thickness variation, $r_{i+1} = r_i$ and $T_{\theta i}$ is calculated from the following equation:

$$T_{web} \cong T_{\theta k} = \sum_{i=1}^{m} (T_{\theta i} A_i) / \sum_{i=1}^{m} A_i$$

where, $A_i = ((h_{i+1} + h_i) w_i / 2)$ with w_i is the width of each modeled segment and $h_{i+1}=h_i$ since thickness variation is not considered in this thesis.

Now, using the relaxation radius a pre-strain is defined as follows:

$$\varepsilon_0 = \begin{bmatrix} 0 \\ 0 \\ 0 \\ -\left(\dfrac{(r_i + r_{i+1})}{2r_r} - 1\right) \end{bmatrix} \quad \text{..... (2.5) [9]}$$

From the pre-strain we get the following expression for stress

$$\sigma_0 = \begin{bmatrix} 0 \\ 0 \\ 0 \\ -E_{\theta i}\left(\dfrac{(r_i + r_{i+1})}{2r_r} - 1\right) \end{bmatrix} \quad \text{..... (2.6) [9]}$$

Plugging in σ_0 in the following equation we get the nodal elemental forces. $B^T \sigma_0 r dA$

$$\int B^T \sigma_0 r dA = f_i \quad \text{..... (2.10)}$$

These elemental loads are then assembled into a structure load vector and then used in solving for the nodal displacements. Then the average tangential stress ($T_{\theta k1}$) of the last layer is calculated. The average tensile stress in the outer lap ($T_{\theta k1}$) will not equal the web line tensile stress because r_{r1} was in fact a guess. .Hence, the relaxation radius is modified, i.e. a second approximation is made. The second relaxation radius is calculated using the following formula [9]:

$$r_{r2} = r_{r1}(T_{\theta k1} / T_{web}) \quad \text{..... (2.11)}$$

The system is again solved for the second relaxation radius. After second solution, average tangential stress is again calculated for the outer layer. Then, using the second and first relaxation radii, a third relaxation radius is obtained by means of linear interpolation using the following equation [9]:

$$r_{r3} = r_{r1} - \frac{(r_{r1} - r_{r2})(T_{web} - T_{\theta k1})}{(T_{\theta k2} - T_{\theta k1})} \quad \text{..... (2.12)}$$

The third relaxation radius is used as input for the final solution for the last layer. After the final solution, calculated average tangential stress will be very close to the web line tension typically:

$$\left|T_{\theta k3} - T_{web}\right| \leq \varepsilon$$

Where $\varepsilon \approx .001$. In units of psi, winding tensions range from hundreds to thousands of psi. Thus, errors on the order of 0.001 are acceptable. At this point another layer is added and the process repeats until the desired outer radius of the winding roll is achieved. After each layer has been added and the average tension in the outer lap converges to the winding stress the increments in all stresses ($\Delta\sigma_r$, $\Delta\sigma_z$, $\Delta\tau_{rz}$ and $\Delta\sigma_\theta$) are used to update the total stresses in all laps. Any state dependant properties such as the radial modulus

(E_r) are updated within each lap as a function of the total radial pressure ($-\sigma_r$). After all the laps have been added, the final total stress and strain state of the wound roll is known and defect analysis can begin. Similar to the stresses the increments in strain ($\Delta\varepsilon_r$, $\Delta\varepsilon_z$, $\Delta\gamma_{rz}$, $\Delta\varepsilon_{\theta\theta}$) are used to update the total strain in all the laps. In experimental analysis it is often more straight forward to measure strains than stresses and hence these computed total strains will be compared to strains measured experimentally.

Winding Simulations

In this section we shall run some simulations that depict the different cases run in the actual laboratory experiments using the DuPont 377 200 gage PET. Two different widths of webs, 6 inch and 24 inch were used. The reason for this is that we hoped to obtain a near plane stress condition in the 6 inch wide roll and a condition that approached plane strain state in the 24 inch wide roll. The wound roll properties along with the core dimensions are listed below in table 1.

Wound roll and core dimensions		
roll width	24inch	6inch
core inner radius	1.512inch	1.512inch
core outer radius	1.886inch	1.662inch
roll outer radius	3.947inch	3.162inch

Table 1: Wound Roll Dimensions

At this point we state the different material properties used in the simulations and then why these values were used.

The material properties used are shown in table2:

Material Properties		
	6 inch web	24 inch web
K1	1.049211	1.049211
K2	40.85841	40.85841
Ewt (psi)	711000	711000
Ewz (psi)	711000	711000
ν_{wrz}	0.01	0.01
ν_{wrt}	0.01	0.01
ν_{wtz}	0.38	0.38
E_{cr} **(psi)**	30000000	30000000
E_{ct} **(psi)**	30000000	30000000
E_{cz} **(psi)**	30000000	30000000
ν_{crz}	0.3	0.3
ν_{crt}	0.3	0.3
ν_{ctz}	0.3	0.3
G_c **(psi)**	11538462	11538462
T_{web}	1000	1000

Table 2: Material properties

Tests were performed by Good and Beisel [18] to determine the value of Young's Modulus E_θ .These tests resulted in a value of 711000 psi. This value was accepted for this study as these tests were run in the recent past. Young's Modulus (E_z) in the cross machine direction was assumed to be equal to the value of E_θ . We know that the value of Young's Modulus E_r is not constant and depends on the constants K_1 and K_2 . So, the values of these constants are provided in the table and are based on tests run by Good and Markum [16] since these tests had been run in the recent past. The shear modulus, like the Young's Modulus in the radial direction, is also dependent on the radial position and here is assumed to be twice the value of E_r in accordance with the results of the tests that Srinivasan Ganapathi had carried out in his study [17].

The value of Poisson's ratio for the θr and zr was considered to be 0.01 in this study. This value was measured by Willet and Poesch [8] and accepted for use by Hakiel [1]. So, this is the value that was used in this study. The Poisson's ratio for the θz direction was chosen as .38 is this study. This is the maximum value of Poisson's ratio claimed by DuPont for the PET [19].

The material properties, E, G, and ν, of the steel core were obtained from a general materials science text [19].

Now, we use these values in the model and run some simulations. 3D plots are presented to show how each of the three stresses change as a function of radius of the wound roll and segment of width being analyzed. The three-dimensional analysis will be done for both the 6 inch material and the 24 inch material. The first set of plots is for the 6 inch wide material.

In the following figure we see that the radial pressure is highest at the core. However, it is not uniform across the width of the web at the core. The edges are under greater pressure than the center of the roll's width. This deviation in pressure at the roll edges near the core is due to the transition to plane stress conditions near the roll edge and the large differences between the core and web properties. Pressure is near zero at the outside of the wound roll because of surface equilibrium in the radial direction.

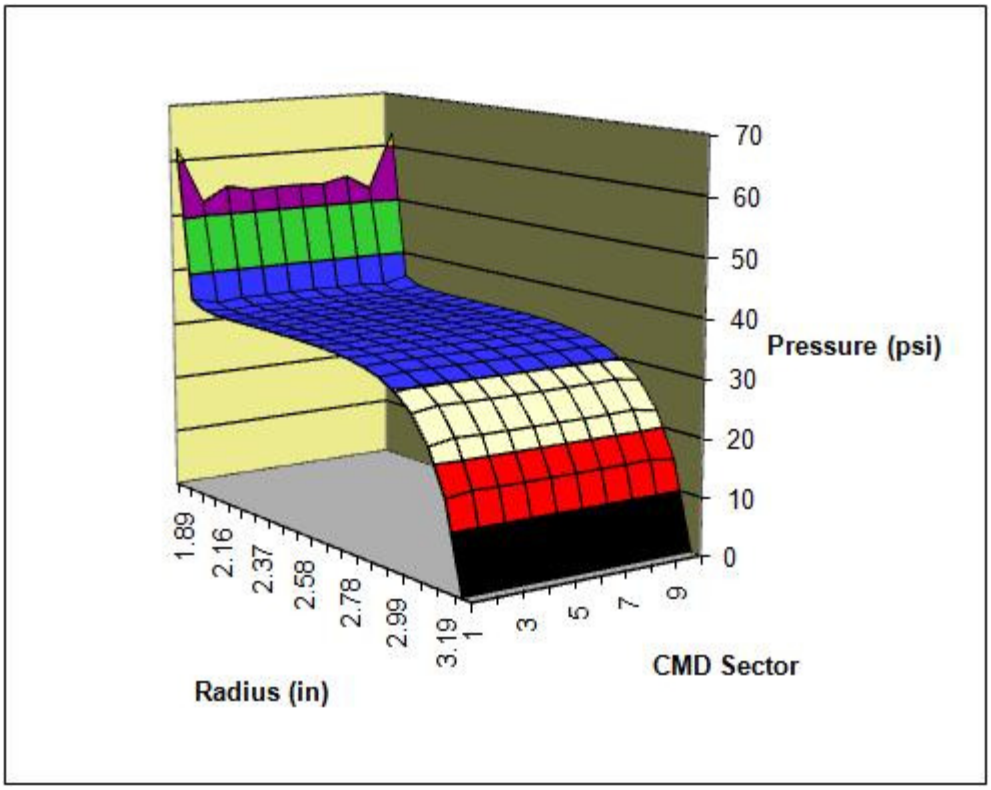

Figure 5: Model Output of Pressure in a 6 inch Wide Web

In the next figure we see the axial stresses produced due to winding. We notice that there is a sharp dip in the axial stress in radii close to the core. The negative σ_z web stresses at the core are due to $\nu_{\theta z,web}$ being fixed at 0.38 while $\nu_{\theta z,core}$ is 0.30. The web wants to expand more than the core does which results in compression of the web.

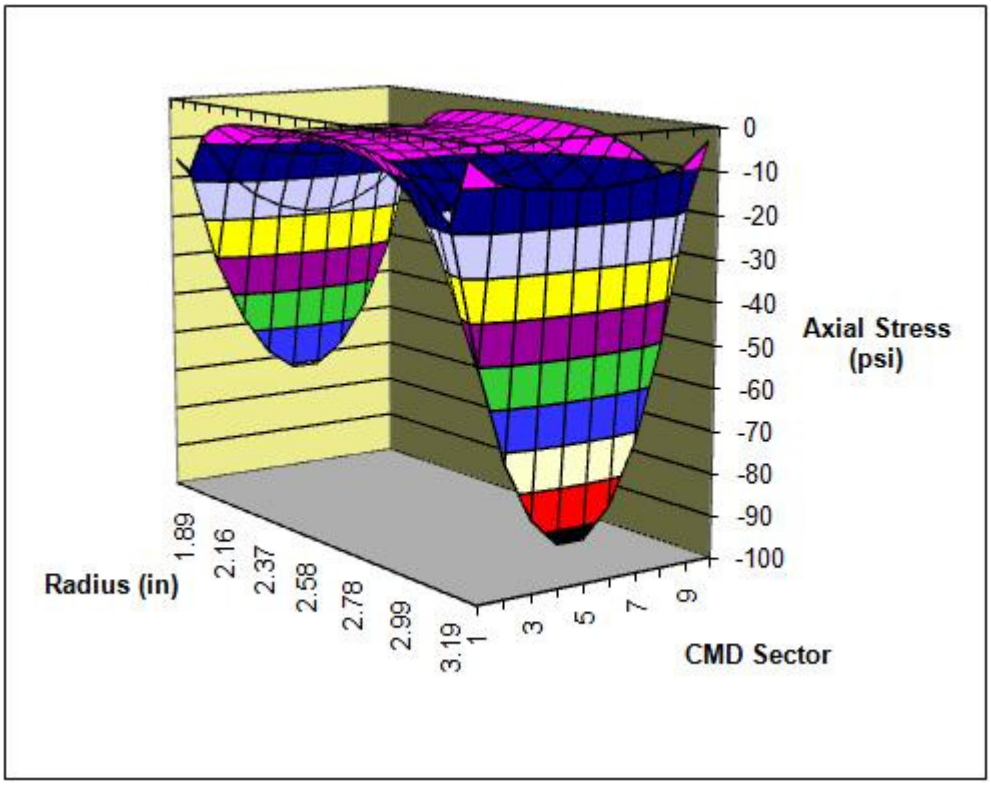

Figure 6: Model Output of Axial Stress in a 6 inch Wide Web

Hence, the axial stress approaches zero as it reaches nearly plane stress conditions.

The next figure shows the change of tangential stress as a function of radial location and widthwise position. We see that the tangential stress starts off high and then goes to zero. The outside edges dip more than the central part. Lower tangential stresses are observed within the winding roll because of radial compression. Furthermore, the edges see even more drop because of the transition to plain stress conditions. The tangential stress in the web is generally calculated by dividing the web tension by the thickness of the web which in this case yields 1000 psi. This is the stress level we ought to see at the core and at the outer layer. In the figure, we see that the tangential stress at the outer layer is mostly 1000psi (except for the edges) and over 1000psi in some of the middle segments. The tangential stress on the core however, are lower that 1000psi,

around 900psi. The reason for this is the radially inward deformation of the steel core due to the initial pressure (on the order of 55-60 psi) on the core as seen in figure 8.

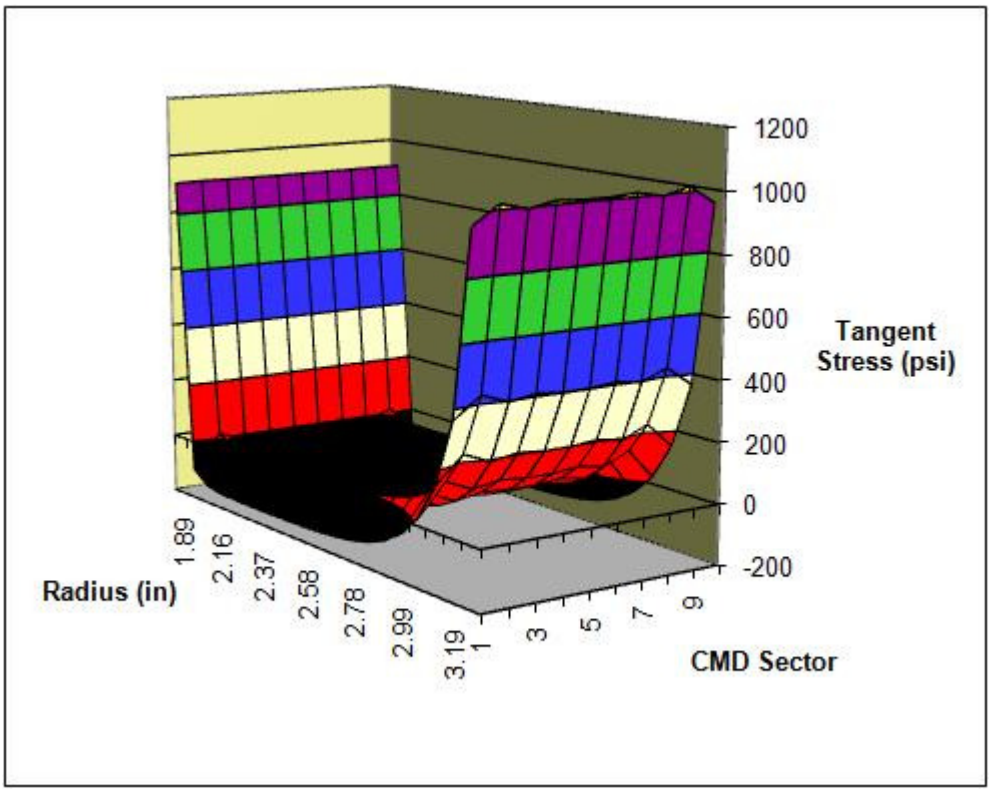

Figure 7: Model Output of Tangential Stress in a 6 inch Wide Web

The next three figures show pressure and stress change as a function of radial location and widthwise position for a 24" wide web. Figure shows the pressure distribution. Similar behavior to that of a 6" wide web is observed here. Pressure is high near the core and approaches zero on the outer layer.

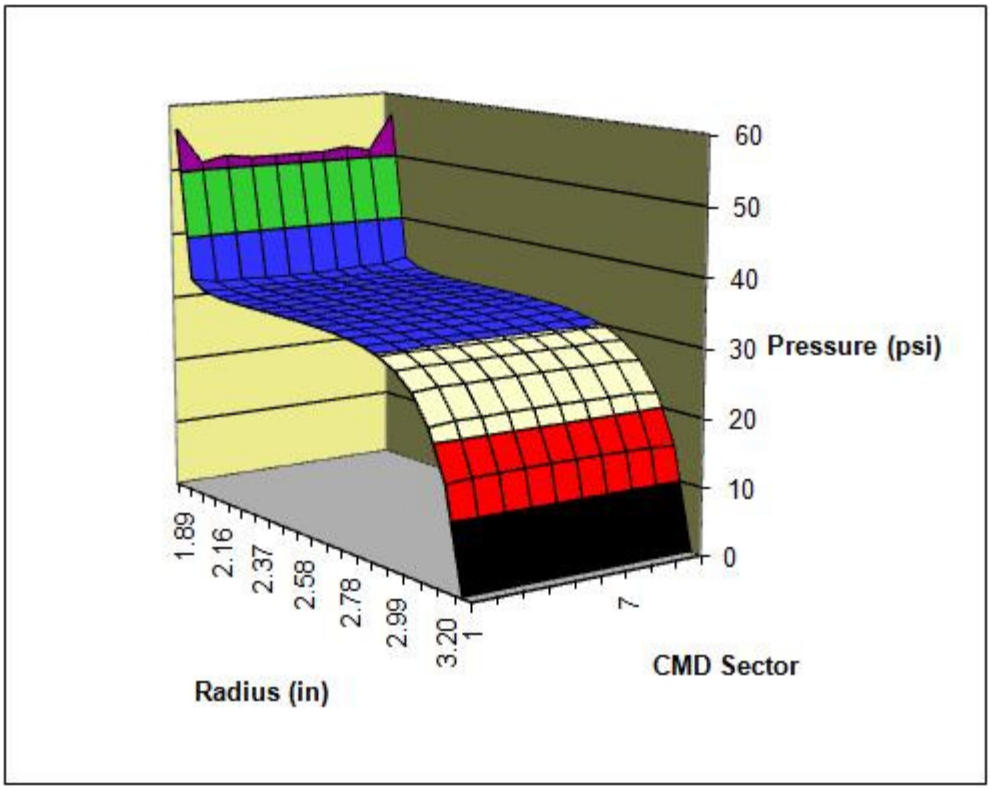

Figure 8: Model Output of Pressure in a 24 inch Wide Web

The next figure shows variation of axial stress the 24” wide roll. A Similar distribution of stress to that of a 6” wide web is seen here. However, the axial stresses in this case are a lot higher than that of the 6” wide roll.

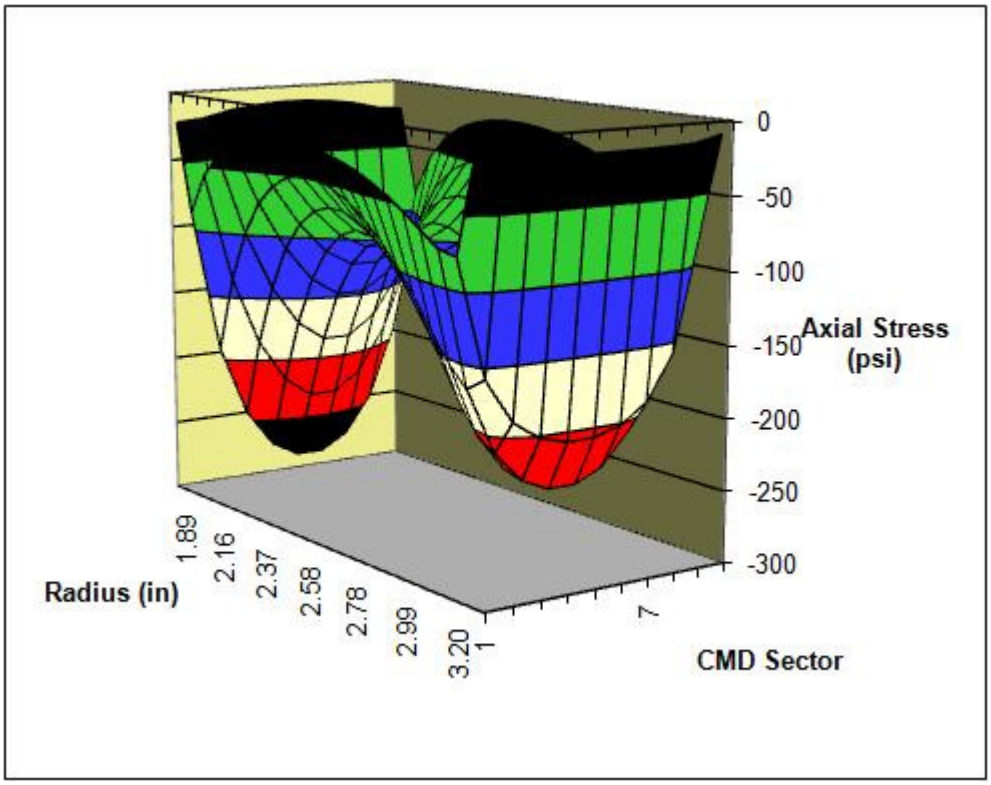

Figure 9: Model Output of Axial Stress in a 24 inch Wide Web

The next figure shows variation of tangential stress. Similar behavior to that of a 6" wide web is seen here in that the tangential stress is the highest at the inner and outer radius with the outer radius experiencing 1000psi and the inner radius experiencing a little less than that at around 900psi.

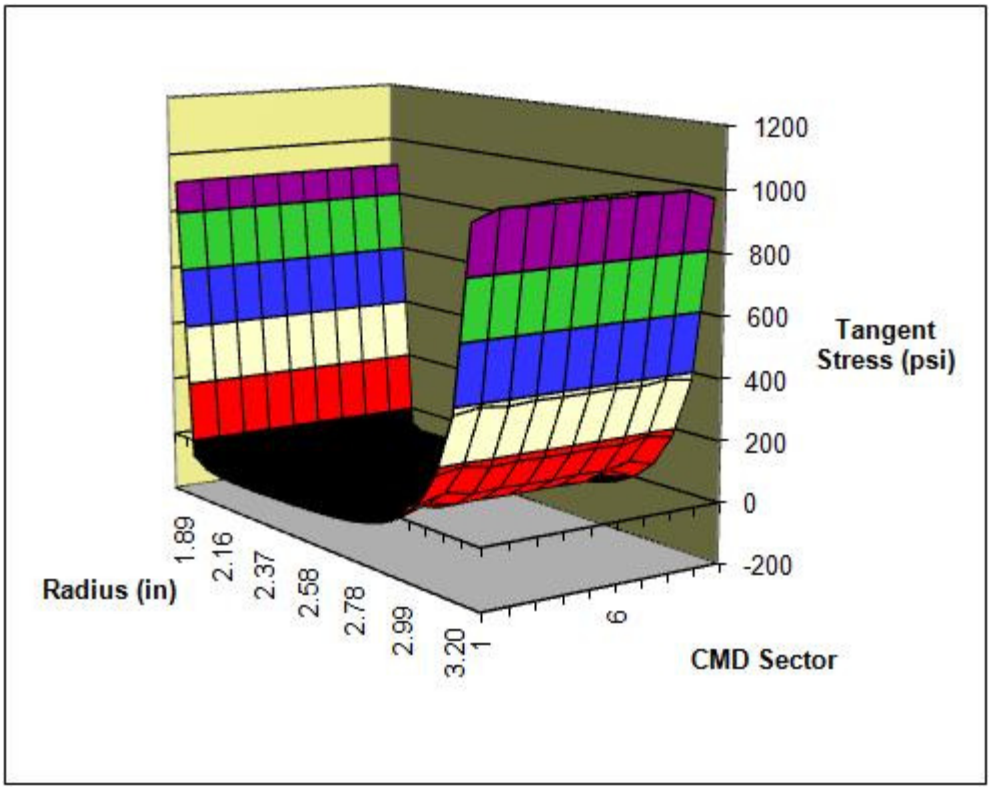

Figure 10: Model Output of Tangential Stress in a 24 inch Wide Web

The theoretical data has so far been presented in this chapter as stress as a function of radius of the wound roll. Now we convert this theoretical data from stress to strain for comparison with the experimental results.

After solution of the finite element set of equations we know all the deformations of the nodes due to the addition of the last lap. These are changes in deformation (Δq) not the total deformations that have been computed. We then calculate changes in strain due to the addition of the last lap.

$$[\Delta\varepsilon]_{i,layer} = \begin{bmatrix} \Delta\varepsilon_r \\ \Delta\varepsilon_z \\ \Delta\gamma_{rz} \\ \Delta\varepsilon_\theta \end{bmatrix} = [B][\Delta q] \quad \text{..... (2.13)}$$

We now update the total strains in all laps by summing these changes in strain for each layer to the strains that exist in these layers that were due to previous layers being added.

$$[\varepsilon_{Total}]_{i,layer} = \begin{bmatrix} \varepsilon_r \\ \varepsilon_z \\ \gamma_{rz} \\ \varepsilon_\theta \end{bmatrix} = [\varepsilon_{Total}]_{i,layer} + [\Delta\varepsilon]_{i,layer} \quad \text{..... (2.14)}$$

The 6 inch wide web strains are shown first. Here it must be mentioned that the model was run using 10 widthwise segments of the roll. This means that the roll was divided into 10 segments and the data from the 5th segment are taken for study since the strain gages were placed at approximately the centre of the web. The following figure shows the MD strain as a function of wound roll radius. The strains shown represent the strains at the centerline of the roll so a comparison could be made with the experimental data, which was taken at the centerline of the roll as mentioned before.

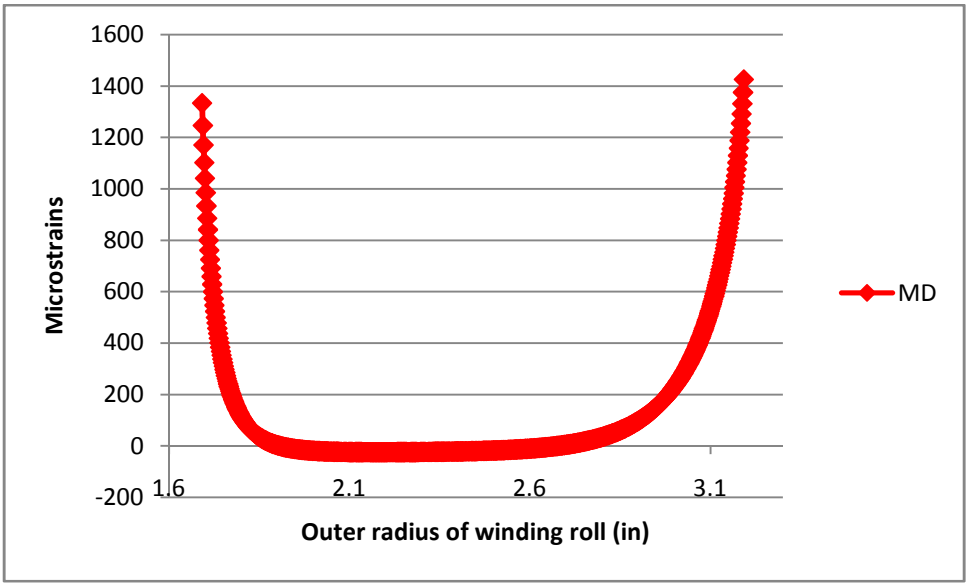

Figure 11: MD Strain for 6 inch Wide Web

The next figure shows the CMD strain as a function of wound roll radius. Once

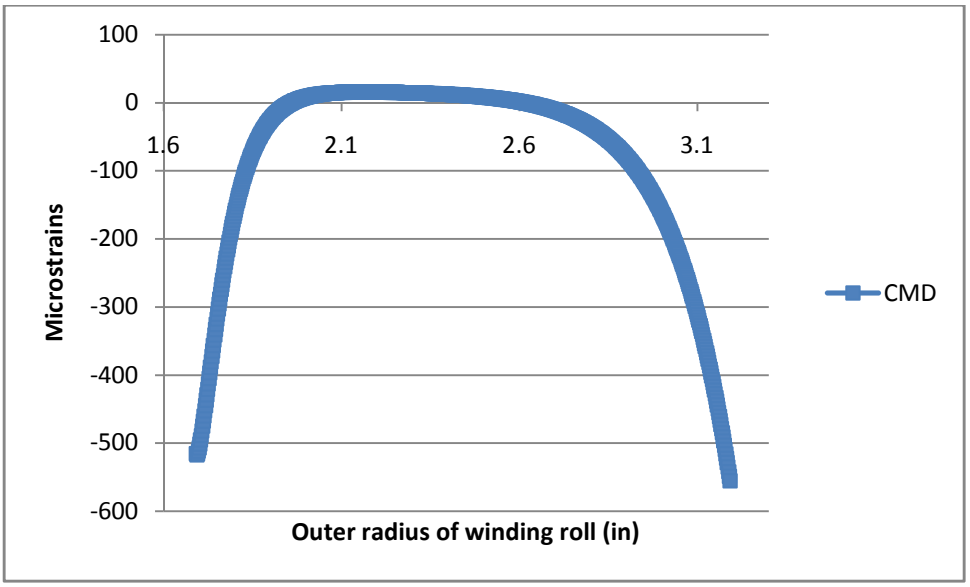

Figure 12: CMD Strain for 6 inch Wide Web

again, segment 5 is being plotted.

Now, the 24 inch wide web stresses are converted to strains. The following figure shows the MD strain as a function of wound roll radius. MD strains for the 24 inch wide web were similar to the MD strains in 6 inch wide web.

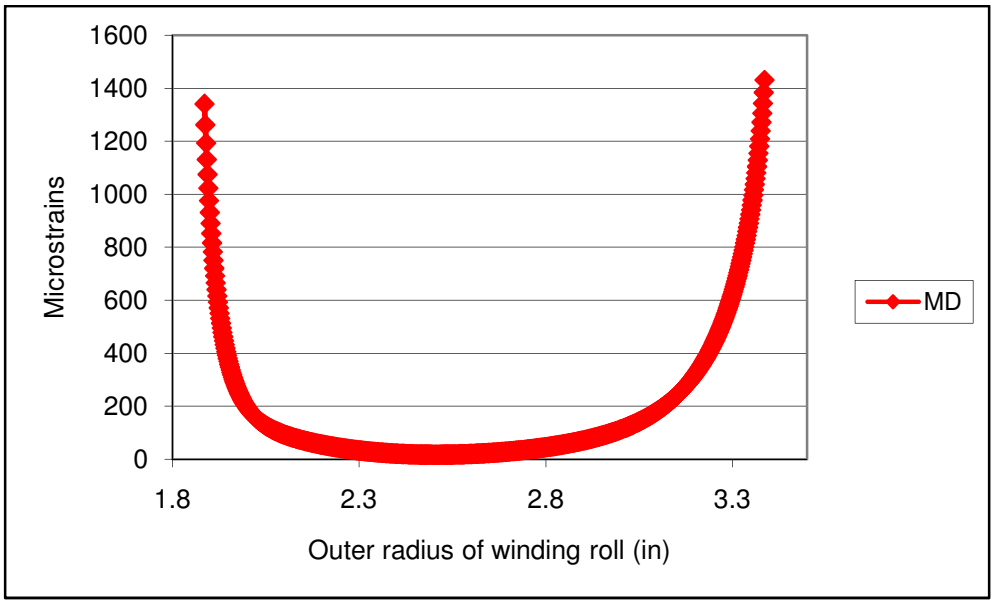

Figure 13: MD Strain for 24 inch Wide Web

The next figure shows the CMD strain as a function of radius.

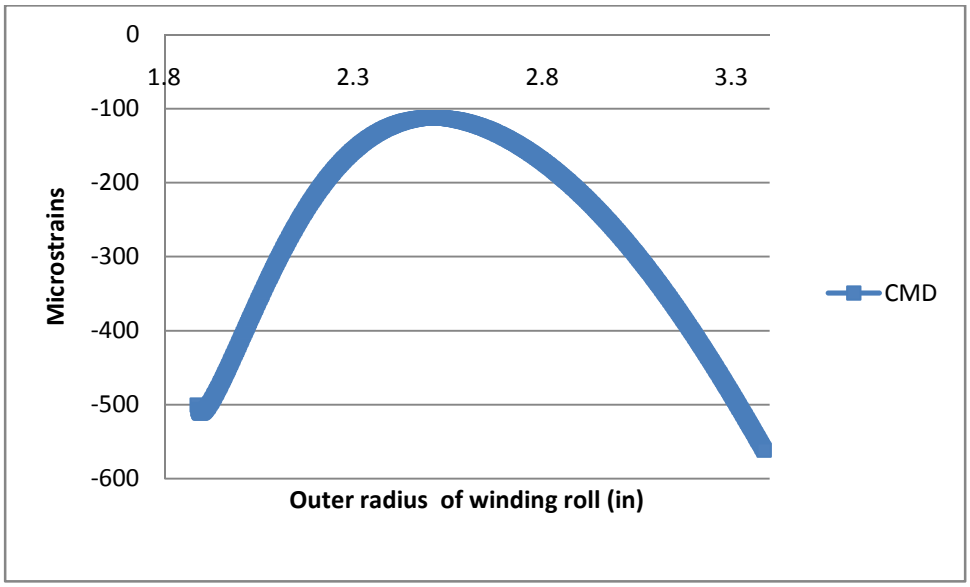

Figure 14: CMD Strain for 24 inch Wide Web

All of the four theoretical plots that we have seen so far show strains for the final wound roll radius. Later in chapter III you will find various types of strain measurements were employed to validate this model. These measurements all involve attaching a strain sensor to the web and winding it into the roll. These sensors allow measurements of changes of strain from a reference level to a different level. The strain in the free web span prior to the winder has nonzero strains in both the MD and CMD due to web tension. Typically these strains were nulled or balanced electronically such that the strains that were measured were changes in strain from the free web span levels. Thus the strain recordings through time begin at zero, since they were nulled, and then increase or decrease depending on the direction they were mounted in. So, in essence a strain gage is mounted on the web which becomes a lap in the wound roll. Changes are then recorded in the strain level in that lap as additional layers are wound onto the roll. So, in order to simulate this balancing method, the strain at the depth at which the strain gage was

attached was subtracted from the strain at each successive depth. Now, the theoretical and experimental results can be plotted and compared on the same scale.

Figure 18 shows the final theoretical MD strain for the 6 inch wide web for comparison with the experimental results.

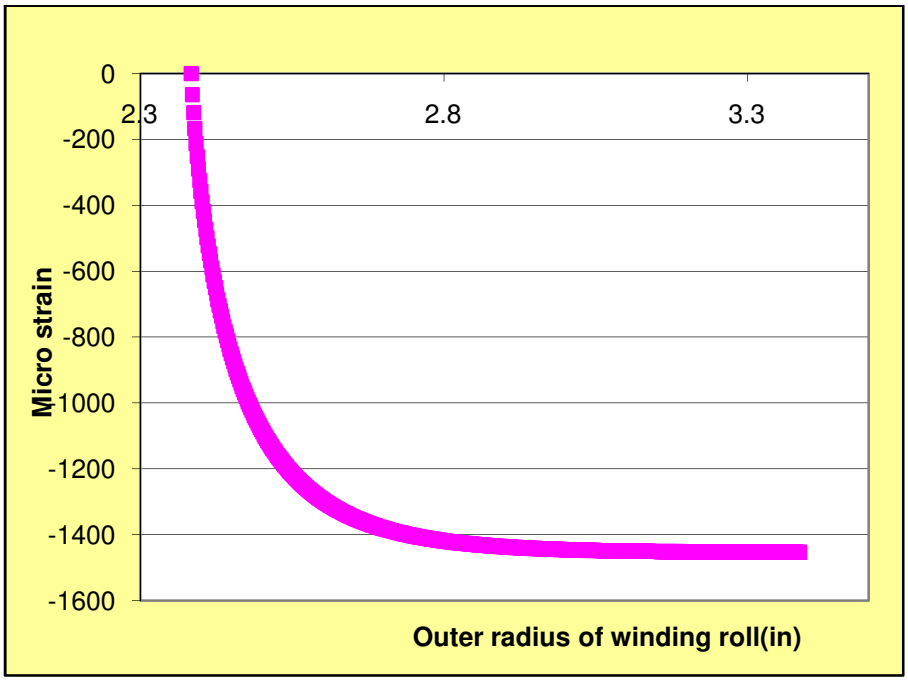

Figure 15: MD Strain for 6 inch Wide Web for Comparison with Experimental Results

Figure 19 shows the final theoretical CMD strain for the 6 inch wide web for comparison with the experimental results.

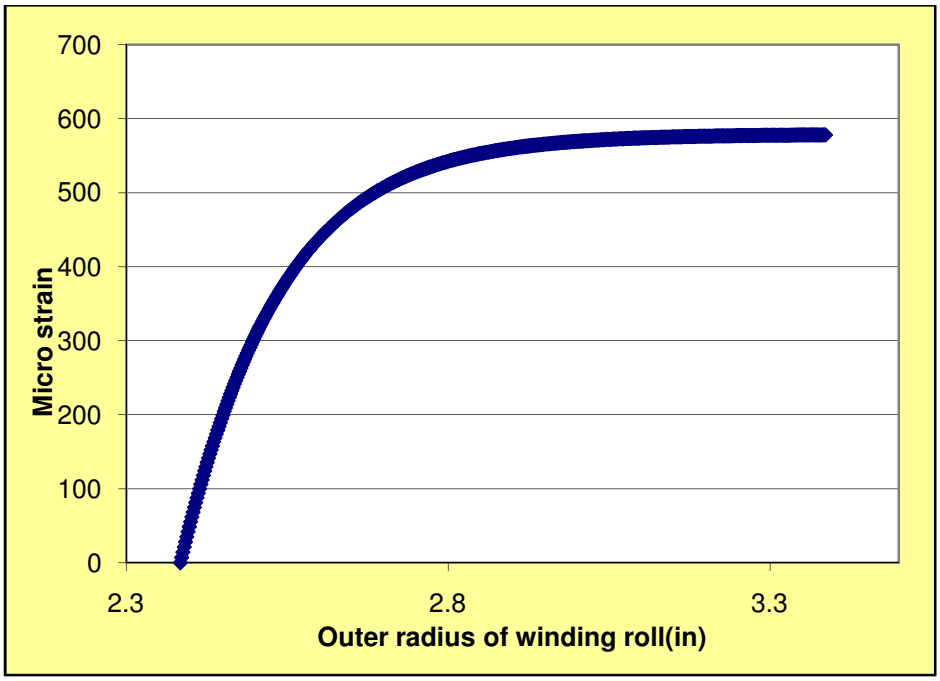

Figure 16: CMD Strain for 6 inch Wide Web for Comparison with Experimental Results

Figure 17 shows the final theoretical MD strain for the 24 inch wide web for comparison with the experimental results.

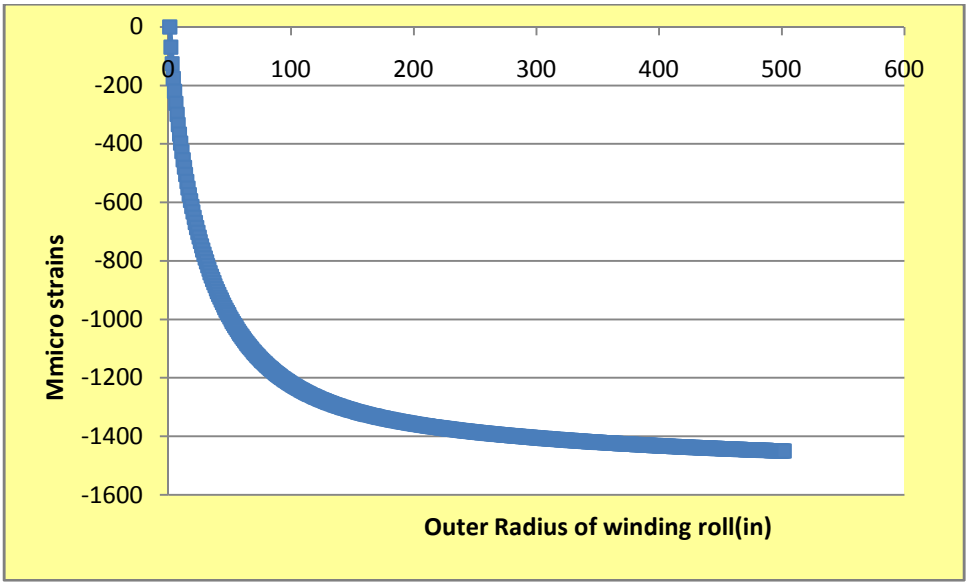

Figure 17: MD Strain for 24 inch Wide Web for Comparison with Experimental Results

Figure 18 shows the final theoretical CMD strain for the 24 inch wide web for comparison with the experimental results.

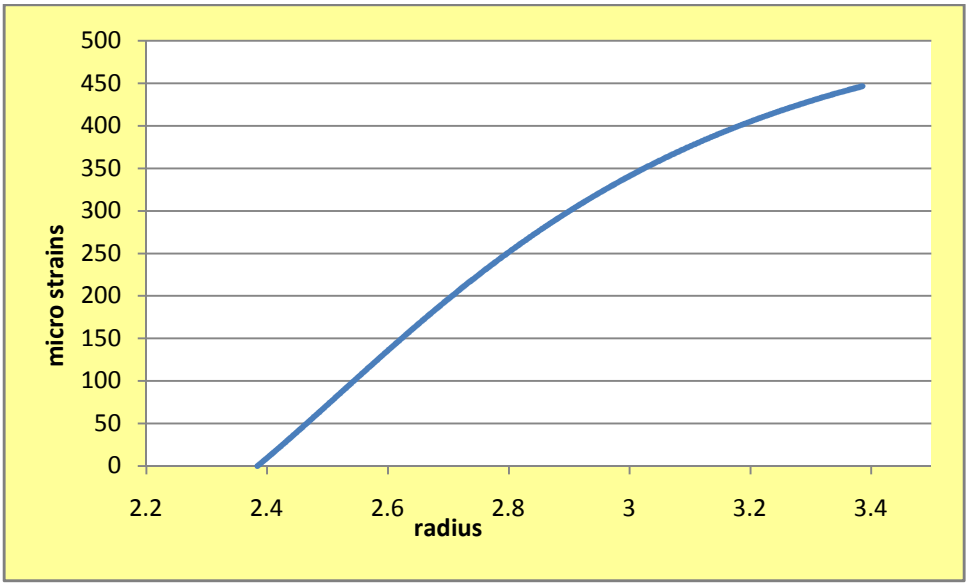

Figure 18: CMD Strain for 24 inch Wide Web for Comparison with Experimental Results

In the next chapter we shall describe the experimental procedure that was implemented to explore whether these stresses that were produced by Mollamahmutoglu's model are correct.

CHAPTER III

EXPERIMENTAL PROCEDURE

Several methods were used to measure the changes in strain in a web due to winding. Strain measurement methods are more common than stress measurements in the laboratory. At the end of chapter II a description was given of how the strain measured by a single gage in either the MD or CMD direction would be expected to vary as the roll is wound.

Preliminary stages

In order to measure the strain inside a wound roll an optical strain measurement system was first tested. This strain gage was manufactured by Direct Measurements Inc (DMI). It used a small strain gage in the form of a 2D bar code and a camera that took pictures of the strain gage, compared the picture of a certain initial time to a reference picture taken at zero strain and calculated the strain change using software. The following diagrams show a close up view of the camera and the DMI gage.

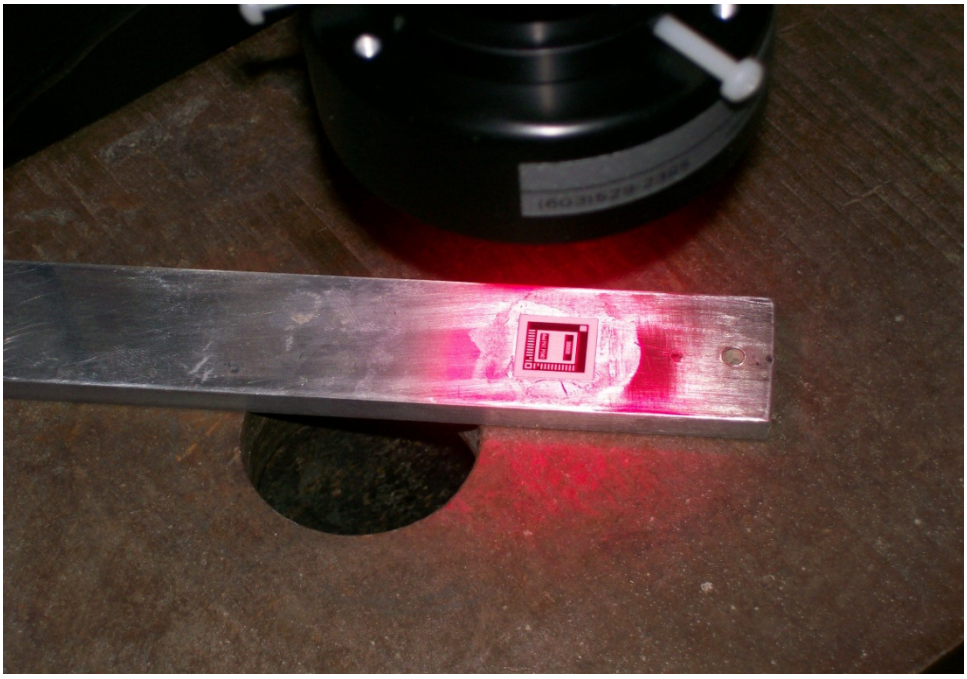

Figure 19: Close up View of the DMI Optical Strain Measuring System

.

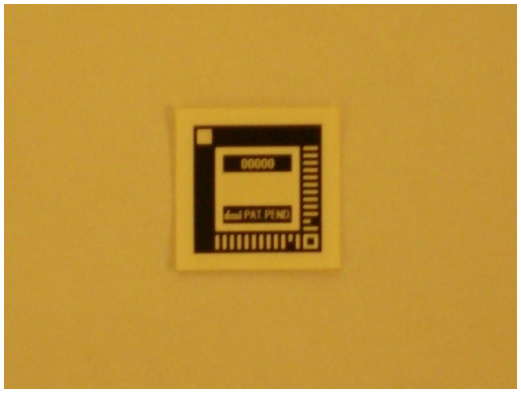

Figure 20: DMI Strain Gage

There were several difficulties faced using this system and eventually it was not used anymore. The following figure shows the comparison of DMI strain gage data with the theoretical value.

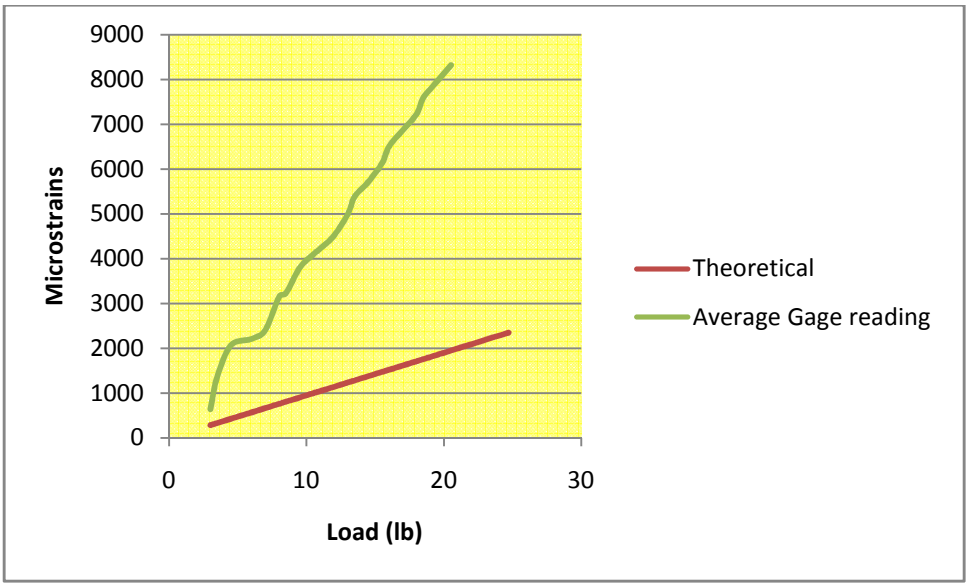

Figure 21: Comparison of DMI Strain Gage Data with Theoretical Values

These data were obtained by loading a PET coupon with dead weights. First, the weight holder was loaded and then the vertical position of the camera was adjusted to focus on the strain gage that had been mounted already. The picture of the strain gage taken by the camera at this point was used by the software as a reference image. Then weights were added and strain changes were recorded by comparing with the reference image each time. The figure shows an average of the strain readings using the DMI strain gage. From the figure we see that the DMI gage was not giving dependable outputs.

Another problem that was faced during the use of the DMI optical system was that there was considerable drift in the data. This means that, after loading the web coupon with a certain load. The reading wouldn't always stay constant at or around a certain value. Hence to find out the amount of drift in the measuring system a drift test was run. The DMI gage was mounted on a calibration bar and load was applied. The

following figure shows that strain readings or rather the change in strain readings with time for a constant load.

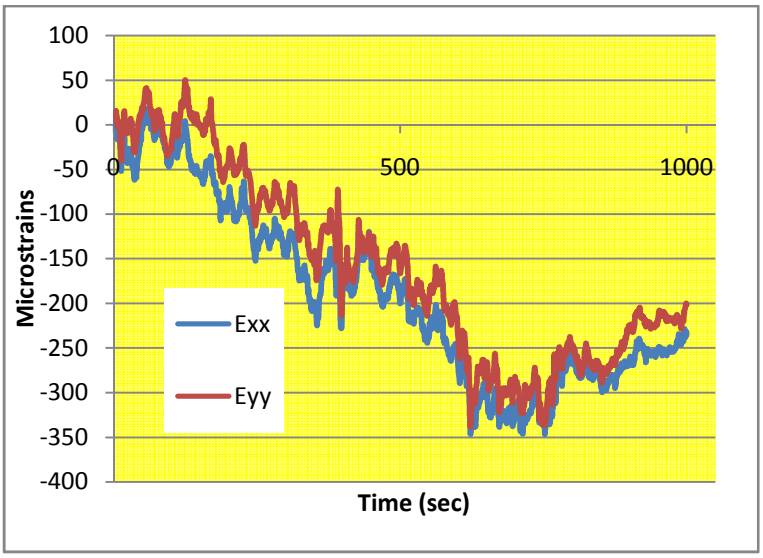

Figure 22: Drift test data.

We see that there was huge drift. This was another reason the DMI optical system wasn't used further. Electrical resistance strain gages were employed next. The details of these strain gages are given below:

4 Inch Long Single Element Gage:

This strain gage was a Micro-Measurement Precision Strain Gage. It was 4 inches long, single element. The gage had 350 ohms of resistance and a nominal gage factor of 2.20 +/- 0.5%. Figure 16 shows an example of one these strain gages.

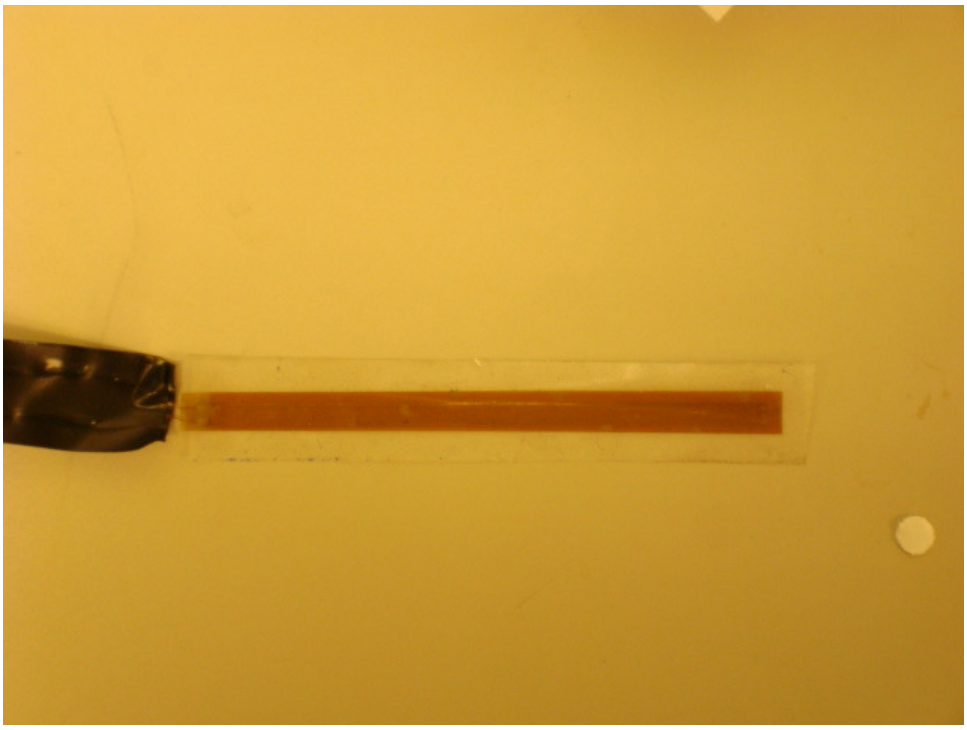

Figure 22: 4 inch Long, Single Element Strain Gage

The Rosette Gage (Dual 90 degree)

The Rosette gage used was a Micro-Measurement Precision Strain Gage (type CEA-13-250UT-350). The gage had 350 ohms of resistance and a nominal gage factor of 2.10 +/- 1.5%. The Rosette gage was actually two single element gages on a single backing that were turned 90º to one another, so that one measured CMD strain and the other measured MD strain. Figure 17 shows an example of a rosette strain gage. These gages are similar to those used by Angela Welch in a previous study [15].

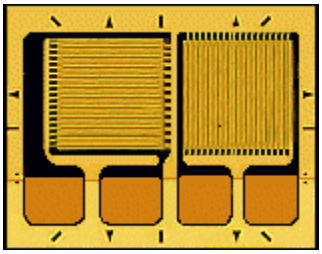

Figure 23: Rosette Strain Gage

Smaller Single element strain gage

Eventually a smaller single element strain gage was used. It was a Vishay Micro-Measurement Student Gage (type CEA-13-240UZ-120). The gage had 120 ohms of resistance and a gage factor of 2.10 +/- 0.5%. The single element gage can measure either the MD or the CMD strain at a time as opposed to the Rosette which could measure both at the same time. So, the MD and CMD strains were measured separately.

Strain gage attachment

The same method was used for attaching all of the strain gages to the web. First, the web surface was prepared. Very fine grit sand paper was used to roughen the surface so that the strain gages adhered to them well and thereby making a better connection to the web. Then the surface was cleaned using first a degreaser, then an acid, and finally a neutralizer to balance the pH of the surface. Then a catalyst was used which helps the bonding process of the adhesive which is applied subsequently. Then the strain gage was attached to the web using a cyanoacrylate, or M-Bond, adhesive. Figure 19 shows an example of the completion of the strain gage attachment.

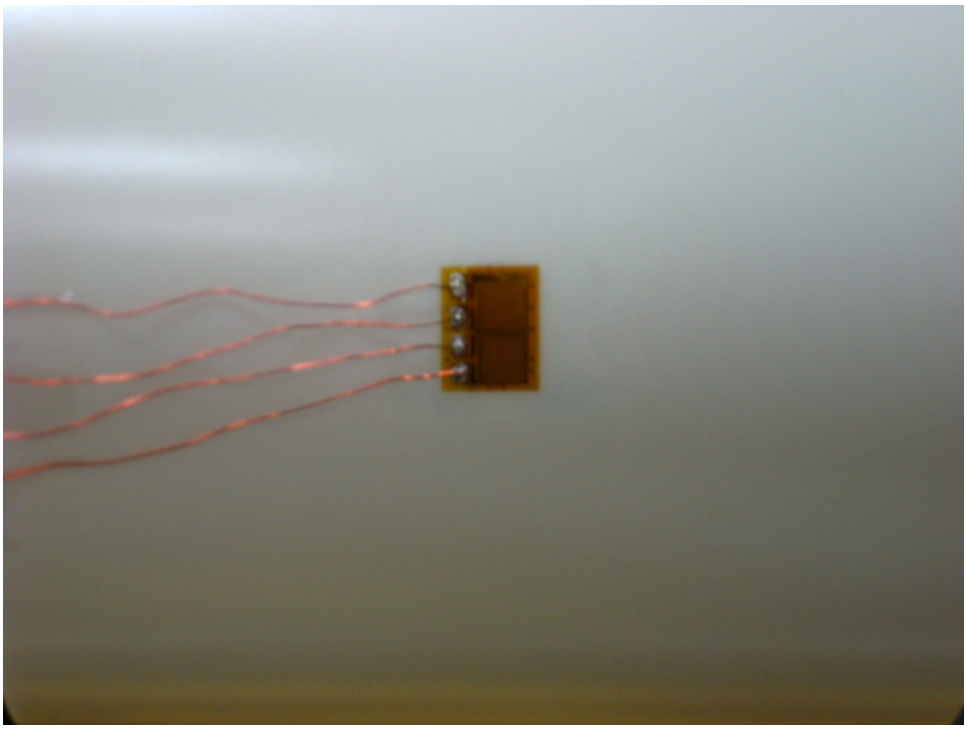

Figure 24: Attachment of Rosette to the web surface

Strain indicators

In addition to the strain indicator that came with the DMI optical strain measurement system, three types of strain indicators were used in the experimental part of this study. They are as follows:

1. A wide-range strain indicator (P3800 Measurements Group)
2. P3 Strain indicator and recorder(Measurements Group)
3. Micro Measurement Telemetry system with Agilelink software.

They are mentioned here in short.

Wide-Range Strain Indicator

A wide-range strain indicator was used during the period when the 4 inch long strain gage was being tested for use and a reinforcement factor was being estimated. These

Figure 25: Wide-Range Strain Indicator (Model 3800)

measurements were reported in units of micro-strain from the strain indicator. Figure 20 shows a picture of the wide-range strain indicator.

The P3 Strain indicator and Recorder:

A wide-range strain indicator was used during the second phase of the study to measure strains when the cantilever winder was being used for strain measurements. These measurements were reported in units of micro-strain from the strain indicator. This strain indicator could take data dynamically and at a frequency of one data point per second. It also stored the data for subsequent use. Figure 21 shows a picture of the wide-range strain indicator used in the experimental portion of the study.

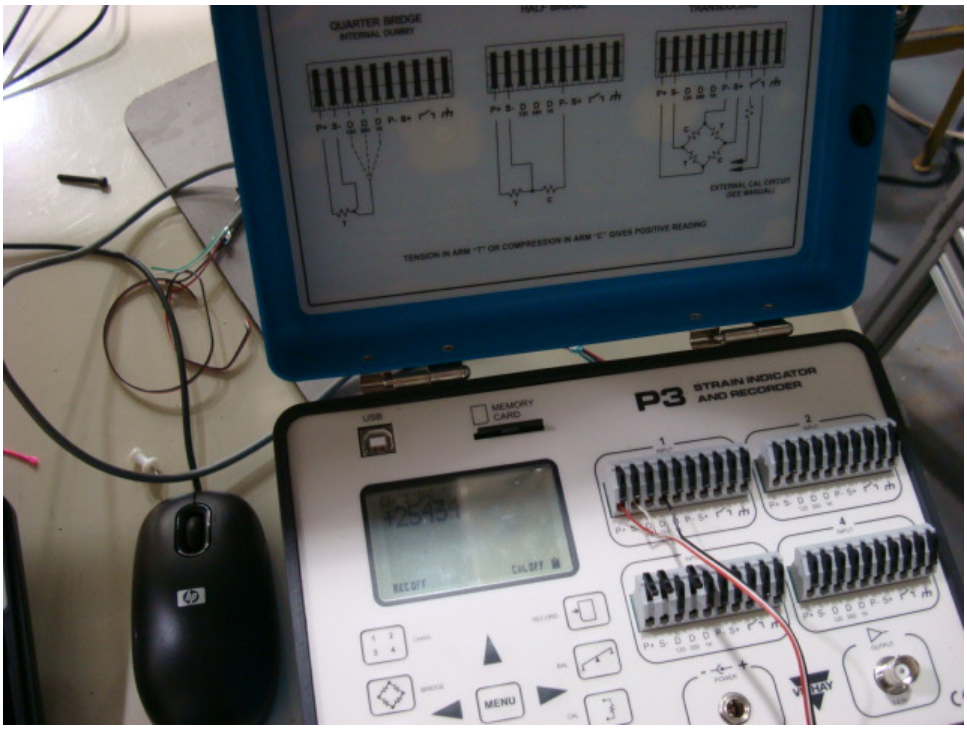

Figure 26: P3 Strain Indicator and Recorder

Micro Measurement Telemetry System with Agilelink Software.

This is the strain measurement system that was eventually used for the final portion of our study and it proved to provide the most reasonable results. It had a transmitter that was hooked up to the strain gage; a receiver that received the data from the transmitter and a software that translated the collected data into strain readings. The following figure shows the telemetry system at work.

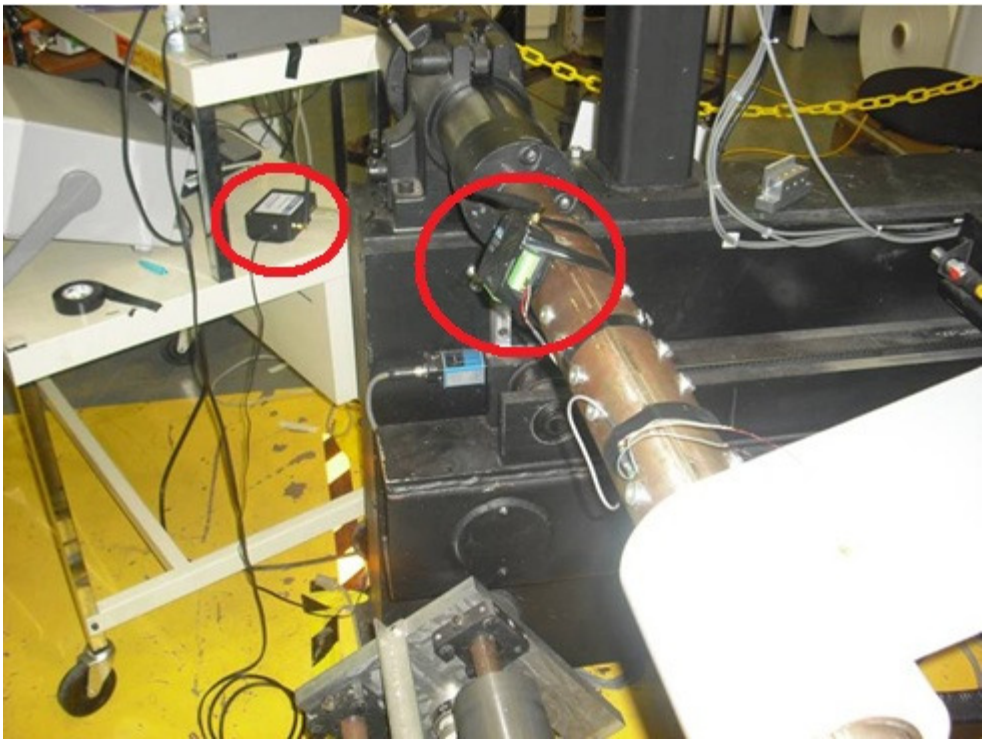

Figure 27: Micro Measurement Telemetry system

Description of Strain Measurement Using Small Scale Winder

The small scale winder was used primarily to measure CMD strains. An inch of pile height of web was wound on to the core at 20 RPM. As the small scale winder could not hold tension at zero velocity the strain gage was mounted on the web on the fly, i.e. it was stuck to the web using a double sided tape as the web was moving towards the wound roll. The applied tension was 1.33pli. As mentioned before, the P3 Strain Indicator and Recorder was being used in this experiment. One data point indicating a strain value was being recorded every second. As the web was moving towards the roll, the strain gage was attached to it on the fly. Prior to attaching the strain gage, the recorder was turned on and recording had started and the recorder was indicating the number of data points recorded. This was increasing every second by one data point. So, as soon as

the strain gage was attached to the web, the data point at which this had occurred was recorded manually by an observer. This would be considered as the point where the strain gage was inserted and hence the starting point. However, as soon as the strain gage was wound into the roll, there would be a big drop in the strain value. The onset of the drop would be considered as the point where the strain gage, along with the web, had entered the roll. As the strain gage was wound in, data was recorded and stored in the P3 strain indicator and recorder. The data that was collected is provided in the appendix. The following figure shows the data obtained by using the cantilever winder. It must be mentioned here that only the CMD strains were measured using this winder.

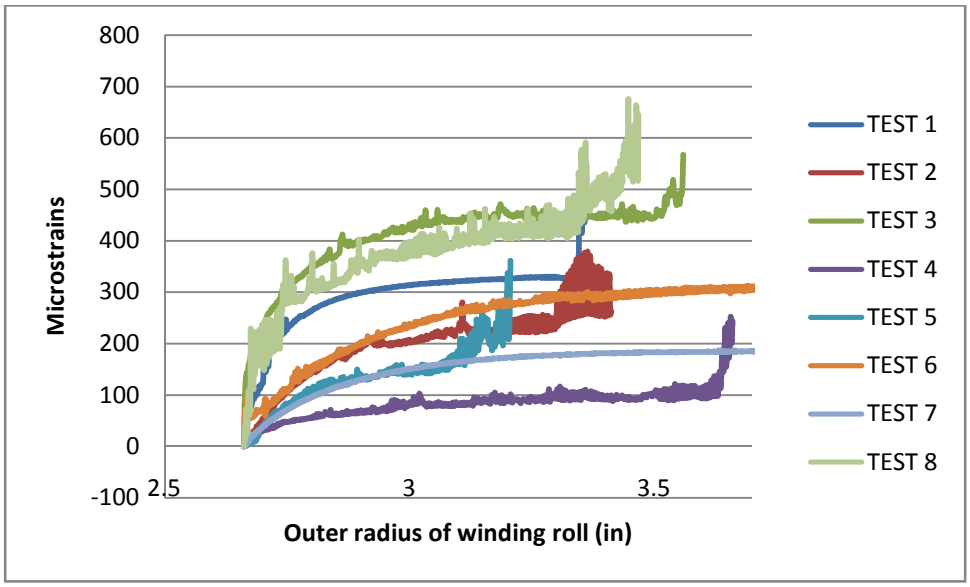

Figure 28: CMD Strains Measured Using the Cantilever Winder.

From Figure 28 we see that the repeatability was poor. Furthermore, the curves do not follow the trends of the strains produced by the model. The possible reasons behind this maybe:

- As the strain gage was attached to the web on the fly, the strain gage may not have properly adhered to the surface of the web and therefore unable to measure

strain properly.

- There may have been stress developing in the strain gages simply because of the poor attachment and the strain indicated may have been a combination of this and the strain reading from the web.
- At 20 RPM, the machine was struggling to hold web tension constant. This may have caused problems in proper winding, in that; proper tension was not being imparted in the web.

Hence, after several failed attempts at getting reasonable data from this machine and the instruments discussed the study was moved to the High Speed Web Line and a radio telemetry system was used to acquire the strain data. The high speed web line can hold tension at zero web speed which allows us to stop the web, attach a strain gage and then continue winding.

Description of Strain Measurement Using High Speed Web Line

During this part of the experimental study, the Micro Measurement Telemetry system was used. The transmitter was attached to the winding shaft and the receiver was placed at a distance and close to the computer that had the Agilelink software. Since the High Speed Web Line is capable of holding tension at zero velocity, about half an inch (pile height) of web was wound on to the core at 50 FPM and then the machine was set to run at zero velocity. The strain gage was mounted on the web using techniques discussed previously and the telemetry transmitter was connected to the strain gage by soldering copper wires to it, the other ends of which were connected to the transmitter. Then the machine was again run at 50 RPM for one more inch of pile height. Data was recorded at

1200 sweeps/second. The same process was repeated several times. The following figure shows dynamic data collection using the Agilelink software. The stair steps in the data

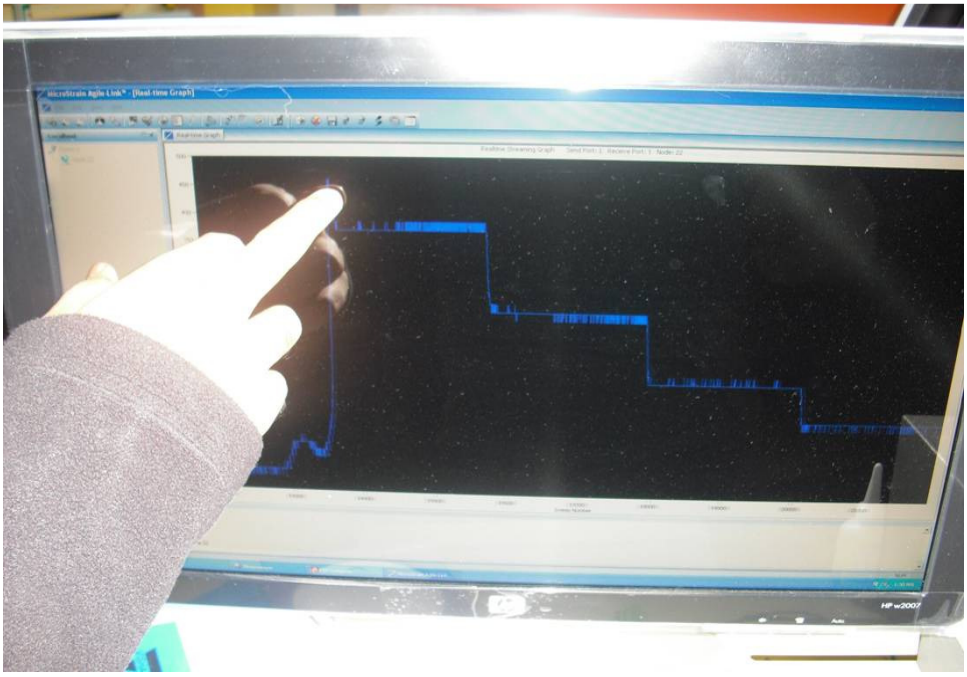

Figure 29: Dynamic Data Collection (CMD) Using Agilelink Software

Show the effect of individual laps being wound on top of the lap that was instrumented with the strain gage.

At first a Rosette strain gage was used to measure both MD and CMD strains at the same time. We failed to acquire any consistent, repeatable data and then upon further investigation of the mounting process of the strain gage we concluded that the Rosette was too big and the pressure being applied to it while it was being mounted on the web was leaving a fairly large amount of indentation on the surface of the wound roll. That is why a smaller single element gage was chosen next. This was less than 25% the size of the earlier Rosette. However, a single element gage could only measure either MD or CMD strains. So, two sets of tests were run.

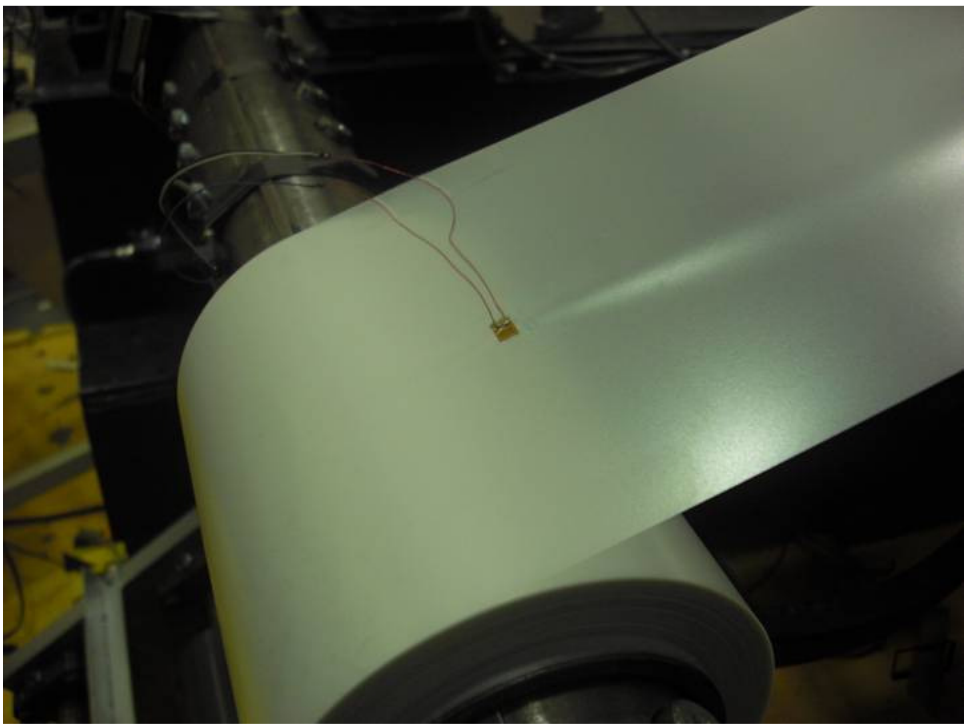

Figure 30: Strain Gage Mounted in the Span.

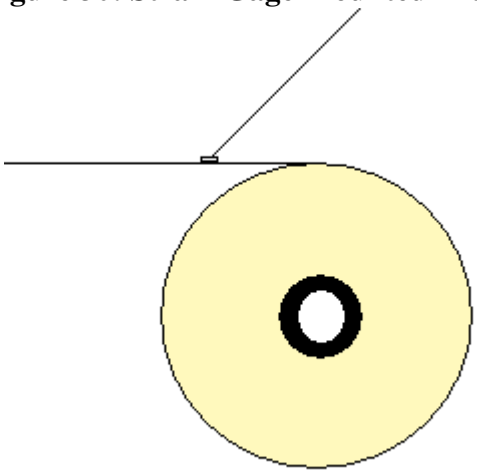

Figure 31: Mounting of Strain Gage

The strain gage was mounted on the web at two positions of the web relative to the wound roll during the testing: when the web was in the span and when it was a part of the roll. In both cases, the MD and CMD strains were measured. Now, when the strain

gage is mounted and subsequently balanced on the web span, the web and the gage move and enter the roll together. So, they bend together and as a result, a sudden change in the strain value is observed which can be interpreted as the associated bending strain. However, when the gage is mounted and balanced when the web was already wound on to the roll the bending strains cannot be seen as the balancing process had already cancelled it.

The balancing of the strain gage using the Agilink Software is done in the following way. After the strain gage is mounted on the web, the machine velocity is set at 50 FPM while maintaining web tension. So, 1000 psi of tension is being imparted on the web and hence the strain gage. Now, using the auto-balance option in the Agilink Software, the output of the strain gage was nulled.

The Agilink Software has the option of continuous data streaming which allows us to observe the change in strain values. It outputs strains as a function of sweep values. Every second, 1200 sweeps are reported to the software that contains strain data. So, in effect, we get 1200 strain indications every second. This results in a large amount of strain data. In most cases around 900000 strain values were obtained before the test concluded.

It must be mentioned that in some cases the strain gage was mounted on the free span of the web and in some cases on the outside of the roll. In the first case, the bending strains and membrane strains could be identified as the web and gage bent together. However, in the second case, the bending strains were always built-in. The first method worked well for MD strains and the second method worked well for CMD strains. This may be due to restriction of lateral movement of web layer.

CHAPTER V

EXPERIMENTAL RESULTS AND COMPARISON WITH MODEL

In this chapter the results of the experimental data are presented. Numerous tests were performed with the three different setups described in Chapter IV. Here, the results obtained by using the High Speed Machine and the Telemetry data acquisition system will be shown. A total of 28 tests are shown here.

Two different roll widths were tested; 6 inch and 24 inch wide webs. The same strain gage was used for both rolls. Now we will review the experimentally obtained data.

First, the experimental results for the 6" wide web are shown in Figure 32. The following diagram shows a total of 8 experimental readings taken for measuring the MD strains. An experimental reading consists of a test that began with the strain gage at the surface of the winding roll and completed when about ¾" of web layers had been wound onto the roll above the layer with the gage. Since the web line can be reversed, it is possible that one strain gage can be used several times. In Figure 32 the results for 8 winding tests are shown but only two 2 strain gages were used. Each gage was used for 4

winding tests. The variation in results among 4 tests using one strain gage must be due to either winding tension varying or due to balance conditions at the start of the test.

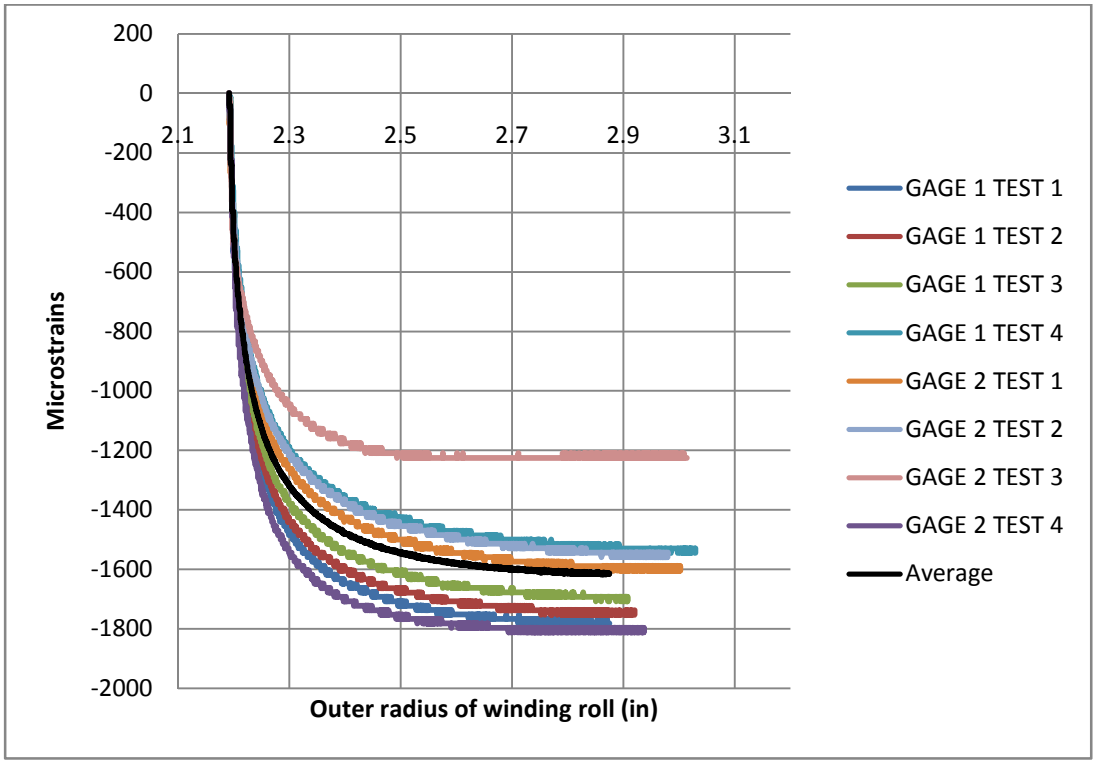

Figure 32: MD Strains in 6 inch Wide PET

Statistical analysis will be used to compare the data at 5 winding radii after the gage was inserted. The data is presented in table 3. Except for the 7th reading, the repeatability for this set of data was moderate, which is seen in Figure 32 and in

6 inch MD						
	Average	Median	St. Dev	Range	Max	Min
2.2	-490	-498	49	148	-400	-549
2.4	-1477	-1485	179	531	-1176	-1707
2.6	-1580	-1603	184	556	-1225	-1782
2.8	-1614	-1640	189	571	-1225	-1796
2.875	-1614	-1640	192	586	-1225	-1811

Table 3: Statistical Results for MD Strains in 6 inch Wide PET

Table 3. One important value to note in Table 3 is the standard deviation. The standard deviation represents the average distance of the measured strains from the mean strain value. The maximum standard deviation is 192 microstrain and the minimum standard deviation is 49 microstrain. If the results from the 7th winding are not considered, then the standard deviation and range are both significantly lowered. To do this, we apply Chauvenet's rule. The mathematical calculations for applying Chauvenet's criterion is provided in the Appendix. Applying Chauvenet's criterion we find that the standard deviation at the saturation strain drops from 192 microstrain to 120 microstrain and the range drops from 586 microstrain to 297 microstrain. Furthermore, the average saturation strain becomes -1670 microstrain.

Next, the experimental results for the CMD strain measurement of the 6wide web

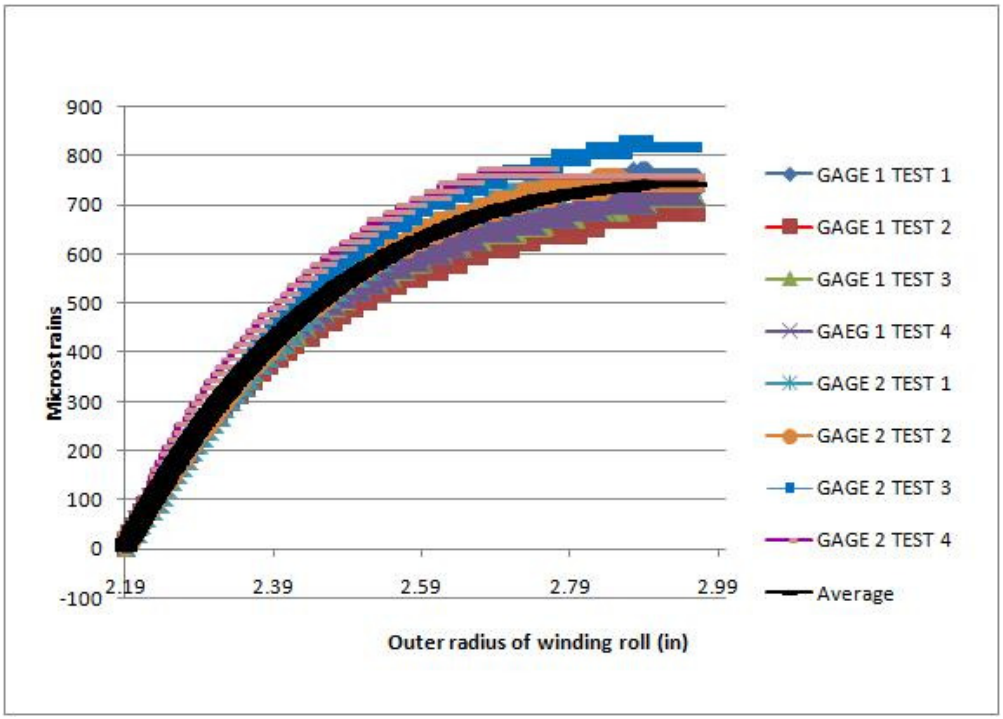

Figure 33: Experimental Readings for CMD Strains in 6 inch Wide Web

are presented. In Figure 33 we see the results of 8 winding tests accomplished using two strain gages similar to Figure 32. The CMD strains saturated at an average value of 740

Statistical analysis was performed on this data. Analysis was conducted at five different points in the depth of the strain gage in the wound roll. These results are shown in Table 4. The standard deviation was low compared to the MD data In fact it was shown in table 3 that the standard deviation at saturation was 192 microstrain which is 12% of the average for the MD data. In table 4 the standard deviation decreased to 40 out of 741 microstrain, or 5% of the average.

6 inch CMD						
	Average	**Median**	**St. Dev**	**Range**	**Max**	**Min**
2.2	31	29	5	14	44	29
2.4	434	423	33	103	504	400
2.6	634	631	51	148	712	564
2.8	720	727	44	133	787	653
2.9	740.6438	742	40	133	816	683

Table 4: Statistical Results for CMD Strains in 6 inch Wide PET

Next the MD strain data for the 24 inch wide PET is presented in Figure 34. A total of 6 readings, taken from two strain gages (3 tests each), are shown here. This set of data has a very broad range. The average MD strains saturate at -1446 microstrain.

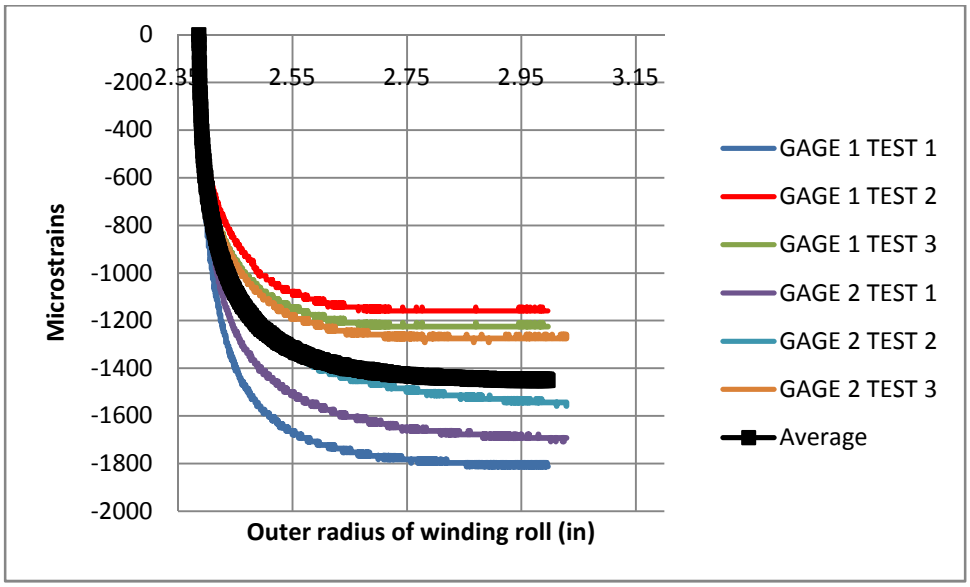

Figure 34: MD Strains in 24 inch Wide PET

The statistics for this data is shown in Table 5. The standard deviation had a minimum value of 86 microstrain and a maximum value of 266 microstrain. Although the standard deviation for the data in Table 5 is high it is comparable to that of the MD data for the 6" wide roll presented in Table 3.

24 inch MD						
	Average	Median	St. Dev	Range	Max	Min
2.4	-643	-620	86	247	-539	-787
2.6	-1370	-1370	233	595	-1127	-1722
2.75	-1426	-1426	252	621	-1160	-1782
2.9	-1446	-1446	266	651	-1160	-1811

Table 5: Statistical Results for MD Strains in 24 inch Wide PET

Next, the experimental CMD strain data for the 24 inch wide PET is presented. 6 winding tests were completed using 2 strain gage installations. These reading are fairly repeatable.

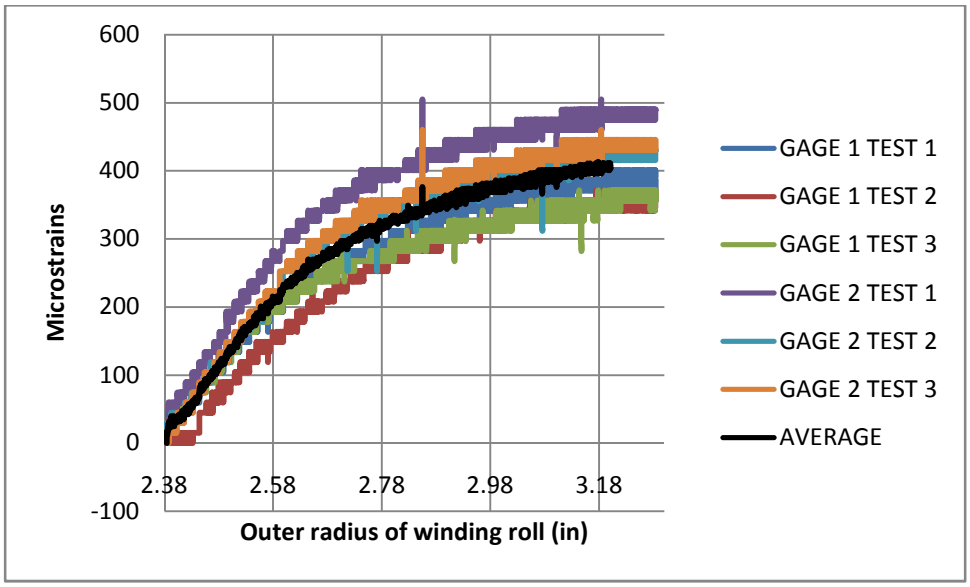

Figure 35: CMD Strains in 24 inch Wide PET

The statistical analysis of this data is presented in table 6. The standard deviation was comparable in magnitude to the CMD data for the 6" wide roll presented in table 4 although the magnitudes of the averages have decreased by factor of 2.

24 inch CMD						
Outer Radius(in)	**Average**	**Median**	**St. Dev**	**Range**	**Max**	**Min**
2.4	29	29	19	59	59	0
2.6	232	232	41	133	297	163
2.75	309	309	46	133	386	252
2.9	348	348	40	118	415	297
3.05	388	388	55	148	475	326

Table 6: Statistical Results for CMD Strains in 24 inch Wide PET

In the next section we compare the experimentally obtained data with the model outputs. But before that, a few things have to be mentioned about the tremendous spread in the data.

- The installation of the strain gage has a huge effect on the data obtained. The backing of the strain gage is as thick as the material itself. As a result, the installation of the strain gage on the web surface causes some degree of reinforcement. Cyanoacrolyte is used as adhesive to mount the strain gage and that has its own properties which have significant effort on the measured strain.
- The strain gage is mounted in a flat state on the web surface. However, it does not remain flat after several laps of winding. This probably has some effect on the strain measurement.
- After each winding experiment, the gage reading is balanced in the same way. But still, the difference in the data suggests that there are some things that are still in the dark, as far as balancing is concerned.
- The copper wires that are attached to the strain gage have a telling effect in case of the 24" PET as copper wires of more than a foot of length is used. The sharp spikes that we see in some of the experimental results are probably due to the copper wires rubbing against each other and in the process removing the varnish that is used as an insulator.
- We've seen that if the copper wires are even slightly taut, the results obtained are very different from the ones in which they are loose and not very taut.

So, all of these things factor in when strain readings are taken. Therefore, it can be said that the experimental process as a whole has a great effect on the quality and dependability on the data obtained.

Comparison with Mollamahmutoglu's model:

In this section we compare the experimentally obtained data with the model results. The average of the experimental results shall be compared to the model output so that an average comparison can be made. Figure 37 shows a comparison of the experimentally obtained MD strains for the 6 inch PET with the model output. In the figure, the average MD strains also have standard deviation bars (yellow). We see that the average of the MD strains were quite close to the model output in the sense that the model output (specially the saturation region) falls in the area encompassed by the standard deviation of the experimental results. At the saturation strain the percent

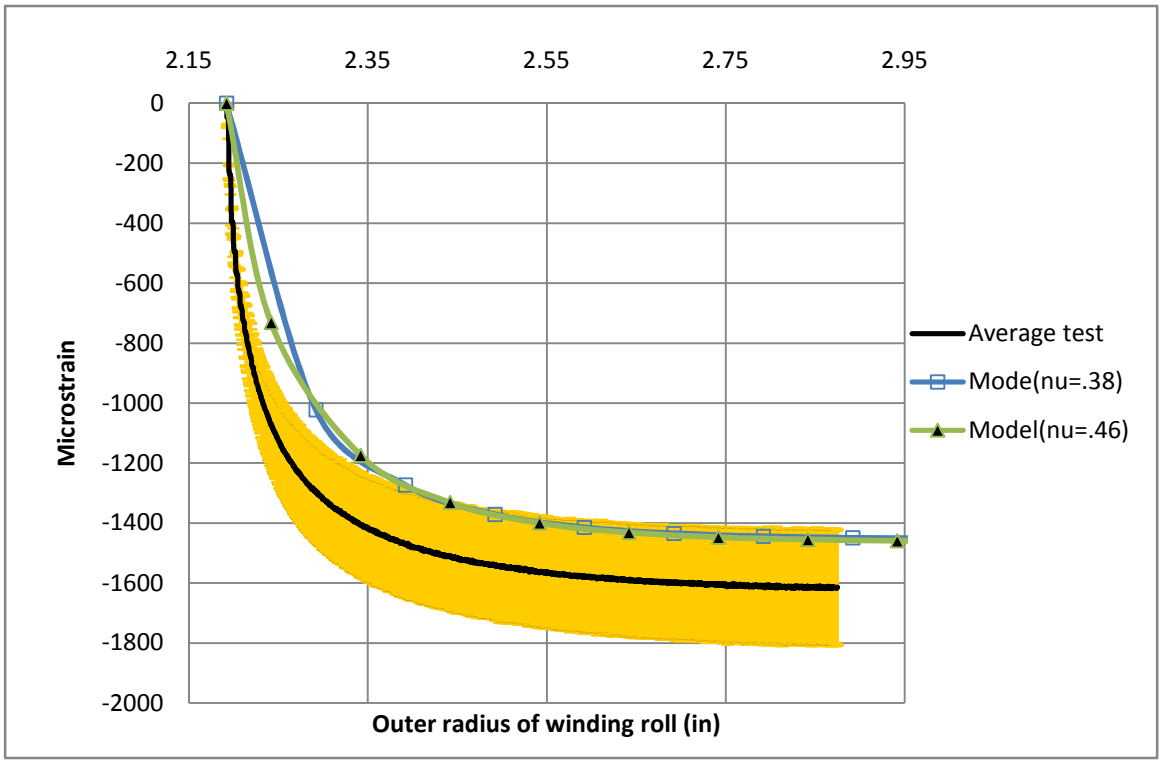

Figure 37: Comparison of Model Output with Averaged Experimental MD Strains for 6 inch Web.

difference between the average of the experimental values and the model output is 11%. The comparison between the CMD strains for the 6 inch PET and the model output is shown in Figure 38. At the saturation strain the difference between the average experimental strain and the model output is 26% of the model output. The experimental strains and the model output have the same contour and values for about 0.2 inches of pile height. However, the model strains then start to saturate whereas the experimental strains still keep increasing. This results in a difference of about 160 microstrain at saturation. In Figure 38 we see that the average of the CMD test strain saturates at about 750 microstrain. In Figure 37 the average of the MD test strain saturates at about -1625 microstrain. If this roll was narrow enough to achieve plane stress condition we could

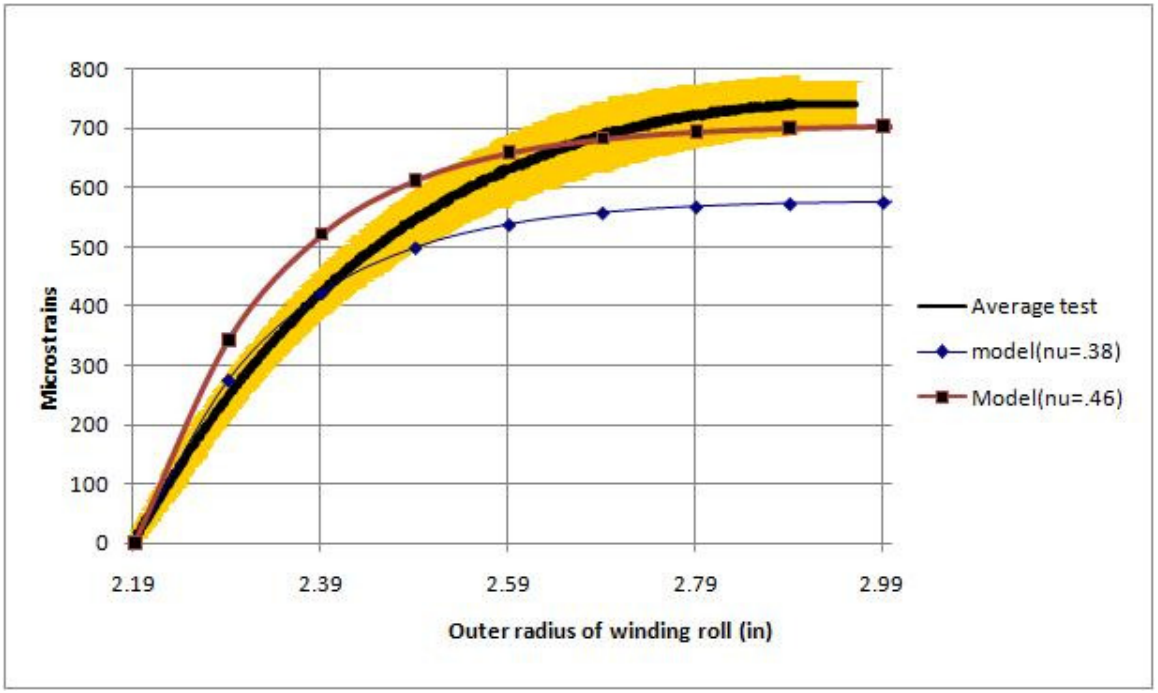

Figure 38: Comparison of Model Output with Averaged Experimental CMD Strains for 6 inch Web.

infer from the test data that Poissons ratio in the theta-z plane becomes –(750/-1625) = .46. A model result is also shown in which nu theta-z was set to .46 rather than the .38 value stated earlier.

Next, we look at the average MD strains in comparison with the model outputs. We see that the average MD strains for the 24 inch PET is fairly close to the model results. Although the average of the experimental results and the model output don't have the same contour, the model results fall in the area encompassed by the range of the experimental data. Furthermore, at saturation strain, the difference between the two are just 3%. Again, model results were produced for both a $\nu_{\theta z}$ set to .38 and .46.

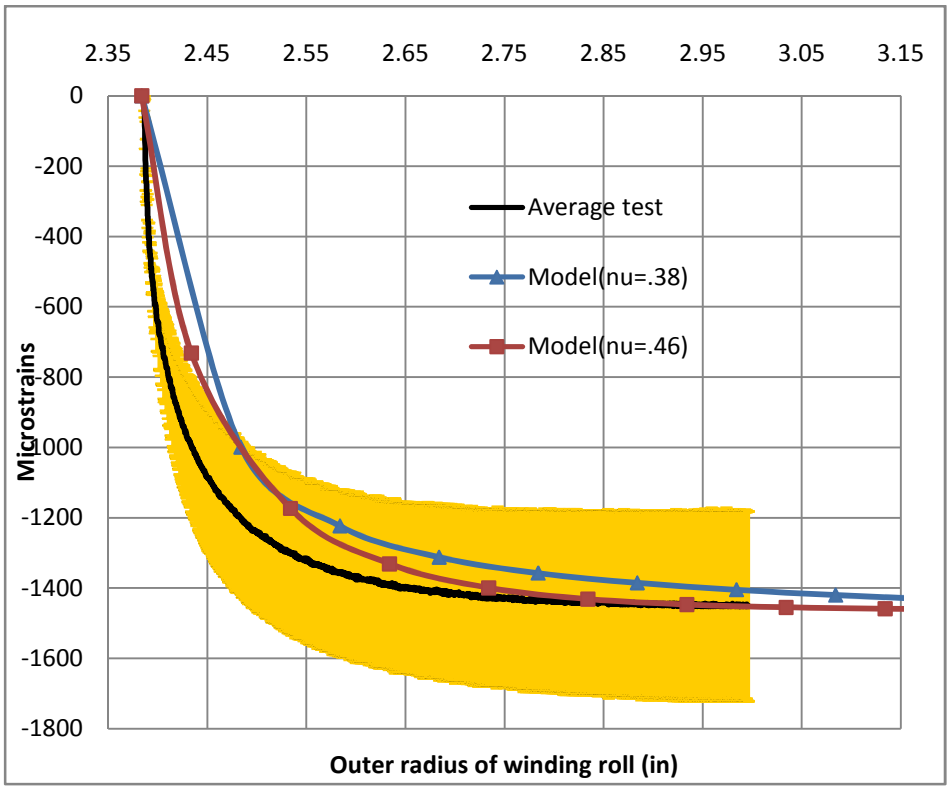

Figure 39: Comparison of Averaged Experimental MD Strain Data with Model for the 24 inch Web.

Next we compare the average of the experimental data of the CMD strains for the 24 inch PET with the model output in Figure 40. We see that the contour of the average of the experimental data is very different from that of the model output. The experimental strains start saturating after 0.8 inches of pile height. But, the model output ($\nu_{\theta z}$=.38) still

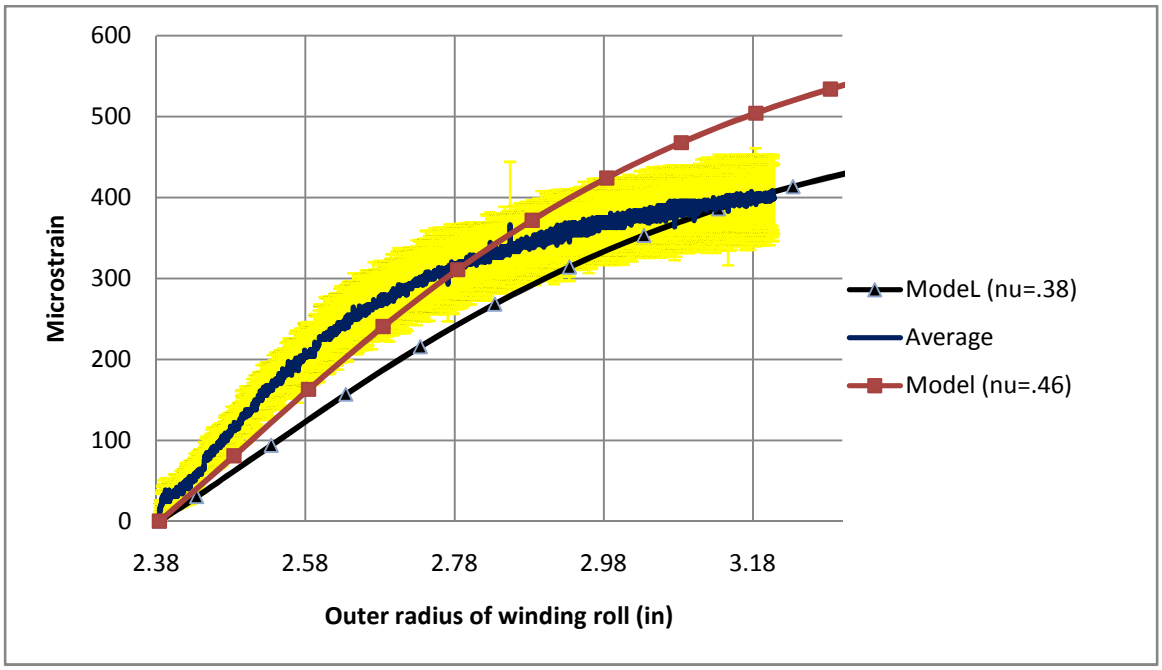

Figure 40: Comparison of average of experimental data with model for the 24 inch PET

increases at that point, and almost linearly. The model results for the higher Poisson's ratio ($\nu_{\theta z}$=.46) falls closer to the test data but as seen, the character of the test curve is still much different.

Comparison with Angela Welch's study:

Now we compare our experimentally obtained data and model output with a previous set of experimental data obtained by Welch [15]. There was one notable

difference with this study. Welch used the Rosette strain gage in her experiments and in this study a much smaller gage was used as mentioned before.

The next four figures show comparison of the data obtained in this study, Mollamahmutoglu's model output and Angela Welch's experimental data. It must be mentioned here that in her work, Welch compared the median of her data to the model she was using. So, the medians of her data are presented here. The following figure shows a comparison of the MD strains in the 6 inch wide PET.

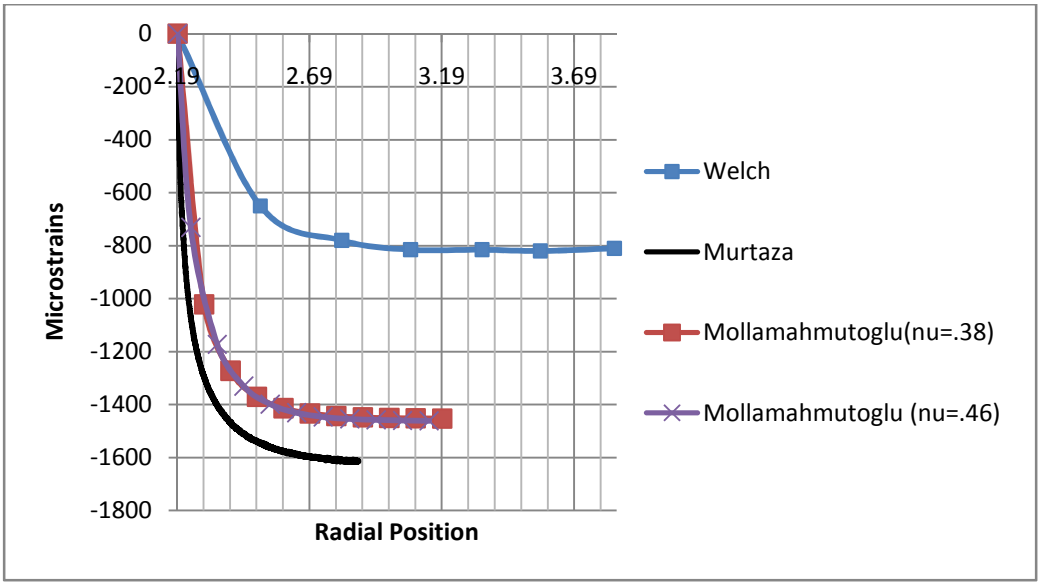

Figure 41: Comparison of MD Strains in 6 inch PET

We see that the Murtaza and Mollamahmutoglu MD strains are significantly larger than the Welch MD strains and saturate at a much larger strain value. The saturation MD strain in Welch's study is -817 microstrain. The saturation MD strain in this study is -1614.4 microstrain and form Mollamahmutoglu's model is -1453.56 microstrain.

The next figure shows a comparison of the CMD strains in the 6 inch PET. Similar behavior to the one seen for the MD strains is seen in the comparison of the CMD strains as in the saturation value for the Welch CMD strains is much lower than the ones

in this study. The saturation value for the Welch strains is less than 50% of the Model strains and less than 70% of the strains derived experimentally in this study.

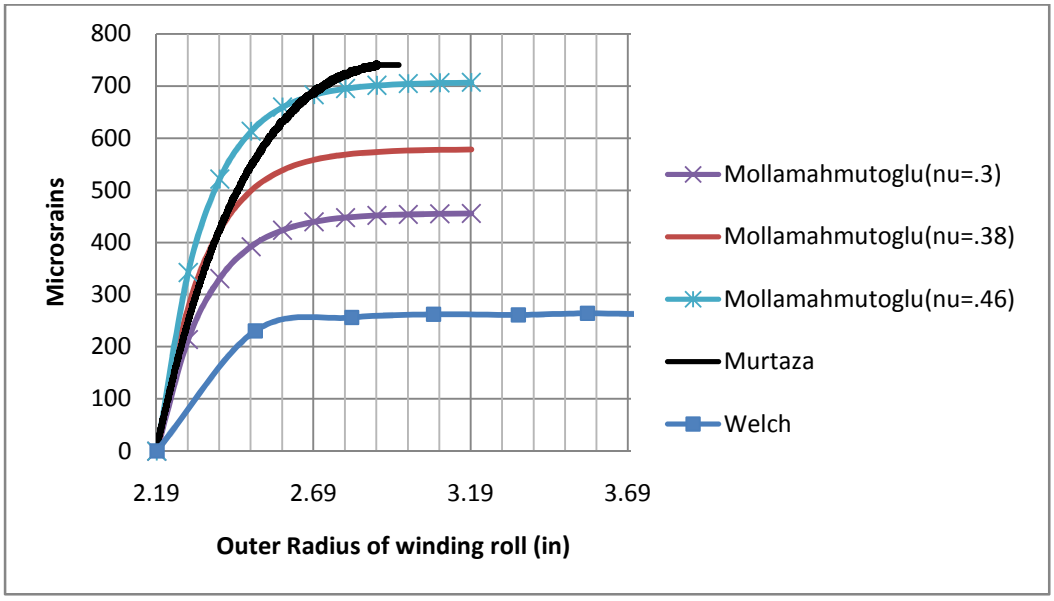

Figure 42: Comparison of CMD Strains in 6 inch PET

The next figure shows a comparison of the MD strains in the 24 inch PET. Similar behavior to the ones seen for the MD strains in the 6 inch wide PET is seen here.

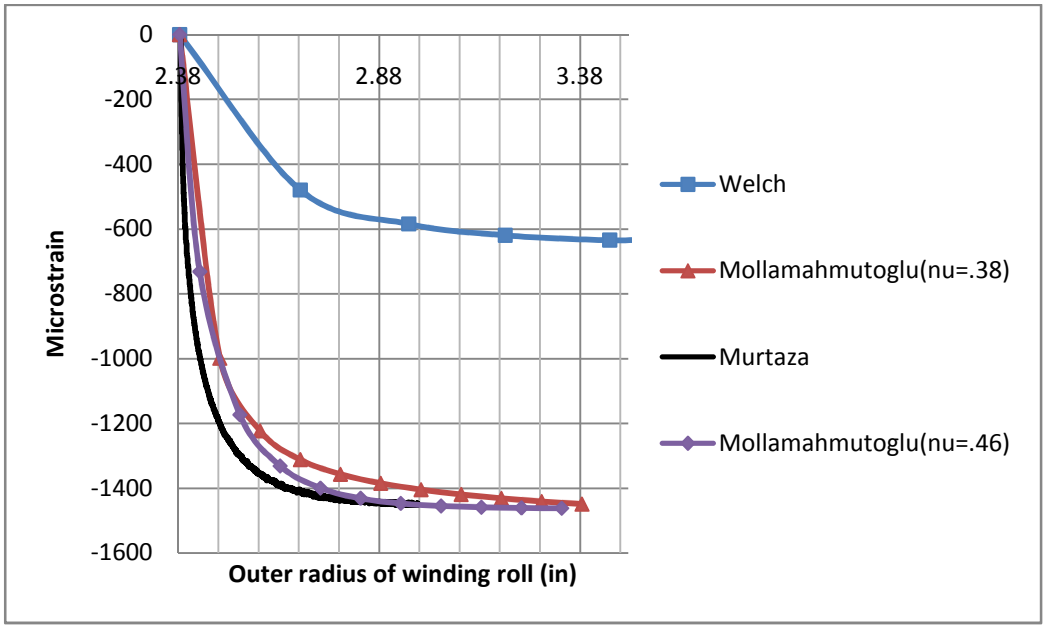

Figure 43: Comparison of MD Strains in the 24 inch PET

The next figure shows a comparison of the CMD strains in the 24 inch PET. Similar behavior to the one seen in the comparison of the 6 inch PET CMD stains is seen here. However, we see that the contour of the Mollamahmutoglu, in the initial stages is

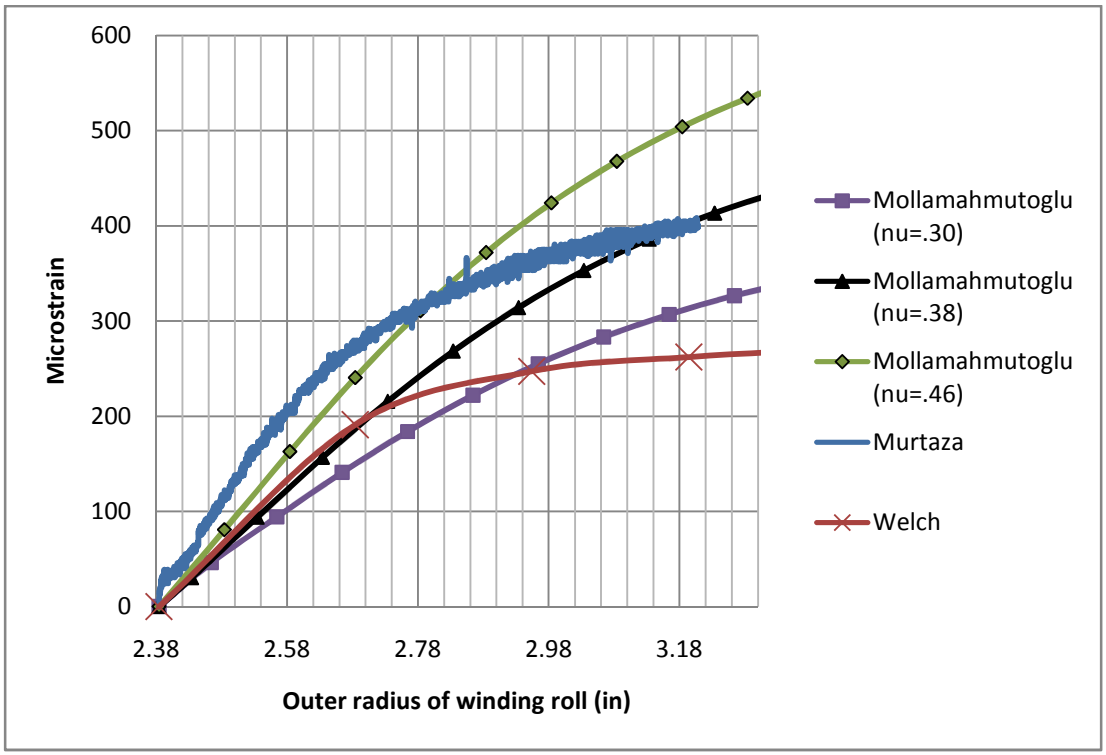

Figure 44: Comparison of CMD Strains in the 24 inch PET

Close to the Welch strains, but rises almost linearly and does not saturate while the Welch strains saturate at 270 microstrain.

We have seen that there is great difference between the data obtained experimentally in the two studies although the same material and testing conditions were used in that, the same tension applied and machine run at same speed etc. However, there are two major differences in the data collection technique. In this study data was collected using a telemetry system and therefore continuously. On the other hand, in Welch's study in order to take the strain reading at a certain depth of the roll, the machine would be stopped and the copper wires reattached every time. This may have been

responsible for the large difference between the data obtained in the two studies. Furthermore, in her experimentation she used a Rosette, while in this study a much smaller strain gage was used. The backing of the strain gage has a significant effect on the measured strain value. Hence, a larger strain gage means more reinforcement of the web and therefore smaller strains. As mentioned in Chapter IV, in the initial stages of this study a Rosette was used for measurement of strain. So, we now compare the data obtained using the Rosette gage with Welch's results.

Figure 45 shows the data obtained for the MD strains using the Rosette gage in both studies. One thing must be mentioned here, and that is in her study Welch used a much bigger strain gage compared to the one used in this study. Now, in te following figure we see that using the Rosette gage yielded lower saturation strains in this

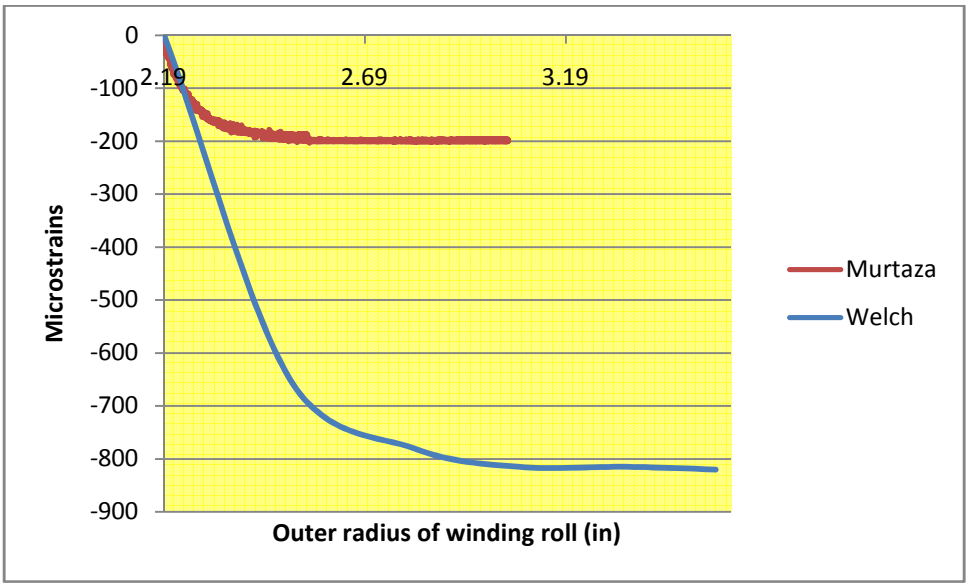

Figure 45: Comparison of MD strains for the 6" PET using Rosette gage

study. Figure 46 shows the data obtained for the CMD strains using the Rosette gage in both studies. Again we see that using the Rosette gage resulted in a much smaller saturation strain in this study.

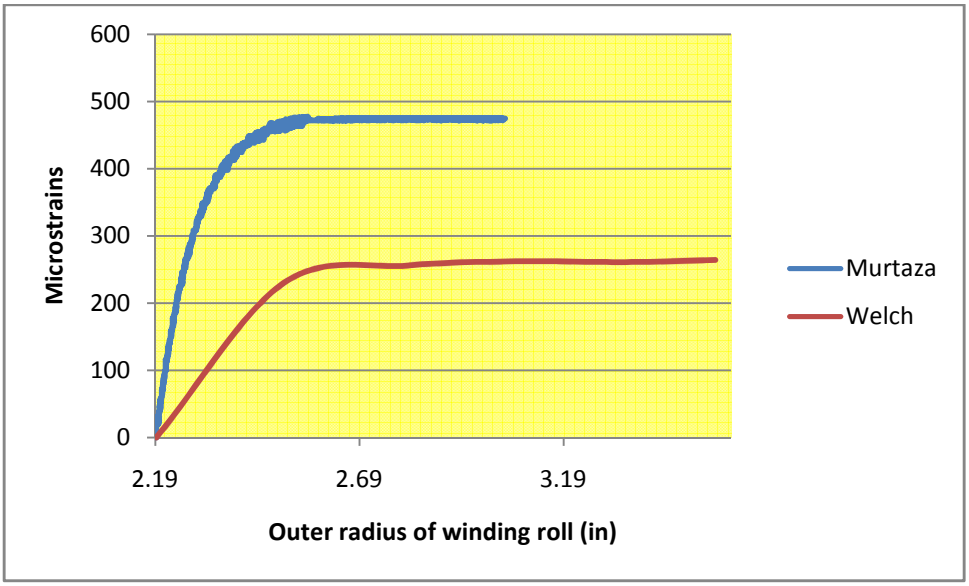

Figure 46: Comparison of CMD strains for the 6" PET using Rosette gage

Although the results are still not comparable, it can be said that it is evident that using the Rosette has resulted in lower saturation strain. Therefore, we can say that the backing of the larger strain gage (Rosette), as opposed to the smaller strain gage used in eventually in this study, had reinforced the web and this resulted in smaller strains.

CHAPTER V

CONCLUSIONS

From the comparisons between experimental data and model output in this study we can conclude that the model is able to predict the MD strains for both the 6 inch and 24 inch web. This is evident from observation of Figures 37 and 39 where we see that the range of the experimental MD strains encompasses the model output. In case of the CMD strains the model fails to predict correctly in two different ways. From Figure 42 we see that there is agreement in the CMD strains for the 6 inch web with the model for the first 200-220 laps of winding. But after that the CMD strains saturate at a much higher (approximately 170 microstrain higher) level. In case of the CMD strains of the 24 inch web, the contour of the model output is entirely different from the experimental results (Figure 44). Although the experimental strains tend to saturate on an average around 410 microstrain, the model output keeps on increasing almost linearly. So, there is not enough agreement between the experimental and model output to say that the model is able to predict the CMD strains with any accuracy.

The value of Poisson's ratio $\nu_{\theta z}$ is a very significant factor in the prediction of CMD strains using Mollamahmutoglu's model. This is evident from Figures 42 and 44 where we compare the CMD strains using $\nu_{\theta z} = .3$, .38 and .46. We see that the CMD

strains increase with an increase in the value of $\nu_{\theta z}$. A higher $\nu_{\theta z}$ results in a model output which is closer to the test data.

There is a great deal of variation in the experimental results which appears to depend on the experimental method. From Figures 36 through 39 we observed that the standard deviation in the saturation value of the experimental strains were very high. For the MD and CMD strains for the 6 inch wide roll it was more than 11% and 8% respectively. For the MD and CMD strains for the 24 inch wide roll it was more than 18% and 10% respectively. This is indeed a huge variation. Furthermore, comparison with Angela Welch's data shows that a different experimental technique adapted in this study resulted in almost double MD and CMD strains.

Future Work:

It is evident that experimental techniques play a big role in the determination of strain. More accurate and dependable experimental methods need to be devised in order to accurately measure strain in wound rolls. Temperature effects need to be accounted for as heat is produced when the strain gage is acquiring data.

In this study we focused on the center winding of a PET film at 0.002 inches thick and at two different widths – 6" and 24". To further validate the model, testing of other materials at different widths and thicknesses would be a good idea. Mollamahmutoglu's models are still in development; Poisson's ratio ($\nu_{\theta z}$) has shown to be a sensitive parameter. But Mollamahmutoglu is also investigating allowing slippage between layers of the winding roll which also may be important in producing better agreement between model and tests.

REFERENCES

1. Hakiel, Z., "Nonlinear Model for Wound Roll Stresses," *Tappi Journal*, Vol. 70, No. 5, May 1987.
2. Pfeiffer, J. D., "Internal Pressures in a Wound Roll," *Tappi Journal*, Vol. 49, No. 8, August 1966.
3. Cole, K. A. and Z. Hekiel, "A Nonlinear Wound Roll Stress Model Accounting for Widthwise Web Thickness Nonuniformities," *AMD*, Vol. 149, 1992.
4. Hoffecker, P. and Good, J. K., "An Axisymmetric Finite Element Model for Center Winding Webs," *Proceedings of the Eighth International Conference on Web Handling*, 2005.
5. Altmann, H. C., "Formulas for Computing the Stresses in Center-Wound Rolls," *Tappi Journal,* Vol. 51, No. 4, April 1968.
6. Yagoda, H. P., "Integral Formulas for Wound Rolls," *Mechanics Research Communications*, Vol. 7, No. 2, 1980.
7. Boutaghou, Z. E. and Chase, T. R., "Formulas for Generating Prescribed Residual Stress Distributions in Center Wound Rolls," *ASME Journal of Applied Mechanics*, Vol. 58, September 1991.
8. Willett, M.S. and Poesch, W. L., "Determining the Stress Distributions in Wound Reels of Magnetic Tape Using a Nonlinear Finite-Difference Approach," *Journal of Applied Mechanics*, Vol. 55, June 1988.

9. Mollamahmutoglu, C, “A Novel Algorithm for Predicting Internal Stresses in 2D Axis-symmetrical Wound Roll Models”. Jan, 2007.
10. Lee, Y. M. and J. A. Wickert, “Stress Field in Finite Width Axisymmetric Wound Rolls,” *Transactions of the ASME*, Vol. 69, March 2002.
11. Hoffecker, P. and Good, J. K., “An Axisymmetric Finite Element Model for Center Winding Webs,” *Proceedings of the Eighth International Conference on Web Handling*, 2005.
12. Kedl, D. M., “Using a Two Dimensional Winding Model to Predict Wound Roll Stresses that Occur Due to Circumferential Steps in Core Diameter or to Cross-Web Caliper Variation,” *Proceedings of the First International Conference on Web Handling*, May 1991.
13. Bathe K.J. “Finite Element Procedures”, Prentice-Hall inc. 1996.
14. Hoffeceker P. “Analysis of Nip Impinged Three Dimensional Wound Roll”, PhD Dissertation, Oklahoma State University, May 2006.
15. Angela De’on Welch, “Study On The Development Of Axial Stresses in Wound Rolls”, Master’s Thesis, December 2006.
16. Good, J. K., “Winding and Unwinding Webs: A Review of the State of Science in 2005,” *Proceedings of the Eighth International Conference on Web Handling*, June 2005.
17. Srinivasan Ganapathi, “Diametral Compression of Wound Rolls \with State Dependent Properties”, Master’s Thesis, December 2007.
18. J. Beisel and Good, J. K., “Buckling of Orthotropic Webs in Process Machinery.” *Proceedings of the Seventh International Conference on Web Handling*, 2003.

19. DuPont Teijin Films, “Product Information: Mylar Polyester Films”, June 2003.

APPENDIX

Test data for CMD strains in 6” wide PET

Gage 1

Outer radius	Test 1	Test 2	Test 3	Test 4
2.19200121	0	0	0	0
2.195023046	14.85	14.85	14.85	14.85
2.198040729	14.85	29.7	29.7	14.85
2.201054277	29.7	29.7	29.7	44.55
2.204063707	29.7	44.55	44.55	44.55
2.207069035	44.55	44.55	44.55	59.4
2.210070279	59.4	59.4	59.4	59.4
2.213067453	74.25	59.4	59.4	74.25
2.216060577	74.25	74.25	74.25	74.25
2.219049664	74.25	74.25	74.25	74.25
2.222034733	74.25	89.1	89.1	89.1
2.225015799	89.1	89.1	103.95	89.1
2.227992878	103.95	89.1	103.95	103.95
2.230965985	103.95	103.95	118.8	103.95
2.233935138	118.8	103.95	118.8	118.8
2.236900352	118.8	118.8	118.8	118.8
2.239861641	118.8	118.8	133.65	133.65
2.242819023	118.8	133.65	148.5	133.65
2.245772512	133.65	133.65	148.5	148.5
2.248722123	163.35	133.65	163.35	148.5
2.251667872	163.35	148.5	163.35	163.35
2.254609775	163.35	163.35	163.35	163.35
2.257547845	178.2	163.35	178.2	163.35
2.260482098	193.05	178.2	178.2	178.2
2.263412549	193.05	178.2	178.2	178.2
2.266339212	207.9	193.05	193.05	193.05
2.269262103	207.9	193.05	207.9	193.05
2.272181235	222.75	193.05	207.9	207.9

2.275096623	222.75	193.05	222.75	207.9
2.278008282	222.75	207.9	222.75	222.75
2.280916226	237.6	207.9	222.75	222.75
2.283820469	252.45	207.9	222.75	237.6
2.286721025	252.45	222.75	237.6	237.6
2.289617908	267.3	222.75	237.6	237.6
2.292511132	267.3	237.6	237.6	252.45
2.29540071	267.3	237.6	252.45	252.45
2.298286658	267.3	252.45	252.45	252.45
2.301168987	267.3	252.45	267.3	267.3
2.304047713	267.3	252.45	267.3	267.3
2.306922848	282.15	267.3	267.3	282.15
2.309794405	282.15	267.3	282.15	282.15
2.312662398	282.15	267.3	282.15	282.15
2.315526841	297	282.15	297	297
2.318387746	297	282.15	297	297
2.321245127	311.85	297	297	297
2.324098996	311.85	297	311.85	297
2.326949367	311.85	297	311.85	311.85
2.329796251	326.7	311.85	311.85	311.85
2.332639663	326.7	311.85	326.7	311.85
2.335479615	326.7	311.85	326.7	326.7
2.338316118	341.55	326.7	341.55	326.7
2.341149187	341.55	311.85	341.55	341.55
2.343978833	341.55	326.7	341.55	341.55
2.346805068	356.4	326.7	341.55	341.55
2.349627905	356.4	326.7	356.4	341.55
2.352447357	371.25	326.7	356.4	356.4
2.355263435	371.25	341.55	356.4	356.4
2.358076151	371.25	341.55	356.4	356.4
2.360885517	386.1	341.55	356.4	356.4
2.363691546	386.1	356.4	371.25	371.25
2.366494249	386.1	356.4	371.25	371.25
2.369293638	386.1	356.4	371.25	371.25
2.372089725	386.1	356.4	386.1	386.1
2.374882522	400.95	371.25	386.1	386.1
2.377672039	400.95	371.25	386.1	386.1
2.380458289	400.95	371.25	386.1	386.1
2.383241282	415.8	371.25	386.1	386.1
2.386021031	415.8	386.1	400.95	400.95
2.388797547	415.8	386.1	400.95	400.95

2.391570841	430.65	386.1	400.95	400.95
2.394340924	430.65	386.1	400.95	400.95
2.397107807	430.65	386.1	400.95	400.95
2.399871501	445.5	400.95	415.8	415.8
2.402632018	445.5	400.95	415.8	415.8
2.405389367	445.5	400.95	430.65	415.8
2.408143561	445.5	415.8	430.65	415.8
2.41089461	445.5	415.8	430.65	430.65
2.413642525	445.5	415.8	430.65	430.65
2.416387316	460.35	415.8	430.65	430.65
2.419128994	460.35	430.65	445.5	430.65
2.421867569	475.2	430.65	445.5	445.5
2.424603053	475.2	430.65	445.5	445.5
2.427335455	475.2	430.65	460.35	445.5
2.430064786	475.2	430.65	445.5	445.5
2.432791057	475.2	445.5	460.35	460.35
2.435514276	475.2	445.5	460.35	460.35
2.438234456	490.05	445.5	460.35	460.35
2.440951605	490.05	445.5	460.35	460.35
2.443665735	490.05	445.5	460.35	460.35
2.446376854	490.05	445.5	460.35	475.2
2.449084974	504.9	445.5	475.2	475.2
2.451790103	504.9	460.35	475.2	475.2
2.454492253	490.05	460.35	475.2	475.2
2.457191432	504.9	460.35	475.2	475.2
2.45988765	504.9	460.35	490.05	490.05
2.462580918	519.75	460.35	490.05	490.05
2.465271244	519.75	475.2	490.05	504.9
2.467958639	519.75	475.2	490.05	490.05
2.470643112	519.75	475.2	504.9	504.9
2.473324673	519.75	475.2	504.9	504.9
2.47600333	519.75	475.2	504.9	504.9
2.478679094	534.6	490.05	504.9	504.9
2.481351974	534.6	490.05	504.9	504.9
2.484021978	534.6	490.05	504.9	504.9
2.486689117	534.6	490.05	504.9	504.9
2.4893534	534.6	490.05	504.9	519.75
2.492014835	534.6	504.9	519.75	519.75
2.494673432	549.45	504.9	519.75	519.75
2.4973292	549.45	490.05	519.75	519.75
2.499982148	549.45	490.05	519.75	519.75

2.502632285	549.45	504.9	519.75	519.75
2.505279619	549.45	504.9	534.6	519.75
2.50792416	549.45	504.9	519.75	534.6
2.510565916	564.3	504.9	534.6	534.6
2.513204897	564.3	504.9	534.6	534.6
2.515841111	564.3	504.9	534.6	534.6
2.518474566	564.3	519.75	534.6	534.6
2.521105271	564.3	519.75	549.45	534.6
2.523733236	564.3	519.75	549.45	549.45
2.526358468	579.15	519.75	549.45	549.45
2.528980975	579.15	534.6	549.45	549.45
2.531600768	579.15	519.75	549.45	549.45
2.534217853	579.15	519.75	549.45	549.45
2.536832239	579.15	534.6	564.3	549.45
2.539443934	594	534.6	549.45	549.45
2.542052948	579.15	534.6	549.45	549.45
2.544659287	594	549.45	549.45	549.45
2.547262961	594	549.45	564.3	564.3
2.549863977	608.85	549.45	564.3	564.3
2.552462344	594	549.45	564.3	564.3
2.55505807	594	549.45	564.3	564.3
2.557651162	608.85	549.45	564.3	564.3
2.560241628	608.85	549.45	564.3	564.3
2.562829478	608.85	549.45	579.15	564.3
2.565414718	608.85	549.45	564.3	579.15
2.567997356	608.85	549.45	579.15	579.15
2.570577401	608.85	549.45	579.15	579.15
2.573154859	608.85	549.45	579.15	579.15
2.57572974	608.85	564.3	579.15	579.15
2.57830205	608.85	549.45	579.15	579.15
2.580871797	623.7	564.3	579.15	594
2.583438989	623.7	564.3	579.15	594
2.586003633	608.85	549.45	579.15	594
2.588565738	623.7	564.3	579.15	594
2.59112531	623.7	564.3	594	594
2.593682357	623.7	564.3	594	594
2.596236887	623.7	564.3	594	594
2.598788906	638.55	564.3	594	594
2.601338423	638.55	579.15	594	608.85
2.603885445	623.7	579.15	594	594
2.606429979	638.55	579.15	594	608.85

2.608972032	638.55	579.15	594	608.85
2.611511611	638.55	579.15	608.85	608.85
2.614048724	638.55	579.15	608.85	608.85
2.616583378	638.55	579.15	608.85	608.85
2.61911558	638.55	579.15	608.85	608.85
2.621645337	638.55	579.15	608.85	608.85
2.624172657	653.4	579.15	608.85	608.85
2.626697545	653.4	579.15	608.85	608.85
2.62922001	653.4	579.15	608.85	608.85
2.631740058	653.4	594	623.7	608.85
2.634257696	653.4	594	608.85	608.85
2.636772931	653.4	594	608.85	623.7
2.63928577	653.4	579.15	608.85	608.85
2.64179622	653.4	594	623.7	623.7
2.644304287	668.25	594	623.7	623.7
2.646809979	668.25	594	623.7	623.7
2.649313302	668.25	594	623.7	623.7
2.651814262	668.25	594	623.7	623.7
2.654312867	668.25	608.85	623.7	623.7
2.656809123	668.25	608.85	623.7	638.55
2.659303036	668.25	608.85	623.7	638.55
2.661794614	683.1	608.85	638.55	638.55
2.664283863	668.25	608.85	638.55	638.55
2.666770789	668.25	608.85	638.55	638.55
2.669255398	668.25	608.85	638.55	638.55
2.671737698	668.25	608.85	638.55	638.55
2.674217695	668.25	608.85	638.55	638.55
2.676695395	668.25	608.85	638.55	638.55
2.679170804	668.25	608.85	638.55	638.55
2.681643929	683.1	608.85	638.55	638.55
2.684114777	683.1	608.85	638.55	638.55
2.686583352	683.1	623.7	638.55	638.55
2.689049663	683.1	608.85	638.55	638.55
2.691513714	683.1	623.7	638.55	653.4
2.693975512	683.1	608.85	638.55	653.4
2.696435064	683.1	623.7	638.55	653.4
2.698892375	683.1	623.7	638.55	653.4
2.701347451	683.1	623.7	653.4	653.4
2.703800299	683.1	623.7	638.55	653.4
2.706250925	683.1	623.7	653.4	653.4
2.708699334	683.1	623.7	653.4	653.4

2.711145533	683.1	623.7	638.55	653.4
2.713589528	697.95	623.7	638.55	653.4
2.716031325	697.95	623.7	653.4	653.4
2.718470928	712.8	623.7	653.4	653.4
2.720908346	697.95	623.7	653.4	653.4
2.723343582	712.8	623.7	653.4	653.4
2.725776644	697.95	623.7	653.4	653.4
2.728207537	697.95	638.55	653.4	653.4
2.730636266	697.95	638.55	653.4	653.4
2.733062838	712.8	638.55	653.4	668.25
2.735487258	712.8	638.55	653.4	668.25
2.737909532	712.8	638.55	653.4	668.25
2.740329666	712.8	638.55	668.25	668.25
2.742747665	712.8	638.55	668.25	668.25
2.745163535	712.8	638.55	668.25	668.25
2.747577282	712.8	638.55	653.4	668.25
2.74998891	727.65	638.55	653.4	668.25
2.752398427	712.8	638.55	668.25	668.25
2.754805837	727.65	638.55	668.25	668.25
2.757211145	727.65	653.4	668.25	668.25
2.759614358	727.65	653.4	668.25	668.25
2.76201548	712.8	653.4	668.25	668.25
2.764414518	712.8	653.4	668.25	668.25
2.766811476	712.8	653.4	668.25	668.25
2.769206361	712.8	653.4	668.25	683.1
2.771599176	727.65	638.55	683.1	683.1
2.773989929	727.65	653.4	683.1	668.25
2.776378623	727.65	653.4	668.25	683.1
2.778765265	727.65	653.4	668.25	683.1
2.781149859	727.65	653.4	668.25	668.25
2.783532412	727.65	653.4	668.25	683.1
2.785912927	727.65	653.4	668.25	683.1
2.788291411	727.65	668.25	668.25	683.1
2.790667869	727.65	653.4	683.1	683.1
2.793042305	727.65	653.4	683.1	683.1
2.795414725	727.65	653.4	683.1	683.1
2.797785134	727.65	653.4	683.1	683.1
2.800153537	727.65	653.4	683.1	697.95
2.802519939	727.65	653.4	683.1	683.1
2.804884345	727.65	653.4	683.1	697.95
2.807246761	727.65	668.25	683.1	683.1

2.809607191	727.65	668.25	683.1	683.1
2.811965641	742.5	668.25	683.1	683.1
2.814322114	727.65	668.25	683.1	683.1
2.816676617	727.65	668.25	683.1	683.1
2.819029154	742.5	668.25	683.1	683.1
2.821379731	742.5	668.25	683.1	697.95
2.823728351	742.5	668.25	683.1	697.95
2.82607502	742.5	668.25	697.95	697.95
2.828419742	727.65	668.25	697.95	697.95
2.830762524	742.5	668.25	697.95	697.95
2.833103368	742.5	668.25	697.95	697.95
2.835442281	742.5	683.1	697.95	697.95
2.837779267	742.5	668.25	697.95	697.95
2.84011433	742.5	668.25	697.95	697.95
2.842447476	742.5	668.25	697.95	697.95
2.844778709	742.5	668.25	697.95	697.95
2.847108034	742.5	668.25	697.95	697.95
2.849435456	742.5	668.25	697.95	697.95
2.851760978	742.5	668.25	697.95	697.95
2.854084606	742.5	683.1	697.95	697.95
2.856406345	742.5	668.25	697.95	697.95
2.858726199	757.35	668.25	683.1	697.95
2.861044173	742.5	668.25	697.95	697.95
2.86336027	757.35	668.25	697.95	697.95
2.865674497	757.35	668.25	697.95	697.95
2.867986856	757.35	668.25	697.95	697.95
2.870297354	757.35	668.25	697.95	712.8
2.872605993	757.35	668.25	712.8	697.95
2.87491278	757.35	683.1	697.95	712.8
2.877217718	757.35	683.1	697.95	697.95
2.879520811	757.35	683.1	697.95	697.95
2.881822064	757.35	683.1	712.8	697.95
2.884121482	757.35	683.1	712.8	712.8
2.886419068	757.35	668.25	712.8	697.95
2.888714828	757.35	683.1	697.95	712.8
2.891008766	757.35	683.1	712.8	712.8
2.893300885	757.35	683.1	712.8	712.8
2.89559119	757.35	683.1	712.8	712.8
2.897879686	757.35	683.1	712.8	712.8
2.900166377	757.35	683.1	712.8	712.8
2.902451267	757.35	683.1	712.8	712.8

2.90473436	757.35	683.1	712.8	712.8
2.907015661	757.35	683.1	712.8	712.8
2.909295173	757.35	683.1	712.8	712.8
2.911572902	757.35	683.1	712.8	712.8
2.91384885	757.35	683.1	712.8	712.8
2.916123023	757.35	683.1	712.8	712.8
2.918395424	757.35	683.1	712.8	712.8
2.920666058	757.35	683.1	712.8	712.8
2.922934929	757.35	683.1	712.8	712.8
2.92520204	757.35	683.1	712.8	712.8
2.927467396	757.35	683.1	712.8	712.8
2.929731002	757.35	683.1	712.8	712.8
2.93199286	757.35	683.1	712.8	712.8
2.934252975	757.35	683.1	712.8	712.8
2.936511351	757.35	683.1	712.8	712.8
2.938767993	757.35	683.1	712.8	712.8
2.941022903	757.35	683.1	712.8	712.8
2.943276087	757.35	683.1	712.8	712.8
2.945527547	757.35	683.1	712.8	712.8
2.947777289	757.35	683.1	712.8	712.8
2.950025315	757.35	683.1	712.8	712.8
2.95227163	757.35	683.1	712.8	712.8
2.954516238	757.35	683.1	712.8	712.8
2.956759143	757.35	683.1	712.8	712.8
2.959000348	757.35	683.1	712.8	712.8

Gage 2

Outer radius	**Test 1**	**Test 2**	**Test 3**	**Test 4**
2.192001	0	0	0	0
2.195023	14.85	14.85	14.85	29.7
2.198041	14.85	14.85	29.7	29.7
2.201054	29.7	29.7	29.7	44.55
2.204064	29.7	29.7	44.55	59.4
2.207069	29.7	44.55	44.55	74.25
2.21007	44.55	59.4	59.4	89.1
2.213067	59.4	59.4	59.4	89.1
2.216061	59.4	74.25	59.4	103.95
2.21905	74.25	74.25	74.25	103.95
2.222035	74.25	89.1	74.25	118.8

2.225016	74.25	89.1	74.25	148.5
2.227993	74.25	89.1	89.1	148.5
2.230966	89.1	89.1	103.95	163.35
2.233935	89.1	103.95	103.95	178.2
2.2369	89.1	103.95	103.95	178.2
2.239862	103.95	118.8	118.8	193.05
2.242819	103.95	133.65	118.8	207.9
2.245773	118.8	133.65	133.65	207.9
2.248722	118.8	133.65	148.5	207.9
2.251668	133.65	148.5	148.5	207.9
2.25461	133.65	148.5	148.5	222.75
2.257548	148.5	163.35	163.35	237.6
2.260482	148.5	163.35	163.35	237.6
2.263413	148.5	178.2	178.2	252.45
2.266339	163.35	178.2	178.2	252.45
2.269262	178.2	193.05	193.05	252.45
2.272181	178.2	193.05	193.05	252.45
2.275097	178.2	207.9	207.9	267.3
2.278008	193.05	207.9	207.9	267.3
2.280916	207.9	222.75	222.75	282.15
2.28382	207.9	222.75	222.75	282.15
2.286721	207.9	237.6	222.75	297
2.289618	207.9	237.6	237.6	297
2.292511	222.75	237.6	237.6	311.85
2.295401	237.6	252.45	252.45	311.85
2.298287	222.75	252.45	252.45	326.7
2.301169	237.6	252.45	267.3	326.7
2.304048	252.45	252.45	267.3	341.55
2.306923	252.45	252.45	282.15	341.55
2.309794	267.3	267.3	282.15	341.55
2.312662	267.3	282.15	297	356.4
2.315527	267.3	282.15	297	356.4
2.318388	282.15	282.15	311.85	371.25
2.321245	282.15	297	311.85	371.25
2.324099	297	297	311.85	371.25
2.326949	297	297	326.7	386.1
2.329796	297	311.85	326.7	386.1
2.33264	311.85	326.7	341.55	386.1
2.33548	311.85	326.7	356.4	400.95
2.338316	311.85	326.7	356.4	400.95
2.341149	326.7	326.7	356.4	415.8

2.343979	326.7	341.55	356.4	415.8
2.346805	326.7	341.55	371.25	415.8
2.349628	341.55	356.4	371.25	430.65
2.352447	341.55	356.4	371.25	430.65
2.355263	341.55	356.4	386.1	430.65
2.358076	341.55	371.25	386.1	445.5
2.360886	356.4	371.25	400.95	445.5
2.363692	356.4	371.25	400.95	445.5
2.366494	371.25	386.1	415.8	460.35
2.369294	371.25	386.1	415.8	460.35
2.37209	371.25	386.1	415.8	460.35
2.374883	371.25	400.95	415.8	475.2
2.377672	386.1	400.95	430.65	475.2
2.380458	386.1	400.95	430.65	475.2
2.383241	386.1	415.8	430.65	475.2
2.386021	400.95	415.8	445.5	490.05
2.388798	400.95	415.8	445.5	490.05
2.391571	400.95	430.65	445.5	490.05
2.394341	415.8	430.65	445.5	490.05
2.397108	415.8	430.65	460.35	504.9
2.399872	430.65	430.65	460.35	504.9
2.402632	430.65	445.5	460.35	504.9
2.405389	430.65	445.5	475.2	504.9
2.408144	430.65	445.5	460.35	519.75
2.410895	445.5	460.35	475.2	519.75
2.413643	430.65	460.35	475.2	519.75
2.416387	445.5	460.35	475.2	534.6
2.419129	445.5	460.35	490.05	534.6
2.421868	460.35	475.2	490.05	534.6
2.424603	460.35	475.2	490.05	534.6
2.427335	460.35	475.2	490.05	549.45
2.430065	475.2	490.05	504.9	534.6
2.432791	460.35	490.05	504.9	549.45
2.435514	475.2	490.05	519.75	549.45
2.438234	475.2	490.05	519.75	549.45
2.440952	490.05	490.05	519.75	564.3
2.443666	490.05	504.9	519.75	564.3
2.446377	490.05	504.9	519.75	564.3
2.449085	490.05	504.9	534.6	579.15
2.45179	504.9	504.9	534.6	579.15
2.454492	504.9	504.9	549.45	579.15

2.457191	504.9	504.9	549.45	594
2.459888	519.75	504.9	549.45	594
2.462581	519.75	519.75	564.3	594
2.465271	504.9	519.75	564.3	594
2.467959	519.75	519.75	564.3	608.85
2.470643	519.75	519.75	564.3	608.85
2.473325	519.75	534.6	564.3	594
2.476003	519.75	534.6	579.15	608.85
2.478679	534.6	534.6	579.15	608.85
2.481352	519.75	534.6	579.15	608.85
2.484022	534.6	549.45	594	608.85
2.486689	534.6	534.6	579.15	608.85
2.489353	534.6	549.45	594	608.85
2.492015	549.45	549.45	594	623.7
2.494673	549.45	549.45	594	623.7
2.497329	549.45	549.45	594	623.7
2.499982	549.45	564.3	594	638.55
2.502632	549.45	564.3	594	638.55
2.50528	549.45	564.3	608.85	638.55
2.507924	564.3	564.3	608.85	638.55
2.510566	564.3	564.3	608.85	638.55
2.513205	579.15	579.15	608.85	638.55
2.515841	579.15	579.15	623.7	653.4
2.518475	579.15	579.15	623.7	653.4
2.521105	579.15	579.15	623.7	653.4
2.523733	579.15	594	623.7	653.4
2.526358	579.15	594	623.7	653.4
2.528981	594	594	623.7	668.25
2.531601	579.15	594	638.55	668.25
2.534218	579.15	594	638.55	668.25
2.536832	594	594	638.55	668.25
2.539444	594	594	638.55	668.25
2.542053	594	608.85	638.55	668.25
2.544659	594	608.85	638.55	668.25
2.547263	608.85	608.85	653.4	668.25
2.549864	608.85	608.85	653.4	683.1
2.552462	608.85	608.85	653.4	683.1
2.555058	608.85	608.85	653.4	683.1
2.557651	608.85	623.7	653.4	683.1
2.560242	623.7	623.7	653.4	683.1
2.562829	623.7	608.85	668.25	697.95

2.565415	623.7	623.7	653.4	697.95
2.567997	623.7	623.7	668.25	697.95
2.570577	623.7	623.7	668.25	697.95
2.573155	623.7	623.7	668.25	697.95
2.57573	638.55	623.7	668.25	697.95
2.578302	623.7	623.7	683.1	697.95
2.580872	638.55	638.55	683.1	697.95
2.583439	638.55	638.55	683.1	712.8
2.586004	638.55	638.55	683.1	712.8
2.588566	638.55	638.55	683.1	712.8
2.591125	638.55	638.55	683.1	712.8
2.593682	638.55	638.55	697.95	712.8
2.596237	638.55	638.55	683.1	712.8
2.598789	638.55	638.55	697.95	712.8
2.601338	653.4	653.4	697.95	712.8
2.603885	653.4	653.4	697.95	712.8
2.60643	653.4	653.4	697.95	712.8
2.608972	653.4	653.4	697.95	712.8
2.611512	653.4	653.4	697.95	727.65
2.614049	668.25	653.4	712.8	727.65
2.616583	668.25	653.4	712.8	712.8
2.619116	668.25	653.4	697.95	727.65
2.621645	668.25	653.4	697.95	727.65
2.624173	668.25	668.25	712.8	727.65
2.626698	668.25	668.25	712.8	727.65
2.62922	668.25	668.25	712.8	742.5
2.63174	668.25	668.25	712.8	742.5
2.634258	668.25	668.25	712.8	727.65
2.636773	668.25	668.25	712.8	742.5
2.639286	683.1	668.25	727.65	742.5
2.641796	683.1	668.25	727.65	742.5
2.644304	683.1	683.1	727.65	742.5
2.64681	683.1	668.25	727.65	742.5
2.649313	683.1	683.1	727.65	742.5
2.651814	683.1	668.25	712.8	757.35
2.654313	683.1	683.1	727.65	757.35
2.656809	683.1	683.1	727.65	757.35
2.659303	683.1	683.1	727.65	757.35
2.661795	683.1	683.1	727.65	757.35
2.664284	697.95	683.1	727.65	757.35
2.666771	683.1	683.1	742.5	757.35

2.669255	683.1	683.1	742.5	757.35
2.671738	697.95	683.1	742.5	757.35
2.674218	697.95	683.1	742.5	757.35
2.676695	697.95	697.95	757.35	757.35
2.679171	697.95	697.95	742.5	757.35
2.681644	697.95	683.1	742.5	757.35
2.684115	697.95	697.95	742.5	757.35
2.686583	712.8	697.95	742.5	757.35
2.68905	712.8	697.95	757.35	757.35
2.691514	712.8	697.95	742.5	757.35
2.693976	712.8	697.95	757.35	757.35
2.696435	712.8	697.95	757.35	757.35
2.698892	712.8	697.95	742.5	757.35
2.701347	712.8	712.8	757.35	757.35
2.7038	712.8	712.8	757.35	757.35
2.706251	712.8	712.8	772.2	772.2
2.708699	712.8	697.95	757.35	757.35
2.711146	712.8	712.8	757.35	757.35
2.71359	712.8	697.95	757.35	757.35
2.716031	727.65	712.8	772.2	757.35
2.718471	727.65	712.8	757.35	757.35
2.720908	727.65	712.8	757.35	757.35
2.723344	727.65	712.8	757.35	757.35
2.725777	727.65	712.8	772.2	757.35
2.728208	727.65	712.8	772.2	757.35
2.730636	727.65	712.8	772.2	757.35
2.733063	727.65	727.65	772.2	757.35
2.735487	727.65	712.8	772.2	772.2
2.73791	727.65	712.8	772.2	772.2
2.74033	727.65	727.65	772.2	757.35
2.742748	742.5	712.8	772.2	757.35
2.745164	727.65	712.8	772.2	757.35
2.747577	727.65	712.8	772.2	757.35
2.749989	742.5	727.65	772.2	757.35
2.752398	727.65	727.65	772.2	772.2
2.754806	742.5	712.8	772.2	757.35
2.757211	742.5	727.65	772.2	757.35
2.759614	742.5	727.65	772.2	757.35
2.762015	742.5	727.65	787.05	757.35
2.764415	742.5	727.65	787.05	757.35
2.766811	742.5	727.65	787.05	757.35

2.769206	742.5	727.65	787.05	757.35
2.771599	742.5	727.65	787.05	757.35
2.77399	742.5	727.65	787.05	757.35
2.776379	742.5	727.65	787.05	757.35
2.778765	742.5	727.65	787.05	757.35
2.78115	742.5	727.65	787.05	757.35
2.783532	742.5	727.65	787.05	757.35
2.785913	742.5	742.5	787.05	757.35
2.788291	742.5	727.65	801.9	757.35
2.790668	742.5	742.5	801.9	757.35
2.793042	742.5	727.65	801.9	757.35
2.795415	742.5	742.5	787.05	757.35
2.797785	742.5	742.5	801.9	757.35
2.800154	742.5	727.65	787.05	757.35
2.80252	742.5	727.65	801.9	757.35
2.804884	742.5	742.5	801.9	757.35
2.807247	742.5	742.5	801.9	757.35
2.809607	742.5	742.5	801.9	757.35
2.811966	742.5	742.5	801.9	757.35
2.814322	742.5	742.5	801.9	757.35
2.816677	742.5	742.5	816.75	757.35
2.819029	742.5	742.5	801.9	757.35
2.82138	742.5	742.5	801.9	757.35
2.823728	742.5	742.5	801.9	757.35
2.826075	742.5	742.5	801.9	757.35
2.82842	742.5	742.5	801.9	757.35
2.830763	742.5	742.5	801.9	757.35
2.833103	742.5	742.5	801.9	757.35
2.835442	742.5	742.5	801.9	757.35
2.837779	742.5	742.5	816.75	757.35
2.840114	742.5	742.5	816.75	757.35
2.842447	742.5	742.5	816.75	757.35
2.844779	742.5	742.5	816.75	757.35
2.847108	742.5	757.35	801.9	757.35
2.849435	742.5	757.35	801.9	757.35
2.851761	742.5	757.35	801.9	757.35
2.854085	742.5	742.5	801.9	757.35
2.856406	742.5	742.5	816.75	757.35
2.858726	742.5	742.5	816.75	757.35
2.861044	742.5	742.5	816.75	757.35
2.86336	742.5	742.5	816.75	757.35

2.865674	742.5	742.5	816.75	757.35
2.867987	742.5	742.5	801.9	757.35
2.870297	742.5	742.5	816.75	757.35
2.872606	742.5	742.5	816.75	757.35
2.874913	742.5	742.5	816.75	757.35
2.877218	742.5	742.5	816.75	757.35
2.879521	742.5	742.5	831.6	757.35
2.881822	742.5	742.5	816.75	757.35
2.884121	742.5	742.5	816.75	757.35
2.886419	742.5	742.5	816.75	757.35
2.888715	742.5	742.5	816.75	757.35
2.891009	742.5	742.5	816.75	757.35
2.893301	742.5	742.5	816.75	757.35
2.895591	742.5	742.5	816.75	757.35
2.89788	742.5	742.5	816.75	757.35
2.900166	742.5	742.5	816.75	757.35
2.902451	742.5	742.5	816.75	757.35
2.904734	742.5	742.5	816.75	757.35
2.907016	742.5	742.5	816.75	757.35
2.909295	742.5	742.5	816.75	757.35
2.911573	742.5	742.5	816.75	757.35
2.913849	742.5	742.5	816.75	757.35
2.916123	742.5	742.5	816.75	757.35
2.918395	742.5	742.5	816.75	757.35
2.920666	742.5	742.5	816.75	757.35
2.922935	742.5	742.5	816.75	757.35
2.925202	742.5	742.5	816.75	757.35
2.927467	742.5	742.5	816.75	757.35
2.929731	742.5	742.5	816.75	757.35
2.931993	742.5	742.5	816.75	757.35
2.934253	742.5	742.5	816.75	757.35
2.936511	742.5	742.5	816.75	757.35
2.938768	742.5	742.5	816.75	757.35
2.941023	742.5	742.5	816.75	757.35
2.943276	742.5	742.5	816.75	757.35
2.945528	742.5	742.5	816.75	757.35
2.947777	742.5	742.5	816.75	757.35
2.950025	742.5	742.5	816.75	757.35
2.952272	742.5	742.5	816.75	757.35
2.954516	742.5	742.5	816.75	757.35
2.956759	742.5	742.5	816.75	757.35

2.959	742.5	742.5	816.75	757.35

Test data for MD strains in 6” wide PET

Gage 1

Outer radius	Test 1	Test 2	Test 3	Test 4
2.19200121	0	0	0	0
2.201054277	-534.6	-519.75	-490.05	-415.8
2.210070279	-801.9	-772.2	-742.5	-623.7
2.219049664	-935.55	-935.55	-861.3	-727.65
2.227992878	-1069.2	-1039.5	-980.1	-861.3
2.236900352	-1158.3	-1128.6	-1084.05	-920.7
2.245772512	-1232.55	-1188	-1143.45	-994.95
2.254609775	-1291.95	-1262.25	-1202.85	-1039.5
2.263412549	-1336.5	-1306.8	-1247.4	-1084.05
2.272181235	-1381.05	-1351.35	-1291.95	-1113.75
2.280916226	-1410.75	-1366.2	-1321.65	-1143.45
2.289617908	-1440.45	-1410.75	-1351.35	-1173.15
2.298286658	-1470.15	-1425.6	-1366.2	-1188
2.306922848	-1485	-1440.45	-1395.9	-1217.7
2.315526841	-1514.7	-1470.15	-1425.6	-1232.55
2.324098996	-1544.4	-1485	-1425.6	-1247.4
2.332639663	-1559.25	-1514.7	-1455.3	-1262.25
2.341149187	-1574.1	-1529.55	-1455.3	-1291.95
2.349627905	-1574.1	-1544.4	-1470.15	-1291.95
2.358076151	-1588.95	-1544.4	-1499.85	-1306.8
2.366494249	-1618.65	-1559.25	-1499.85	-1321.65
2.374882522	-1618.65	-1574.1	-1514.7	-1336.5
2.383241282	-1633.5	-1574.1	-1529.55	-1336.5
2.391570841	-1633.5	-1588.95	-1529.55	-1351.35
2.399871501	-1648.35	-1603.8	-1544.4	-1351.35
2.408143561	-1648.35	-1603.8	-1544.4	-1366.2
2.416387316	-1663.2	-1618.65	-1559.25	-1381.05
2.424603053	-1663.2	-1618.65	-1559.25	-1381.05
2.432791057	-1678.05	-1633.5	-1574.1	-1381.05
2.440951605	-1678.05	-1633.5	-1574.1	-1395.9
2.449084974	-1692.9	-1648.35	-1588.95	-1395.9
2.457191432	-1692.9	-1648.35	-1588.95	-1410.75

2.465271244	-1692.9	-1648.35	-1603.8	-1410.75
2.473324673	-1707.75	-1663.2	-1603.8	-1410.75
2.481351974	-1707.75	-1663.2	-1603.8	-1425.6
2.4893534	-1707.75	-1663.2	-1603.8	-1410.75
2.4973292	-1722.6	-1678.05	-1618.65	-1425.6
2.505279619	-1707.75	-1678.05	-1618.65	-1440.45
2.513204897	-1722.6	-1678.05	-1618.65	-1440.45
2.521105271	-1722.6	-1678.05	-1618.65	-1440.45
2.528980975	-1722.6	-1678.05	-1633.5	-1440.45
2.536832239	-1722.6	-1692.9	-1633.5	-1455.3
2.544659287	-1737.45	-1692.9	-1633.5	-1455.3
2.552462344	-1737.45	-1692.9	-1633.5	-1455.3
2.560241628	-1737.45	-1692.9	-1633.5	-1470.15
2.567997356	-1737.45	-1692.9	-1648.35	-1470.15
2.57572974	-1752.3	-1707.75	-1663.2	-1470.15
2.583438989	-1752.3	-1707.75	-1648.35	-1470.15
2.59112531	-1752.3	-1707.75	-1663.2	-1470.15
2.598788906	-1752.3	-1707.75	-1663.2	-1470.15
2.606429979	-1752.3	-1707.75	-1663.2	-1485
2.614048724	-1752.3	-1707.75	-1663.2	-1485
2.621645337	-1752.3	-1707.75	-1663.2	-1485
2.62922001	-1767.15	-1722.6	-1663.2	-1485
2.636772931	-1752.3	-1722.6	-1663.2	-1485
2.644304287	-1767.15	-1722.6	-1663.2	-1485
2.651814262	-1767.15	-1722.6	-1663.2	-1485
2.659303036	-1767.15	-1722.6	-1678.05	-1499.85
2.666770789	-1767.15	-1722.6	-1678.05	-1485
2.674217695	-1767.15	-1722.6	-1678.05	-1485
2.681643929	-1767.15	-1722.6	-1678.05	-1499.85
2.689049663	-1767.15	-1737.45	-1678.05	-1499.85
2.696435064	-1767.15	-1722.6	-1678.05	-1499.85
2.703800299	-1767.15	-1722.6	-1678.05	-1499.85
2.711145533	-1782	-1737.45	-1678.05	-1499.85
2.718470928	-1767.15	-1737.45	-1678.05	-1499.85
2.725776644	-1782	-1737.45	-1678.05	-1499.85
2.733062838	-1767.15	-1737.45	-1678.05	-1514.7
2.740329666	-1767.15	-1737.45	-1678.05	-1514.7
2.747577282	-1767.15	-1737.45	-1692.9	-1514.7
2.754805837	-1767.15	-1737.45	-1692.9	-1514.7
2.76201548	-1782	-1737.45	-1692.9	-1514.7
2.769206361	-1767.15	-1737.45	-1678.05	-1514.7

2.776378623	-1767.15	-1737.45	-1692.9	-1514.7
2.783532412	-1767.15	-1737.45	-1678.05	-1514.7
2.790667869	-1782	-1737.45	-1692.9	-1514.7
2.797785134	-1782	-1752.3	-1692.9	-1529.55
2.804884345	-1782	-1737.45	-1692.9	-1529.55
2.811965641	-1782	-1737.45	-1692.9	-1529.55
2.819029154	-1767.15	-1752.3	-1692.9	-1514.7
2.82607502	-1782	-1737.45	-1692.9	-1514.7
2.833103368	-1782	-1737.45	-1692.9	-1529.55
2.84011433	-1782	-1752.3	-1692.9	-1529.55
2.847108034	-1782	-1752.3	-1692.9	-1529.55
2.854084606	-1782	-1752.3	-1692.9	-1529.55
2.861044173	-1782	-1752.3	-1692.9	-1529.55
2.867986856	-1782	-1752.3	-1692.9	-1529.55
2.87491278	-1782	-1752.3	-1692.9	-1514.7

Gage 2

Outer radius	Test 1	Test 2	Test 3	Test 4
2.19200121	0	0	0	0
2.201054277	-490.05	-445.5	-522.824	-549.45
2.210070279	-697.95	-653.4	-637.192	-846.45
2.219049664	-801.9	-757.35	-718.883	-1024.65
2.227992878	-920.7	-861.3	-784.236	-1113.75
2.236900352	-980.1	-935.55	-833.251	-1217.7
2.245772512	-1054.35	-994.95	-882.266	-1291.95
2.254609775	-1098.9	-1039.5	-931.281	-1366.2
2.263412549	-1143.45	-1084.05	-947.619	-1395.9
2.272181235	-1173.15	-1113.75	-980.295	-1455.3
2.280916226	-1202.85	-1158.3	-1012.97	-1485
2.289617908	-1232.55	-1173.15	-1029.31	-1514.7
2.298286658	-1262.25	-1202.85	-1045.65	-1529.55
2.306922848	-1277.1	-1232.55	-1061.99	-1559.25
2.315526841	-1306.8	-1247.4	-1078.32	-1574.1
2.324098996	-1321.65	-1262.25	-1094.66	-1588.95
2.332639663	-1336.5	-1277.1	-1111	-1603.8
2.341149187	-1351.35	-1291.95	-1111	-1633.5
2.349627905	-1366.2	-1306.8	-1127.34	-1633.5
2.358076151	-1381.05	-1321.65	-1143.68	-1648.35

2.366494249	-1395.9	-1336.5	-1143.68	-1663.2
2.374882522	-1395.9	-1336.5	-1160.02	-1678.05
2.383241282	-1410.75	-1351.35	-1160.02	-1678.05
2.391570841	-1410.75	-1366.2	-1176.35	-1692.9
2.399871501	-1425.6	-1381.05	-1176.35	-1707.75
2.408143561	-1440.45	-1381.05	-1176.35	-1707.75
2.416387316	-1440.45	-1395.9	-1176.35	-1707.75
2.424603053	-1455.3	-1410.75	-1192.69	-1722.6
2.432791057	-1455.3	-1410.75	-1192.69	-1722.6
2.440951605	-1470.15	-1410.75	-1192.69	-1722.6
2.449084974	-1470.15	-1425.6	-1192.69	-1737.45
2.457191432	-1470.15	-1425.6	-1209.03	-1737.45
2.465271244	-1485	-1440.45	-1209.03	-1752.3
2.473324673	-1485	-1440.45	-1209.03	-1752.3
2.481351974	-1485	-1440.45	-1209.03	-1752.3
2.4893534	-1485	-1455.3	-1209.03	-1752.3
2.4973292	-1499.85	-1440.45	-1209.03	-1767.15
2.505279619	-1499.85	-1455.3	-1209.03	-1767.15
2.513204897	-1499.85	-1455.3	-1209.03	-1752.3
2.521105271	-1514.7	-1470.15	-1225.37	-1767.15
2.528980975	-1514.7	-1455.3	-1225.37	-1767.15
2.536832239	-1514.7	-1470.15	-1225.37	-1767.15
2.544659287	-1529.55	-1470.15	-1225.37	-1767.15
2.552462344	-1529.55	-1470.15	-1225.37	-1782
2.560241628	-1529.55	-1485	-1225.37	-1782
2.567997356	-1529.55	-1485	-1225.37	-1782
2.57572974	-1529.55	-1485	-1225.37	-1782
2.583438989	-1544.4	-1485	-1225.37	-1782
2.59112531	-1544.4	-1485	-1225.37	-1796.85
2.598788906	-1544.4	-1499.85	-1225.37	-1782
2.606429979	-1544.4	-1499.85	-1225.37	-1796.85
2.614048724	-1544.4	-1499.85	-1225.37	-1782
2.621645337	-1544.4	-1499.85	-1225.37	-1796.85
2.62922001	-1544.4	-1514.7	-1225.37	-1796.85
2.636772931	-1559.25	-1499.85	-1225.37	-1796.85
2.644304287	-1559.25	-1514.7	-1225.37	-1796.85
2.651814262	-1559.25	-1514.7	-1225.37	-1796.85
2.659303036	-1559.25	-1514.7	-1225.37	-1796.85
2.666770789	-1559.25	-1514.7	-1225.37	-1796.85
2.674217695	-1574.1	-1514.7	-1225.37	-1796.85
2.681643929	-1574.1	-1514.7	-1225.37	-1796.85

2.689049663	-1559.25	-1514.7	-1225.37	-1796.85
2.696435064	-1574.1	-1514.7	-1225.37	-1796.85
2.703800299	-1574.1	-1529.55	-1225.37	-1796.85
2.711145533	-1574.1	-1529.55	-1225.37	-1796.85
2.718470928	-1574.1	-1529.55	-1225.37	-1796.85
2.725776644	-1574.1	-1529.55	-1225.37	-1796.85
2.733062838	-1574.1	-1529.55	-1225.37	-1796.85
2.740329666	-1574.1	-1529.55	-1225.37	-1796.85
2.747577282	-1588.95	-1529.55	-1225.37	-1796.85
2.754805837	-1574.1	-1529.55	-1225.37	-1796.85
2.76201548	-1574.1	-1529.55	-1225.37	-1796.85
2.769206361	-1588.95	-1529.55	-1225.37	-1811.7
2.776378623	-1588.95	-1544.4	-1225.37	-1811.7
2.783532412	-1588.95	-1529.55	-1225.37	-1796.85
2.790667869	-1574.1	-1529.55	-1225.37	-1811.7
2.797785134	-1588.95	-1529.55	-1225.37	-1796.85
2.804884345	-1588.95	-1544.4	-1209.03	-1811.7
2.811965641	-1588.95	-1529.55	-1225.37	-1811.7
2.819029154	-1588.95	-1544.4	-1225.37	-1811.7
2.82607502	-1588.95	-1544.4	-1225.37	-1796.85
2.833103368	-1588.95	-1544.4	-1225.37	-1811.7
2.84011433	-1588.95	-1544.4	-1225.37	-1811.7
2.847108034	-1588.95	-1544.4	-1225.37	-1796.85
2.854084606	-1588.95	-1544.4	-1225.37	-1811.7
2.861044173	-1588.95	-1544.4	-1225.37	-1811.7
2.867986856	-1588.95	-1544.4	-1225.37	-1796.85
2.87491278	-1588.95	-1544.4	-1225.37	-1811.7

Test data for MD strains in 24” wide PET

MD strains for 24 inch wide web

Outer radius	Gage 1 test 1	Gage 1 test 2	Gage 1 test 3	Gage 2 test 1	Gage 2 test 2	Gage 2 test 3
2.386001112	0	0	0	0	0	0
2.394328026	-549.45	-457.4713	-522.8242	-564.3	-445.5	-522.8243

2.402626069	-846.45	-571.8391	-653.5303	-742.5	-653.4	-637.1921
2.41089554	-1024.65	-637.1921	-718.8833	-891	-787.05	-735.2216
2.419136731	-1113.75	-718.8834	-784.2363	-1009.8	-861.3	-800.5746
2.42734993	-1217.7	-767.8981	-833.2511	-1084.05	-950.4	-849.5894
2.435535422	-1291.95	-800.5746	-882.2658	-1158.3	-994.95	-898.6042
2.443693484	-1366.2	-849.5894	-914.9424	-1202.85	-1054.35	-931.2807
2.45182439	-1395.9	-865.9277	-947.6189	-1247.4	-1098.9	-963.9572
2.45992841	-1455.3	-898.6042	-980.2954	-1291.95	-1128.6	-996.6337
2.468005809	-1485	-931.2807	-1012.9719	-1321.65	-1158.3	-1029.3102
2.476056848	-1514.7	-947.619	-1029.3102	-1351.35	-1188	-1045.6485
2.484081782	-1529.55	-980.2955	-1045.6484	-1381.05	-1217.7	-1061.9867
2.492080864	-1559.25	-996.6338	-1061.9867	-1395.9	-1232.55	-1078.325
2.500054342	-1574.1	-1012.972	-1078.3249	-1425.6	-1247.4	-1111.0015
2.508002461	-1588.95	-1029.3103	-1094.6632	-1440.45	-1262.25	-1111.0015
2.515925462	-1603.8	-1045.6485	-1111.0014	-1455.3	-1277.1	-1127.3398
2.52382358	-1633.5	-1061.9868	-1127.3397	-1470.15	-1291.95	-1160.0163
2.531697048	-1633.5	-1061.9868	-1127.3397	-1485	-1306.8	-1160.0163
2.539546097	-1648.35	-1078.3251	-1143.678	-1485	-1336.5	-1160.0163
2.547370951	-1663.2	-1078.3251	-1143.678	-1514.7	-1336.5	-1192.6928
2.555171834	-1678.05	-1094.6633	-1160.0162	-1514.7	-1336.5	-1192.6928
2.562948964	-1678.05	-1094.6633	-1160.0162	-1529.55	-1351.35	-1192.6928
2.570702556	-1692.9001	-1094.6633	-1176.3545	-1544.4	-1366.2	-1192.6928
2.578432824	-1707.75	-1111.0016	-1176.3545	-1544.4	-1381.05	-1209.031
2.586139977	-1707.75	-1111.0016	-1176.3545	-1559.25	-1395.9	-1209.031
2.59382422	-1707.75	-1111.0016	-1192.6927	-1559.25	-1395.9	-1225.3693
2.601485757	-1722.6	-1127.3398	-1192.6927	-1559.25	-1395.9	-1225.3693
2.609124787	-1722.6	-1127.3398	-1192.6927	-1574.1	-1410.75	-1225.3693
2.616741509	-1722.6	-1127.3398	-1192.6927	-1574.1	-1410.75	-1225.3693
2.624336116	-1737.45	-1143.6781	-1209.031	-1588.95	-1410.75	-1225.3693
2.6319088	-1737.45	-1127.3398	-1209.031	-1588.95	-1425.6	-1241.7076
2.63945975	-1752.3	-1127.3398	-1192.6927	-1603.8	-1440.45	-1241.7076
2.646989151	-1752.3	-1143.6781	-1209.031	-1603.8	-1440.45	-1241.7076
2.654497187	-1752.3	-1143.6781	-1209.031	-1603.8	-1440.45	-1258.0458
2.661984039	-1752.3	-1143.6781	-1209.031	-1603.8	-1455.3	-1241.7076
2.669449886	-1767.1501	-1143.6781	-1209.031	-1618.65	-1455.3	-1258.0458
2.676894902	-1767.1501	-1143.6781	-1209.031	-1618.65	-1455.3	-1258.0458
2.684319263	-1752.3	-1143.6781	-1209.031	-1618.65	-1455.3	-1258.0458
2.691723137	-1767.1501	-1143.6781	-1209.031	-1618.65	-1455.3	-1258.0458
2.699106695	-1767.1501	-1160.0163	-1225.3692	-1633.5	-1470.15	-1258.0458
2.706470102	-1767.1501	-1160.0163	-1225.3692	-1633.5	-1470.15	-1258.0458
2.713813522	-1767.1501	-1160.0163	-1225.3692	-1633.5	-1470.15	-1258.0458

2.721137118	-1782	-1160.0163	-1225.3692	-1648.35	-1470.15	-1258.0458
2.72844105	-1782	-1160.0163	-1225.3692	-1648.35	-1485	-1258.0458
2.735725473	-1782	-1160.0163	-1225.3692	-1648.35	-1485	-1258.0458
2.742990545	-1782	-1160.0163	-1209.031	-1648.35	-1485	-1258.0458
2.750236419	-1782	-1160.0163	-1225.3692	-1648.35	-1485	-1258.0458
2.757463245	-1796.85	-1160.0163	-1225.3692	-1648.35	-1485	-1274.3841
2.764671174	-1782	-1160.0163	-1225.3692	-1663.2	-1499.85	-1274.3841
2.771860353	-1796.85	-1160.0163	-1225.3692	-1663.2	-1499.85	-1274.3841
2.779030927	-1782	-1160.0163	-1225.3692	-1663.2	-1499.85	-1274.3841
2.78618304	-1796.85	-1160.0163	-1225.3692	-1663.2	-1499.85	-1274.3841
2.793316834	-1796.85	-1160.0163	-1225.3692	-1663.2	-1499.85	-1274.3841
2.800432449	-1796.85	-1160.0163	-1225.3692	-1663.2	-1499.85	-1274.3841
2.807530023	-1796.85	-1160.0163	-1225.3692	-1663.2	-1514.7	-1274.3841
2.814609694	-1796.85	-1160.0163	-1225.3692	-1663.2	-1514.7	-1274.3841
2.821671595	-1796.85	-1160.0163	-1225.3692	-1678.05	-1514.7	-1274.3841
2.828715859	-1796.85	-1160.0163	-1225.3692	-1663.2	-1514.7	-1274.3841
2.835742619	-1796.85	-1160.0163	-1225.3692	-1678.05	-1514.7	-1274.3841
2.842752004	-1796.85	-1160.0163	-1225.3692	-1678.05	-1514.7	-1274.3841
2.849744142	-1796.85	-1160.0163	-1225.3692	-1678.05	-1514.7	-1274.3841
2.85671916	-1796.85	-1160.0163	-1225.3692	-1678.05	-1529.5501	-1274.3841
2.863677184	-1796.85	-1160.0163	-1225.3692	-1678.05	-1514.7	-1274.3841
2.870618336	-1796.85	-1160.0163	-1209.031	-1678.05	-1529.5501	-1274.3841
2.877542739	-1796.85	-1160.0163	-1225.3692	-1678.05	-1529.5501	-1274.3841
2.884450514	-1796.85	-1160.0163	-1225.3692	-1692.9	-1529.5501	-1274.3841
2.891341779	-1796.85	-1160.0163	-1225.3692	-1678.05	-1529.5501	-1274.3841
2.898216654	-1796.85	-1160.0163	-1225.3692	-1678.05	-1529.5501	-1274.3841
2.905075253	-1796.85	-1160.0163	-1225.3692	-1678.05	-1529.5501	-1274.3841
2.911917692	-1796.85	-1160.0163	-1225.3692	-1678.05	-1529.5501	-1274.3841
2.918744085	-1796.85	-1160.0163	-1225.3692	-1678.05	-1529.5501	-1274.3841
2.925554544	-1811.7	-1160.0163	-1225.3692	-1678.05	-1529.5501	-1274.3841
2.93234918	-1811.7	-1160.0163	-1225.3692	-1692.9	-1529.5501	-1274.3841
2.939128103	-1796.85	-1160.0163	-1225.3692	-1692.9	-1544.4	-1274.3841
2.945891422	-1811.7	-1143.6781	-1225.3692	-1692.9	-1544.4	-1274.3841
2.952639244	-1796.85	-1160.0163	-1209.031	-1692.9	-1529.5501	-1274.3841
2.959371674	-1796.85	-1160.0163	-1225.3692	-1692.9	-1544.4	-1274.3841
2.966088817	-1811.7	-1160.0163	-1209.031	-1692.9	-1544.4	-1274.3841
2.972790779	-1796.85	-1160.0163	-1225.3692	-1692.9	-1544.4	-1274.3841
2.979477659	-1796.85	-1160.0163	-1225.3692	-1692.9	-1544.4	-1274.3841
2.986149561	-1811.7	-1160.0163	-1225.3692	-1692.9	-1544.4	-1274.3841
2.992806584	-1796.85	-1160.0163	-1225.3692	-1692.9	-1544.4	-1274.3841

CMD strains for 24 inch wide PET

Outer radius	Gage 1 test 1	Gage 1 test 2	Gage 1 test 3	Gage 2 test 1	Gage 2 test 2	Gage 2 test 3
2.384001112	0	0	0	0	0	0
2.392328026	44.55	14.85	14.85	59.4	14.85	29.7
2.400626069	44.55	14.85	29.7	44.55	29.7	14.85
2.40889554	44.55	0	44.55	74.25	29.7	44.55
2.417136731	59.4	14.85	44.55	74.25	59.4	44.55
2.42534993	59.4	14.85	59.4	74.25	59.4	44.55
2.433535422	59.4	14.85	59.4	103.95	59.4	74.25
2.441693484	59.4	14.85	74.25	103.95	74.25	74.25
2.44982439	89.1	44.55	89.1	118.8	89.1	89.1
2.45792841	89.1	44.55	89.1	118.8	89.1	89.1
2.466005809	89.1	44.55	103.95	133.65	103.95	103.95
2.474056848	103.95	59.4	103.95	133.65	103.95	103.95
2.482081782	118.8	74.25	103.95	148.5	133.65	118.8
2.490080864	118.8	74.25	118.8	148.5	118.8	118.8
2.498054342	133.65	89.1	133.65	178.2	133.65	133.65
2.506002461	133.65	89.1	133.65	193.05	133.65	148.5
2.513925462	133.65	89.1	133.65	193.05	148.5	148.5
2.52182358	163.35	118.8	163.35	207.9	163.35	163.35
2.529697048	148.5	103.95	163.35	222.75	163.35	178.2
2.537546097	178.2	133.65	163.35	222.75	178.2	178.2
2.545370951	178.2	133.65	178.2	222.75	193.05	178.2
2.553171834	178.2	133.65	178.2	252.45	193.05	207.9
2.560948964	193.05	148.5	178.2	252.45	193.05	207.9
2.568702556	193.05	148.5	193.05	252.45	207.9	207.9
2.576432824	193.05	148.5	193.05	267.3	207.9	222.75
2.584139977	193.05	148.5	193.05	267.3	222.75	222.75
2.59182422	193.05	148.5	193.05	267.3	222.75	222.75
2.599485757	207.9	163.35	207.9	297	252.45	252.45
2.607124787	222.75	178.2	207.9	297	252.45	252.45
2.614741509	222.75	178.2	207.9	297	252.45	252.45
2.622336116	222.75	178.2	207.9	311.85	252.45	267.3
2.6299088	222.75	178.2	222.75	311.85	267.3	267.3
2.63745975	222.75	178.2	222.75	326.7	267.3	282.15

2.644989151	237.6	193.05	222.75	326.7	267.3	282.15
2.652497187	237.6	193.05	237.6	341.55	282.15	297
2.659984039	237.6	193.05	237.6	341.55	282.15	297
2.667449886	252.45	207.9	252.45	341.55	282.15	297
2.674894902	252.45	207.9	267.3	341.55	282.15	297
2.682319263	252.45	207.9	252.45	356.4	297	311.85
2.689723137	252.45	222.75	267.3	356.4	297	311.85
2.697106695	252.45	222.75	252.45	356.4	297	311.85
2.704470102	252.45	222.75	311.85	371.25	297	326.7
2.711813522	252.45	222.75	267.3	371.25	311.85	326.7
2.719137118	267.3	237.6	267.3	371.25	311.85	326.7
2.72644105	267.3	237.6	267.3	371.25	326.7	326.7
2.733725473	267.3	237.6	267.3	371.25	326.7	326.7
2.740990545	267.3	237.6	267.3	386.1	326.7	341.55
2.748236419	282.15	252.45	267.3	386.1	326.7	341.55
2.755463245	282.15	252.45	267.3	386.1	326.7	341.55
2.762671174	282.15	252.45	267.3	386.1	326.7	341.55
2.769860353	297	267.3	267.3	386.1	341.55	341.55
2.777030927	297	267.3	267.3	386.1	341.55	341.55
2.78418304	297	267.3	267.3	400.95	341.55	356.4
2.791316834	297	267.3	267.3	400.95	341.55	356.4
2.798432449	297	267.3	282.15	400.95	356.4	356.4
2.805530023	311.85	282.15	297	400.95	356.4	356.4
2.812609694	297	267.3	282.15	400.95	356.4	356.4
2.819671595	297	267.3	282.15	400.95	356.4	356.4
2.826715859	297	267.3	282.15	400.95	356.4	356.4
2.833742619	311.85	282.15	282.15	400.95	356.4	356.4
2.840752004	326.7	297	297	400.95	356.4	356.4
2.847744142	326.7	297	297	415.8	356.4	371.25
2.85471916	311.85	282.15	297	415.8	356.4	371.25
2.861677184	326.7	297	282.15	415.8	371.25	371.25
2.868618336	311.85	282.15	311.85	415.8	371.25	371.25
2.875542739	326.7	297	311.85	415.8	356.4	371.25
2.882450514	326.7	297	311.85	415.8	356.4	371.25
2.889341779	326.7	297	297	430.65	371.25	386.1
2.896216654	341.55	311.85	297	430.65	371.25	386.1
2.903075253	326.7	297	311.85	430.65	371.25	386.1
2.909917692	341.55	311.85	311.85	415.8	371.25	371.25
2.916744085	341.55	311.85	297	430.65	371.25	386.1
2.923554544	341.55	311.85	311.85	445.5	371.25	400.95
2.93034918	341.55	311.85	326.7	430.65	386.1	386.1

2.937128103	356.4	326.7	326.7	445.5	386.1	400.95
2.943891422	341.55	311.85	311.85	430.65	371.25	386.1
2.950639244	341.55	311.85	326.7	445.5	371.25	400.95
2.957371674	356.4	326.7	326.7	445.5	400.95	400.95
2.964088817	356.4	326.7	311.85	445.5	400.95	400.95
2.970790779	341.55	311.85	326.7	445.5	386.1	400.95
2.977477659	341.55	311.85	326.7	445.5	386.1	400.95
2.984149561	356.4	326.7	311.85	460.35	400.95	415.8
2.990806584	356.4	326.7	326.7	460.35	400.95	415.8
2.997448828	341.55	311.85	341.55	445.5	386.1	400.95
3.00407639	356.4	326.7	326.7	460.35	400.95	415.8
3.010689367	356.4	326.7	326.7	460.35	400.95	415.8
3.017287856	356.4	326.7	326.7	445.5	400.95	400.95
3.023871951	356.4	326.7	326.7	460.35	400.95	415.8
3.030441745	371.25	341.55	326.7	460.35	400.95	415.8
3.036997332	371.25	341.55	341.55	460.35	400.95	415.8
3.043538803	356.4	326.7	326.7	460.35	386.1	415.8
3.05006625	356.4	326.7	326.7	475.2	415.8	430.65
3.056579761	371.25	341.55	341.55	460.35	415.8	415.8
3.063079427	356.4	326.7	326.7	445.5	400.95	400.95
3.069565334	356.4	326.7	341.55	475.2	415.8	430.65
3.076037569	371.25	341.55	341.55	475.2	415.8	430.65
3.08249622	371.25	341.55	326.7	460.35	400.95	415.8
3.088941371	371.25	341.55	341.55	475.2	415.8	430.65
3.095373106	386.1	356.4	326.7	475.2	415.8	430.65
3.101791509	371.25	341.55	341.55	460.35	400.95	415.8
3.108196662	356.4	326.7	356.4	475.2	415.8	430.65
3.114588647	386.1	356.4	326.7	475.2	415.8	430.65
3.120967545	371.25	341.55	356.4	460.35	415.8	415.8
3.127333436	371.25	341.55	341.55	475.2	415.8	430.65
3.1336864	386.1	356.4	356.4	460.35	400.95	415.8
3.140026514	371.25	341.55	356.4	490.05	415.8	445.5
3.146353856	386.1	356.4	341.55	490.05	415.8	445.5
3.152668504	386.1	356.4	356.4	460.35	415.8	415.8
3.158970533	371.25	341.55	341.55	490.05	415.8	445.5
3.165260018	386.1	356.4	356.4	475.2	415.8	430.65
3.171537035	371.25	341.55	326.7	475.2	430.65	430.65
3.177801657	386.1	356.4	371.25	490.05	430.65	445.5
3.184053957	386.1	356.4	341.55	460.35	415.8	415.8
3.190294008	371.25	341.55	356.4	490.05	430.65	445.5
3.196521882	386.1	356.4	341.55	475.2	415.8	430.65

3.202737648	371.25	341.55	341.55	490.05	430.65	445.5
3.208941379	386.1	356.4	356.4	475.2	430.65	445.5
3.215133143	386.1	371.25	371.25	490.05	430.65	445.5
3.221313009	386.1	371.25	371.25	475.2	430.65	430.65
3.227481046	386.1	341.55	371.25	490.05	415.8	430.65
3.233637321	386.1	356.4	356.4	490.05	430.65	430.65
3.239781902	386.1	356.4	356.4	490.05	415.8	445.5
3.245914854	386.1	356.4	371.25	490.05	430.65	430.65
3.252036244	386.1	341.55	356.4	475.2	415.8	430.65
3.258146137	386.1	371.25	356.4	490.05	430.65	430.65
3.264244597	371.25	341.55	356.4	475.2	430.65	445.5
3.270331688	386.1	356.4	371.25	490.05	430.65	430.65
3.276407474	386.1	371.25	371.25	490.05	415.8	430.65
3.282472017	400.95	341.55	341.55	490.05	415.8	445.5

Mathematical calculations for applying Chauvenet's criterion

Gage 2 Test 3 strains saturated at -1225 microstrain. The average saturation strain was -1614 microstrain with a standard deviation of 192 microstrain. Now, the difference between this particular reading and the average reading is 389 microstrain. This is more than twice the standard deviation of 192 microstrain. The probability of taking data more than two standard deviations from the mean is roughly 0.05. Four measurements were taken, so the statistic value (data size multiplied by the probability) is $0.05 \times 4 = 0.2$. Because $0.2 < 0.5$, according to Chauvenet's criterion, the measured value of -1225 should be discarded.

VITA

Kazi Md. Ismael Murtaza

Candidate for the Degree of

Master of Science

Thesis: VERIFICATION OF CIRCUMFERENTIAL AND AXIAL STRAINS IN AXISYMMETRIC WOUND ROLL MODELS.

Major Field: Mechanical Engineering.

Biographical:

Personal Data: Born in Dhaka, Bangladesh 7th October 1981, son of Dr. Kazi Islam and Dr. Azizunnahar Islam

Education: Graduated tenth grade from St. Joseph High School, Dhaka in May, 1998; graduated twelfth grade from Notre Dame college, Dhaka in May, 2000; received Bachelor of Science degree from Bangladesh University of Engineering and Technology, Dhaka, in December 2006; Completed the requirements for the Master of Science majoring in Mechanical Engineering at Oklahoma State University, Stillwater, Oklahoma in December, 2008.

Experience: Worked as Graduate Research Assistant at OSU from August 2007 to present.

Name: Kazi Md. Ismael Murtaza Date of Degree: May, 2009

Institution: Oklahoma State University Location: Stillwater, Oklahoma

Title of Study: VERIFICATION OF CIRCUMFERENTIAL AND AXIAL STRAINS IN AXISYMMETRIC WOUND ROLL MODELS

Pages in Study: 63 Candidate for the Degree of Master of Science

Major Field: Mechanical Engineering

Scope and Method of Study:

The primary goal of this study was to verify the axial and circumferential strains in axisymmetric wound roll models generated by Cagri Mollamahmutoglu's model, i.e. whether his model predicts the Machine Direction and Cross Machine Direction strains correctly or not. In order to do this two different widths of web were tested, a 6 inch wide web and a 24 inch wide web. The model was run to obtain strains and a comparison was made between the experimental strains and the model strains.

Findings and Conclusions:

The model made reasonably good predictions for MD strains in both cases (6 inch and 24 inch). However, in case of CMD strains the model was not very accurate. In case of CMD strains for the 6 inch web, the final saturation value was off and in case of CMD strains for the 24 inch web; the contour of the model output did not match the contour of the experimental results.

ADVISER'S APPROVAL: Dr. J. K. Good